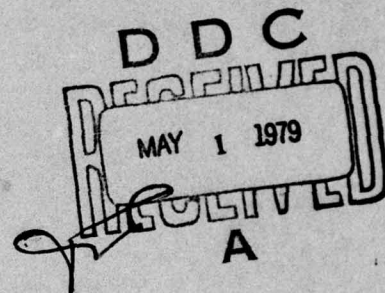LEVEL

RADC-TR-79-7
Final Technical Report
February 1979

ADVANCED MULTIDITHER COAT STUDIES

Hughes Research Lab

D D C
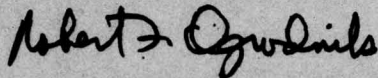
MAY 1 1979

A

The views and conclusions contained in this document are those of
the authors and should not be interpreted as necessarily representing
the official policies, either expressed or implied, of the Defense
Advanced Research Projects Agency or the U.S. Government.

ROME AIR DEVELOPMENT CENTER
Air Force Systems Command
Griffiss Air Force Base, New York 13441

79 04 27 010

This report has been reviewed by the RADC Information Office (OI) and is releasable to the National Technical Information Service (NTIS). At NTIS it will be releasable to the general public, including foreign nations.

RADC-TR-79-7 has been reviewed and is approved for publication.

APPROVED: *Robert F. Ogrodnik*

ROBERT F. OGRODNIK
Project Engineer

ADVANCED MULTIDITHER COAT STUDIES

S.A. Kokorowski
T.R. O'Meara
T. Calderone
R.C. Lind

REPORT DOCUMENTATION PAGE		READ INSTRUCTIONS BEFORE COMPLETING FORM
1. REPORT NUMBER RADC-TR-79-7	2. GOVT ACCESSION NO.	3. RECIPIENT'S CATALOG NUMBER
4. TITLE (and Subtitle) ADVANCED MULTIDITHER COAT STUDIES		5. TYPE OF REPORT & PERIOD COVERED Final Technical Report 1 Jul 77 – 30 Jun 78
		6. PERFORMING ORG. REPORT NUMBER N/A
7. AUTHOR(s) S.A. Kokorowski, T. Calderone T.R. O'Meara, R.C. Lind		8. CONTRACT OR GRANT NUMBER(s) F30602-77-C-0114
9. PERFORMING ORGANIZATION NAME AND ADDRESS Hughes Research Laboratories 3011 Malibu Canyon Road Malibu CA 90265		10. PROGRAM ELEMENT, PROJECT, TASK AREA & WORK UNIT NUMBERS 62301E 12790026
11. CONTROLLING OFFICE NAME AND ADDRESS Defense Advanced Research Projects Agency 1400 Wilson Blvd Arlington VA 22209		12. REPORT DATE February 1979
		13. NUMBER OF PAGES 150
14. MONITORING AGENCY NAME & ADDRESS(if different from Controlling Office) Rome Air Development Center (OCTM) Griffiss AFB NY 13441		15. SECURITY CLASS. (of this report) UNCLASSIFIED
		15a. DECLASSIFICATION DOWNGRADING SCHEDULE N/A

16. DISTRIBUTION STATEMENT (of this Report)

Approved for public release; distribution unlimited.

17. DISTRIBUTION STATEMENT (of the abstract entered in Block 20, if different from Report)

Same

18. SUPPLEMENTARY NOTES

RADC Project Engineer: Robert F. Ogrodnik (OCTM)

19. KEY WORDS (Continue on reverse side if necessary and identify by block number)

Speckle	ABAC
Adaptive optics	Adaptive Systems
Multidither	
COAT	
ASPECT	

20. ABSTRACT (Continue on reverse side if necessary and identify by block number)

Multidither adaptive optics systems are vulnerable to interference caused by the motion of a speckle pattern across the receiver aperture. This program investigated various techniques for reducing or canceling this interference. Several concepts were studied. A very promising one, which we call ASPECT II, was demonstrated with an experimental laboratory COAT system. Computer simulations and experimental data show that with ASPECT-II it is possible to almost completely restore speckle degraded performance of multidither COAT systems.   (Cont'd)

DD FORM 1 JAN 73 1473   EDITION OF 1 NOV 65 IS OBSOLETE

. Items 20 (Cont'd)

An extensive analysis that explicitly illustrates how speckle effects interfere with COAT operation has been developed. It shows that the primary effect is to amplitude modulate the usual point source intensity distribution reflected from a target glint. With large targets, there is also an additive noise contribution from the receiver spatial intensity variations associated with reflections from the area surrounding the target focal spot. This analysis is also used to explain the operations of the ASPECT-I and ASPECT-II speckle cancelation schemes.

Experimental data showing ASPECT cancelation of simulated speckle modulations is presented. The experiments show that the laboratory ASPECT system can cancel single-frequency and broadband modulations within the COAT dither band.

Previous work has also shown that the severity of COAT performance degradation due to speckle interference is related to the COAT servo bandwidth. Generally speaking, the larger the bandwidth, the more severe the degradation. However, if the bandwidth is reduced to decrease speckle interference, the ability of the servo to compensate other disturbances such as atmospheric turbulance will also be reduced. Thus, we have studied a servo technique called ABAC that seeks to optimize the COAT servo bandwidth under arbitrary conditions of speckle interference and atmospheric turbulence. Computer simulation results demonstrate ABAC's ability to achieve this goal.

Analytical work which predicts the amount of COAT target Strehl ratio degradation for a specified but otherwise arbitrary speckle modulation function is also presented. The analytical predictions are compared to computer simulations and good agreement is found.

TABLE OF CONENTS

LIST OF ILLUSTRATIONS

5

7

8

ACRONYMS

COAT – Coherent Optical Adaptive Techniques

ASPECT – Automatic Speckle Cancelation Techniques

ABAC – Automatic Bandwidth Adaptive Control

IMPACT – Image Plane Aperture Censoring Techniques

MAST – Multiple Aperture Sharing Techniques

ABBREVIATIONS

Hz	Hertz
kHz	kilohertz
sec	second
msec	millisecond
Eq	equation
PMT	photo-multiplier
rad	radians
dB	decibles
AGC	automatic gain control
LPF	low-pass filter
HPF	high-pass filter

9

SECTION 1

INTRODUCTION AND SUMMARY

Several investigators have shown that rotating targets generate speckle effects, which have the potential to seriously degrade the performance of all adaptive optics systems operating with single-line laser illuminators.[1,2,3] Accordingly, the primary objective of this program was to investigate techniques that will give improved performance in one class of these systems -- a multidither COAT system -- in the presence of such speckle jamming interference. Thus, we investigated several such concepts and were able to demonstrate one very promising concept that can virtually eliminate the effective speckle interference and the resultant COAT performance degradation. This concept, which we call automatic speckle cancellation techniques (ASPECT), refers to a class of techniques by which speckle noise in a conventional COAT receiver is first estimated and then cancelled. The estimation is achieved by introducing a high-frequency sinusoidal modulation -- the probe frequency -- on either a portion of the outgoing wavefront (ASPECT I) or on the entire wavefront (ASPECT II). The modulation envelope of this carrier, as extracted from the usual multidither detector output, provides the desired speckle estimator. This estimator is used for cancellation in one of two ways: (1) the division scheme or (2) the subtraction scheme.

Basic systems configurations for ASPECT I and II and their relative merits are discussed in Section 2. Since we concluded early in the program that ASPECT II was the preferred approach, it was chosen for laboratory instrumentation. If these systems are to be useful in high-power applications, it is important that reasonably low-cost, high-power configurations be available. Accordingly, two ASPECT II configurations suitable for high-power applications are also discussed in Section 2.

To understand how these systems work requires a detailed analysis of the speckle interference process in multidither COAT systems. Such an

11

analysis is developed in Section 3 and applied to ASPECT systems in Section 4. This analysis shows that the primary effect of speckle on the COAT receiver output signal is indeed a multiplicative noise that can be extracted by an ASPECT I or II estimation system.

We recognized early in the program that, with high power systems, the probe carrier frequency would most conveniently be introduced via phase modulations produced by moving mirrors. Clearly, these have definite frequency limitations that might limit system performance. More specifically, the lower the probe carrier freuency relative to the (highest) normal dither frequency, the higher the likelihood that the probe modulation envelope will be contaminated with undesired high-frequency dither signals and/or their harmonies as well as the multiplicative speckle noise associated with each. The ASPECT frequency ratio* required to avoid such contamination is difficult to ascertain theoretically. This problem was approached in two ways: (1) computer simulation and (2) laboratory system simulation (as discussed in Sections 4 and 5).

We had originally hoped that the ASPECT probe frequency could be the second harmonic of the highest dither frequency (an ASPECT frequency ratio of two) since this would have provided a very simple, low-cost implementation. Unfortunately, the computer simulations indicated that ASPECT frequency ratios of approximately six were required for reasonable performance and that ratios of ten or more are required to ensure the best performance. The experimental laboratory data confirms these same conclusions. In particular, although we were able to demonstrate substantial improvements with the ASPECT correction system operating, we did not see a total performance recovery as large as that achieved in the computer simulations. This was because our maximum achievable probe carrier was 100 kHz, which was about 7 times the maximum COAT dither

---

*Probe carrier divided by the highest COAT dither frequency.

12

frequency of 15 kHz (we used only 7 low-frequency dither channels in the existing system to improve the ASPECT frequency ratio), whereas 10 times is required for best performance.

We have also conducted a computer simulation study of an automatic bandwidth adaptive control (ABAC) system. Briefly, its operating principle is as follows. The amount of energy in the speckle interference signal depends on the COAT servo bandwidth. If we reduce the bandwidth, we reduce the interference. On the other hand, after reducing the bandwidth, the COAT system may not be able to respond fast enough to compensate dynamic phase distortions (such as atmospheric turbulence). The ABAC servo automatically seeks the optimum compromise bandwidth, the bandwidth that allows the highest possible target irradiance in the presence of these constraints. We have demonstrated, using computer simulation, that this concept does perform this task. To implement ABAC, we dither the bandwidth very slowly (about two orders of magnitude slower than the servo bandwidth) and then synchronously detect at the dither frequency to produce a bandwidth correction signal. Since the amount of bandwidth-related degradation is highly dependent on atmospheric conditions and target scenarios, the amount of improvement will vary accordingly.

In Section 7, we show that COAT target irradiance degradation due to speckle interference can be predicted analytically if the power spectrum of the speckle modulation function and the COAT servo bandwidth characteristics are known. The analytical predictions are compared to computer simulation data, with good correlation between the separate results.

13

SECTION 2

ASPECT SYSTEMS

A.   OPERATING PRINCIPLES

ASPECT is a series of techniques for estimating the real-time
jamming or interfering time modulations generated by a moving speckle
pattern[1-3] and for removing their effects (in real time) from the adaptive
optics error signals of a multidither system. This section explores
these techniques in more detail, heuristically describes their operation,
and considers their application at high power levels. These systems
have the following characteristics in common: (1) they share a single
receiver aperature and detector with the basic multidither system;
(2) they inject a probing modulation or wavelength to extract the speckle
waveform estimator via an auxiliary probe beam that shares the main
aperture; (3) they extract the modulation envelope of the probe frequency
in the detector output as a real-time estimator of the speckle jamming
signal: and (4) they divide this signal into or subtract it from the
basic dither encoded signal out of the detector.

If only a single element of a zonal multidither system is modulated
with the probe modulation, we call the resulting system an ASPECT I
system, while if the entire (in the spatial sense) outgoing beam is
modulated, we call the resulting system an ASPECT II system. Further,
as will be discussed in Section 3.E. ASPECT I and ASPECT II estimate
slightly different speckle noise components.

1.   Aspect I Systems

The simplest approach is to extract the ASPECT probe frequency as
the second harmonic of the highest dither frequency in the system. This
has the virtue that no optical modification whatever is required of the
basic multidither outgoing-wave system (illustrated in Figure 1). As
discussed in Section 3.E, it is advantageous to employ a central element

15
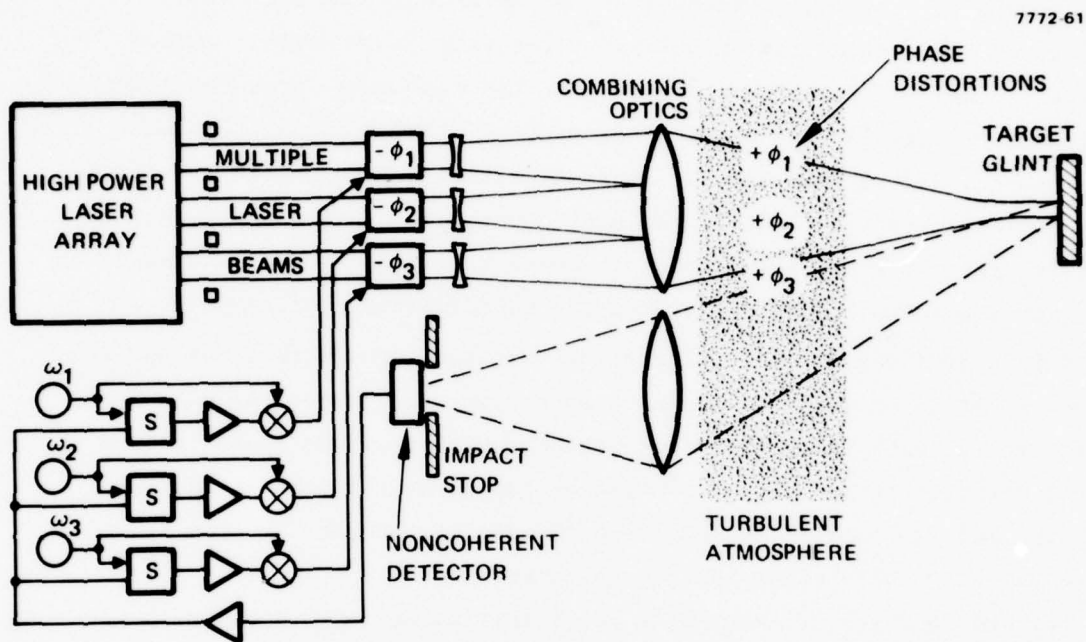
Figure 1. Outgoing-wave multidither or outgoing-wave maximization system. A field of view of stop called an IMPACT stop is often advantageous although it is not essential to system operation if the system has a single dominant glint.

16

in the array for aspect encoding. However, electronic modifications
are required. It is advantageous to raise the probe dither frequency
to the highest possible limit, operating at or above a high-frequency
resonance of the dither mirror, or, if optical power permits, to include
a high-frequency electrooptic dither system for this particular element.
Further, the probe dither amplitude is increased to boost the magnitude
of the second harmonic signal. Specifically, a boosted amplitude ψ_A
for the ASPECT channel of

$$\psi_A \geq 1.8 \text{ rad} \tag{2.1}$$

is recommended for this application. Under these conditions, the
second harmonic, which is the probe frequency, is of strong magnitude
(with good convergence in this channel). Assuming the speckle pattern
scans past the receive aperture and generates a speckle jamming signal
$M_{S2}(t)$, then a nearly equivalent signal $M_{SA}(t)$ also modulates the probe
frequency. Thus, the high-intensity components in the detector output
current are approximately

$$S_o = M_{S2}(t) + CM_{SA}(t) \cos(2\omega_A t + \alpha_A) + \sum_{n=1}^{N} M_{S1}^{(n)}(t) A_n \sin(\omega_n t + \alpha_n),$$

$$\tag{2.2}$$

where $M_{S1}^{(n)}(t)$ and $M_{SA}(t)$ are nearly equal multiplicative noise components,
at least for closely spaced glints; ω_A is the aspect probe frequency,
the variables α_n and α_A are arbitrary reference phases; C is a constant;
and A_n is the modulation index of channel n.

The envelope of the received second harmonic probe signal $M_{SA}(t)$,
is extracted by synchronous detection and forms our estimation signal
$\hat{M}_{SA}(t)$, as illustrated in Figure 2. This signal is then divided into
the basic common dither signal system (as illustrated) or substracted in

17
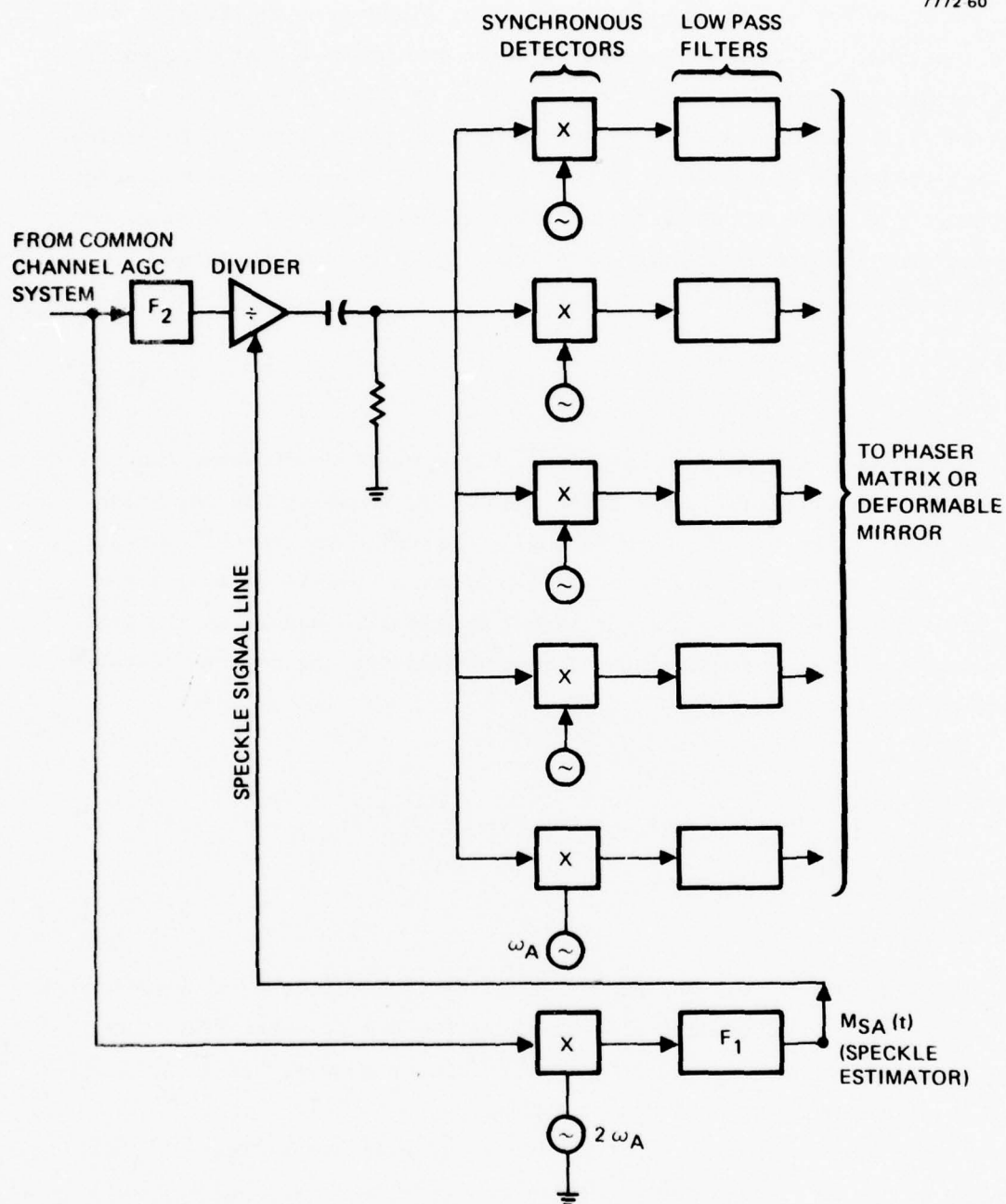
Figure 2. ASPECT I block diagram. This is one system variant. Alter-
native approaches may split off the reference signals after the
divider.

18

the alternate approach. Since $M_{S2}(t)$ is the speckle noise signal of major importance and since $M_{SA}(t)$ is not precisely equal to $M_{S2}(t)$, we believe that these differences may cause some reduction in performance. Additional problems are discussed below. We use matched low-pass filters F_1 and F_2 in Figure 2. Basically, the speckle-estimator low-pass filter F_1 has a cutoff that must fall somewhat above the highest dither frequency and below the ASPECT probe frequency ($2\omega_A$). The filter F_2 is included only to balance the delay times for the true speckle signals and the estimator signal paths going into the divider.

If the probe frequency were sufficiently high and no other types of noise were present, then the speckle estimator $M_{SA}(t)$ and the actual speckle multiplier would be substantially identical. Unfortunately, with second harmonic operation and equally (or near equally) spaced dither signals, a large number of second harmonic signals from the other dithers can fall near the ASPECT probe frequency, as illustrated in Figure 3. In particular, Figure 3 illustrates a "typical" spectrum of the dither channels with all COAT servo loops open, assuming the system is working well. The reference channel at* 7 kHz dominates in intensity because of its high modulation index, if we assume that the dc component is eliminated by high-pass filtering. If the servo loops are closed, as illustrated in Figure 3(b), the fundamental dither frequency components, which represent the error signals, generally reduce in magnitude, particularly at the higher dither frequency, in spite of the speckle jamming, if the ASPECT system functions correctly. In particular, the reference, or probe, channel has a very large expected reduction at its fundamental frequency (good convergence), both because of its high frequency and because its enhanced modulation index makes it less vulnerable to speckle interference. As the fundamental component reduces in amplitude, the second harmonic increases until it becomes the dominant spectral line.

---

*The illustrated frequencies are only examples.

19
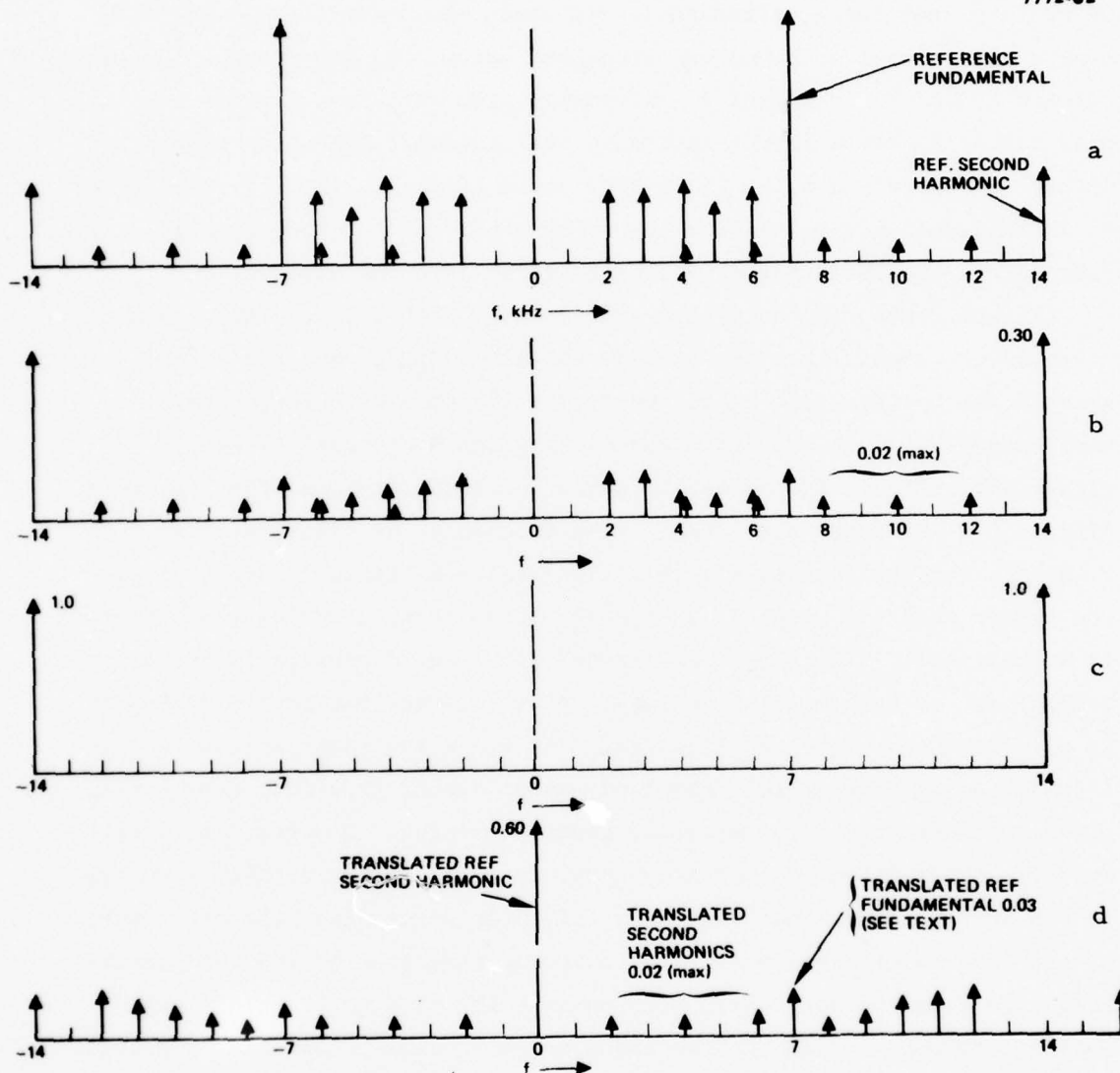
Figure 3. Key voltage (or current) spectra in an ASPECT I system. The indicated magnitudes are discussed in the text. (a) Spectrum of high-pass filter output before convergence. (b) Spectral output of Figure 22(a) after "convergence" (with speckle jamming). (c) Reference oscillator spectrum. (d) Spectrum of reference synchronous detector output, before low pass filtering.

Next we examine the spectrum of the unfiltered output of the ASPECT I
detector. For the moment, we assume that our reference channel second-
harmonic synchronous detector (at 14 kHz) is a true multiplier and
produces an output with the spectrum indicated in Figure 3(d). This
spectrum is the convolution of the reference oscillator spectrum of
Figure 3(c) with the input spectrum of Figure 3(b). The dominant
spectral components are the dc component and second harmonics at 28 kHz,
which are not shown in Figure 3(d).

So far, the effect of the speckle on the spectra in Figure 3 has
not been illustrated. It is easily obtained by convolving the speckle
spectrum with each of the illustrated spectra. In particular, if all
the spectral lines in Figure 3(d), (except the control, or zero frequency,
line) were vanishingly small, then this convolutional process would
simply replicate the speckle spectrum at the detector output and there-
fore the temporal output of the $2\omega_A$ synchronous detector would replicate
$M_{SA}(t)$. As illustrated in Figure 3(d), other spectral lines are present
and contaminate the estimation of the speckle spectra since they couple
erroneous spectral information via the convolution process. However,
the better the estimation, the better the speckle can be removed from
the lower frequency channels, and hence the better the convergence and
the smaller the spectral lines above 7 kHz become, etc. Thus, the effect
of the harmonic jamming signals is a highly nonlinear and very complex
process. This problem is discussed in Sections 4 and 5, which describe
our computer simulations and our laboratory systems investigations.

Similar (but differing in detail) self-jamming problems occur in
all the ASPECT systems dicsussed below if the probe frequency is not
sufficiently well separated from the dither frequencies.

Using computer simulation, we investigated this jamming problem
for ASPECT I and have found, under the assumptions of pure multiplicative
noise as defined in Section 3.C and sufficiently high probe frequencies,
that the system could be made to perform well. However, because of the

21

important advantages of ASPECT II (discussed in Section 2), we elected
to devote the remainder of the report to this class of system.

2. ASPECT II Implementations

ASPECT II systems have demonstrated the best performance in the face
of speckle jamming of all the systems considered in this report and (so
far as is known) elsewhere. These are implemented by splitting off a
portion of the whole beam (in the spatial sense), modulating it or
frequency offsetting it, and recombining it with the main beam ahead of
the wavefront correction system (generally a deformable mirror). Several
modulation techniques potentially are applicable, including (1) frequency
offset of the probe beam, (2) amplitude modulation of the probe beam, and
(3) phase modulation of the probe beam. Primarily because of its high
recombination efficiency, we selected the phase-modulation approach for
initial discussion. Further, since it can employ mechanically moving
mirrors to generate the probe modulation, it appears certain that it
can be implemented at high power levels, without technology challenges.

In addition to the versatility in implementation techniques that
this approach permits in comparison with ASPECT I, it has the property
that is directly estimates $M_{S2}(t)$ in Eq. 2 the speckle noise component
of most importance in speckle jamming. That is, for ASPECT II, $M_{SA}(t)$
is equal to $M_{S2}(t)$ up to a multiplicative constant. This is discussed
in more detail in Section 4.A.

A typical low-power ASPECT II configuration using phase modulation
is illustrated in Figure 4. In this particular implementation, which
closely resembles our laboratory demonstration system, 2% of the main
beam power is split off from the main beam, phase modulated, and then
recombined with the main beam in a Mark-Zender interferometer. A local
null-seeking dither servo holds the interferometer path lengths in
constructive interference on the recombined beams* and in destructive

---

*The in-phase operation of the test beam serves two functions. It pro-
vides the most efficient use of the test beam from a total delivered
power viewpoint, and it also delivers the maximum output signal at the
second harmonic.

22
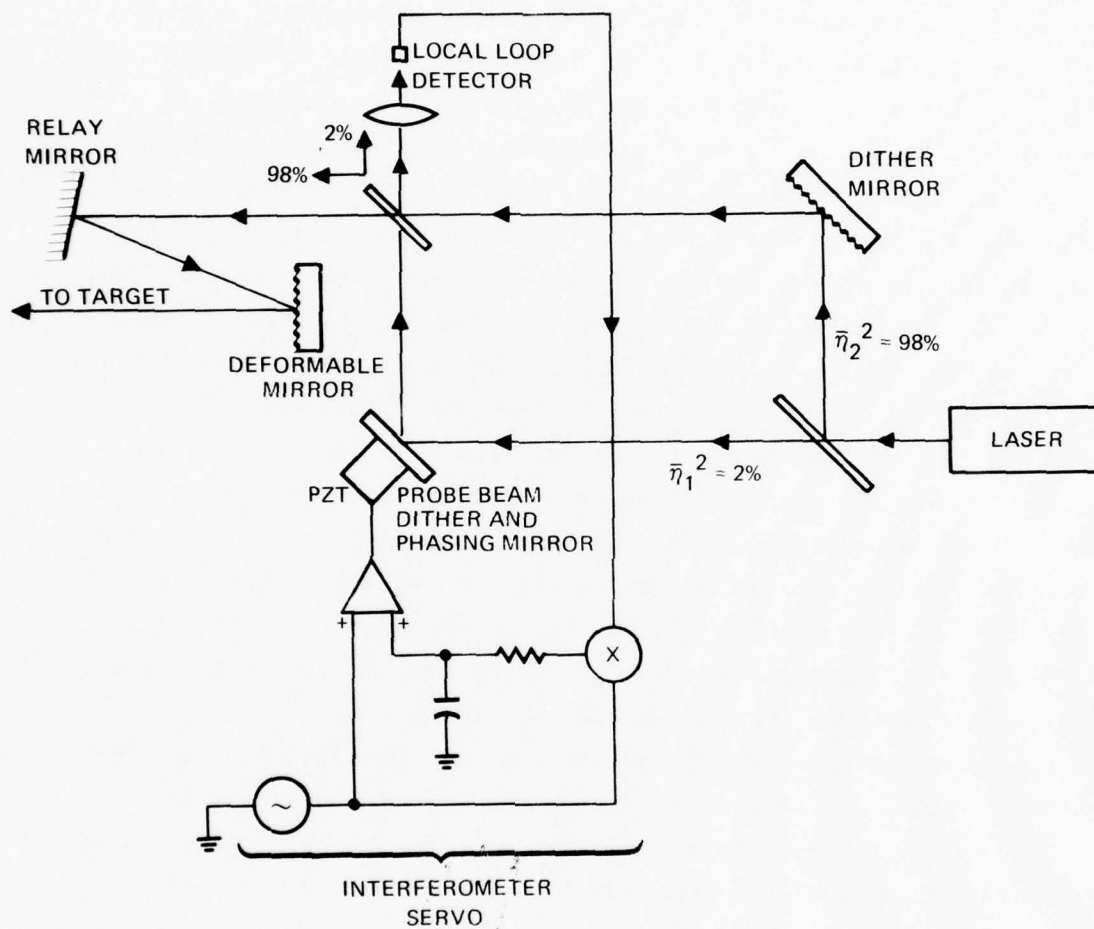
Figure 4. An ASPECT II encoding system. The decoding electronics is
similar to ASPECT I (see Figure 2).

interference at the local loop detector. Separate dither and corrector deformable mirrors are used and are not simply interchangeable in position or combinable without degrading system performance. In particular, if the dither mirror is moved to the position of the deformable mirror (outside the interferometer), the ASPECT output signals will include full strength dither signals and the division operation will cancel the dither and the speckle signals. Although the result of moving the deformable mirror to the position of the dither mirror is less disasterous, it nevertheless compromises the system. Specifically, the probe beam then becomes a badly corrected beam, in the face of propagation path aberrations, and will illuminate a wider portion of the target than the main beam. Consequently, each beam can produce differing speckle fields at the receiver aperture with differing associated amplitude modulations. Thus, the ASPECT cancellation could be less than complete, although possibly still worthwhile. Although both United and Hughes proposed separate dither and corrector mirrors in their HiCLAS design studies, there may be future designs which prefer to combine these functions in one mirror. If so, the preferred location is that of the dither mirror (within the interferometer) of Figure 4. A low-power corrector mirror can be added to the probe beam (in the lower path of the interferometer) if desired to correct the problem just discussed.

The receiver aperture may be off-axis (as illustrated), a shared-aperture annulus, or whatever — it does not matter. Similarly the receiver may be a simple "photon-bucket" collector or an imaging system with a restricted field of view — an "IMPACT" system. The ability to estimate speckle is the same in all cases although the overall speckle suppression may be influenced by these choices.

As in ASPECT I, the speckle modulation envelope is extracted from the second harmonic of the test dither by synchronous detection and is divided into (or subtracted from) the main error signals to cancel the speckle. This is done with an electronic system such as described for the ASPECT I (See Figure 2). For the reasons previously discussed,

24

it is important to have the probe frequency well above the highest dither frequency.

There are some other considerations worth noting. For example, there is an optimum splitter-recombination system for most efficient use of the reinjected power. In particular, the recombination splitter intensity ratio should have the same value of the intensity ratios as in the main and injected beams, with the majority of the power being transmitted through the splitter (when taken one beam at a time). In this way, the two fields transmitted to the local-loop detector are equal in magnitude, and the local-loop system drives them to an out-of-phase condition. This generates an essential* field (and energy) null in this path. In other words, all of the injected power of the test beam is transmitted to the target by virtue of this interference and conservation of energy.

It is helpful to define two kinds of field ratios in this system. The first is the basic splitter field transmission factor, which we call η_1 and η_2 and for the case illustrated in Figure 4:

$$\bar{\eta}_1 = (0.02)^{1/2} \doteq 0.15 \tag{2.3a}$$

$$\bar{\eta}_2 = (0.98)^{1/2} = 0.99 \tag{2.3b}$$

The second factor is the ratio of the fields in the probe beam and the main beam as they exit the second splitter (which we assume are matched, as discussed above). These factors are the squares of the $\bar{\eta}$ factors:

---

*The dithers on the test beam and (to a lesser extent) the dither mirror perturb the null and generate some transmitted energy. This transmission of course provides the source of the error signals in the local detector.

$$\eta_1 = \bar{\eta}_1^2 \qquad\qquad\qquad\qquad (2.4a)$$

$$\eta_2 = \bar{\eta}_2^2 \quad . \qquad\qquad\qquad\qquad (2.4b)$$

For lossless splitter, it follows that

$$\eta_1 + \eta_2 = \bar{\eta}_1^2 + \bar{\eta}_2^2 = 1 \qquad\qquad\qquad (2.5)$$

The efficiency of this system is difficult to replicate with the other approaches, However, these are arguments for operating the test probe beam at a second wavelength or at an offset frequency. The second wavelength must not be far separated from the main beam wavelength to ensure that its speckle patterns replicate those of the main beam. More specifically, if the power levels permit, one may advantageously substitute an acousto-optic modulator for the moving mirror phase modulation system of Figure 4. The probe beam is then up (or down) converted by a convenient frequency (say 1 MHz) and recombined with the main beam, as in the Figure 4 system. In this case, the up-converted beam is reflected and beats with the reflected main beam in the receiver detector to produce a 1-MHz output — the probe frequency. With this approach, control of the recombination path is not required, which simplifies the system. The main advantage is that the probe frequency will be sufficiently high to greatly exceed any dither frequency range available from present or future deformable mirrors. Thus, probe frequency contamination problems are avoided.

B.   HIGH-POWER IMPLEMENTATION OF ASPECT II SYSTEMS

This section illustrates possible approaches to high-power implementations of ASPECT systems. The objective is not so much to identify the "best" configuration as to illustrate the wide variety of possible

26

approaches. Thus, we select two quite different implementations. The first approach, illustrated in Figure 5, is a high-power equivalent of the basic system shown in Figure 4 with diffraction gratings on cooled metal mirrors substituting for the beam splitters and an acousto-optic frequency shifter substituting for the ASPECT (phase modulator) dither mirror (for higher bandwidth, not higher power). To match the interferometer beam sizes to both the deformable mirror and acousto-optic state-of-the-art sizes, we have included a beam reduction optics in the low power path. (We would include such a reduction even with a dither mirror approach since it reduces the size and boosts the resonance frequency of this mirror.) The interferometer as shown in not a balanced path system and is thus applicable only to a single line laser. It can, of course, be balanced by lengthening the upper path.

It is ackward (and expensive) to incorporate a pair of high-power diffraction gratings devoted exclusively to the ASPECT function (after the approach in Figure 5). Fortunately, one can often override or piggyback the ASPECT system on top of an existing grating or gratings system. Thus, no new gratings are required. One such approach is to piggyback the system on top of a MAST grating, illustrated in Figure 6(a). The normal function of the MAST grating is to extract for alignment an IR image of the target and a beam sample of the high-power beam at a common or near-common sensor point. The MAST system works best with polarized laser beams, as illustrated (because of the diffraction sensitivity to polarization). For our ASPECT piggyback system, it is also essential that the laser be polarized.

Figure 6(b) shows the basic MAST system with an ASPECT overlay. Briefly, the MAST grating splits out 1% of the HEL beam in the reflected order, encodes it with an ASPECT modulation, rotates its plane of polarization. The beam then reflects off the MAST grating with high efficiency and is transmitted to the target as illustrated. The ASPECT encoded beam and the main unmodulated beam are both reflected from the target and beat together in a detector to given an i.f. output that is

7772-56
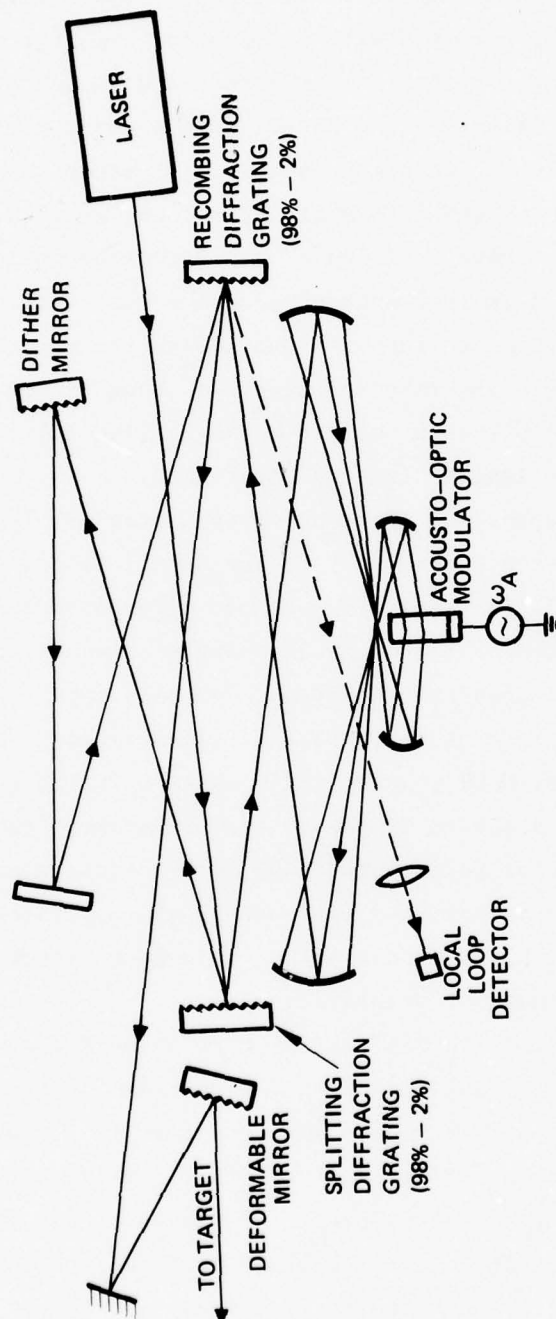
Figure 5. An ASPECT II optical train suitable for higher power level operation. The system is functionally the same as Figure 4 system except that an acousto-optic offset modulator substitutes for the piston mirror modulator of Figure 4.

28
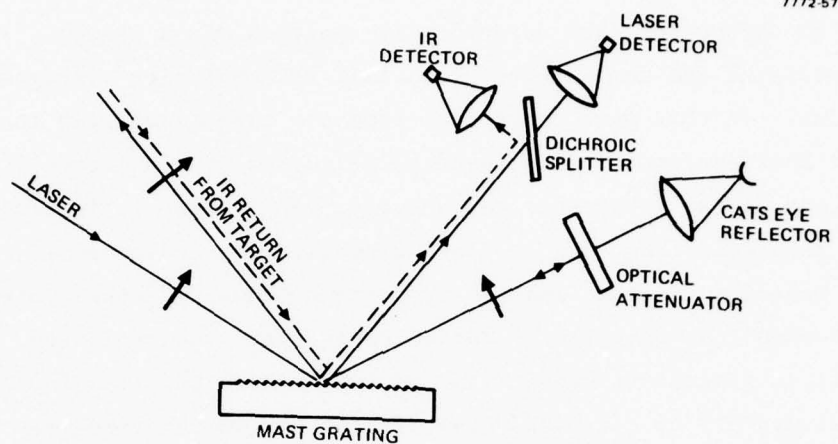
Figure 6(a).
The basic MAST grating system extracts samples of the laser
beam and IR return from the target for purposes of angular
alignment.
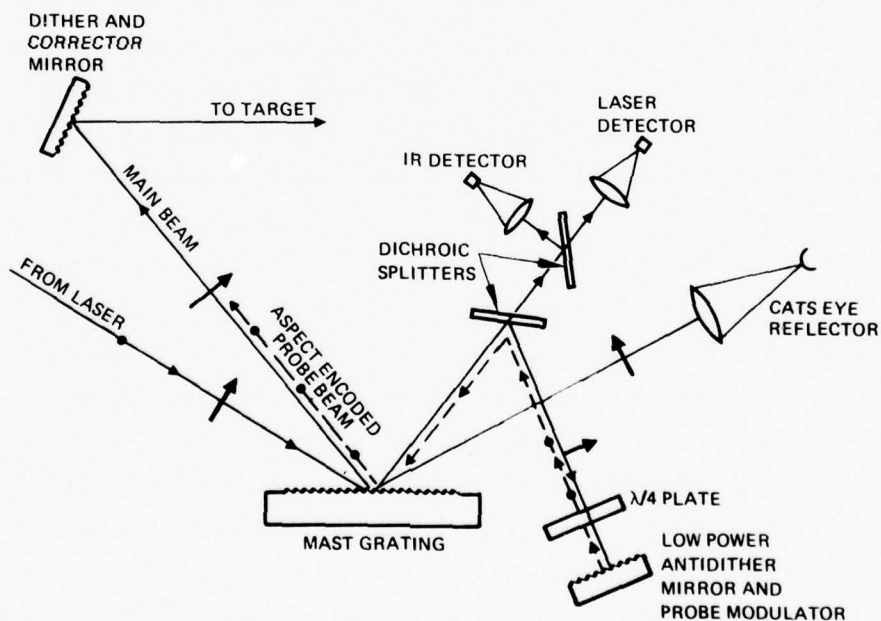
Figure 6(b).
An ASPECT II overlay on a MAST grating system. The anti-
dither mirror effectively removes the dither from the low
power arm of the interferometer. An additional high fre-
quency dither is applied to all elements in parallel to
modulate the probe beam.

29

the ASPECT probe signal. Since the modulated and unmodulated beams experience the same Doppler shift, no Doppler tracking or offset is required even though coherent detection is employed (in a sense).

The modulated and unmodulated beams exit the MAST with orthogonal polarizations. If they were to reflect from the target and pass through a collector aperture optics with these polarization states intact, they would not beat in the detector. Fortunately, many target reflecting structures depolarize the returns, including (1) recessed screws, (2) double bounce speculars, and (3) very rough areas. Further, even with single-pass (curved-surface) target reflectors, the reflected returns will in general be depolarized as they bounce back and forth on the metal mirrors of a typical beam director or in the receiver telescope.

With this approach, it is not feasible to add a dither mirror in the "upper leg" of the interferometer because it is not accessible. Therefore, as illustrated in Figure 6, the dither mirror and deformable mirror must be located either before or (better) after the MAST system (outside the interferometer). To avoid these problems, we added a low-power "anti-dither" mirror as a reflecting element in the ASPECT encoding path. The same mirror can have the ASPECT dither added to all actuators to achieve the ASPECT encoding. Of course, for high frequency encoding, an acousto-optic approach is also applicable to this system.

We require a MAST grating that is extremely efficient in diffraction of one polarization and reasonably efficient in reflection for the other polarization. Fortunately, this is a natural tendency for most designs. Figure 7 illustrates a theoretical prediction for a grating with idealized grooves (designed for 9.28 μm) in which all of the coupling efficiencies are 100%. Measurements on real gratings indicate that at least 75% efficiency is available for the second pass (rotated polarization) reflection of the modulated beam off of the MAST grating and that 98% (or better) efficiency is achievable for the main beam polarization.
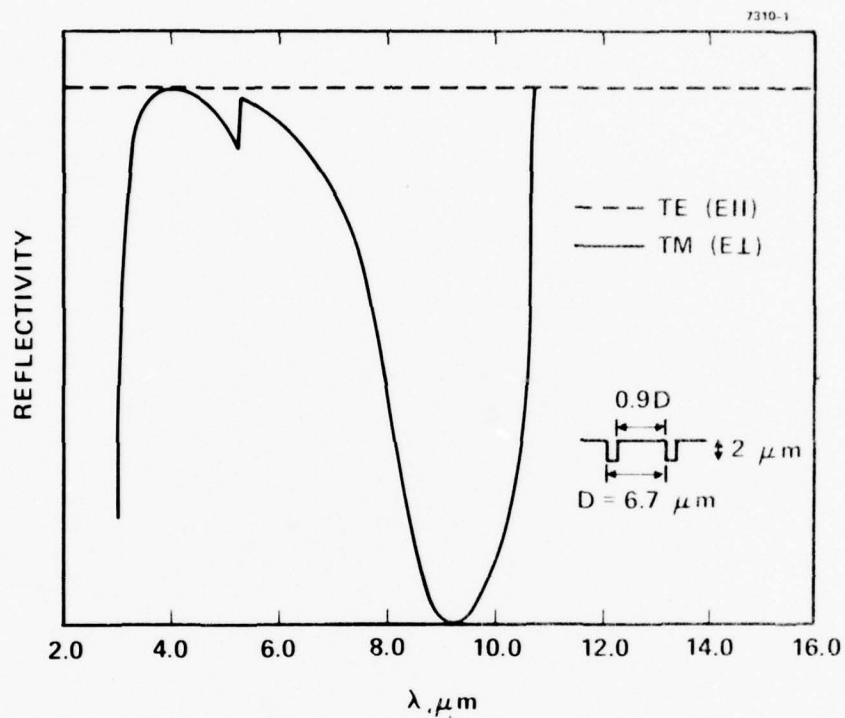
Figure 7. Theoretical performance of a MAST grating system designed for optimum performance at 9.28 μm. Each polarization is transmitted with 100% efficiency.

SECTION 3

SPECKLE INTERFERENCE IN ZONAL MULTIDITHER
COAT SYSTEMS

A. PROBLEM STATEMENT

The analysis presented in this section describes how speckle effects
alter COAT receiver illumination and the resultant photodetector current.
It shows that speckle is primarily a multiplicative phenomenon. That is
to say, the effect of speckle on the COAT receiver is to multiply the
normal COAT signal without speckle (i.e., a signal resulting from an
ideal point source target or gling) by a single temporal modulation func-
tion that can be determined from target surface characteristics and
target illumination. There is also additional additive noise from the
light reflected off of the target surface surrounding the glint. This
additive noise should be treated separately from speckle effects because
it fits more into the category of signal-to-noise problems and/or glint
hopping problems. It is always present and is not appreciably altered
by including speckle effects.

Consider a typical COAT transmitter aperture with an area that has
been divided into N elements or zones for the purpose of adjusting the
phase distribution of the outgoing optical field.[4-6] Referring to the
geometry shown in Figure 8, let $U_{on}(\vec{x}')$ be the incident complex scalar
field on the target plane from the nth element, where the vector $\vec{x}'$ is
the two-dimensional position vector in the target plane. The total
field $U_o(\vec{x}',t)$ is therefore just the sum of all the element fields:

$$U_o(\vec{x}', t) = \sum_{n=1}^{N} U_{on}(\vec{x}',t) \quad .$$ (3.1)

The phase distribution of the nth element field consists of a mean value
$\beta_n(\vec{x}',t)$ and a sinusoidal dither $\psi_n \sin(\omega_n t + \alpha_n)$, where ψ_n is the dither

33
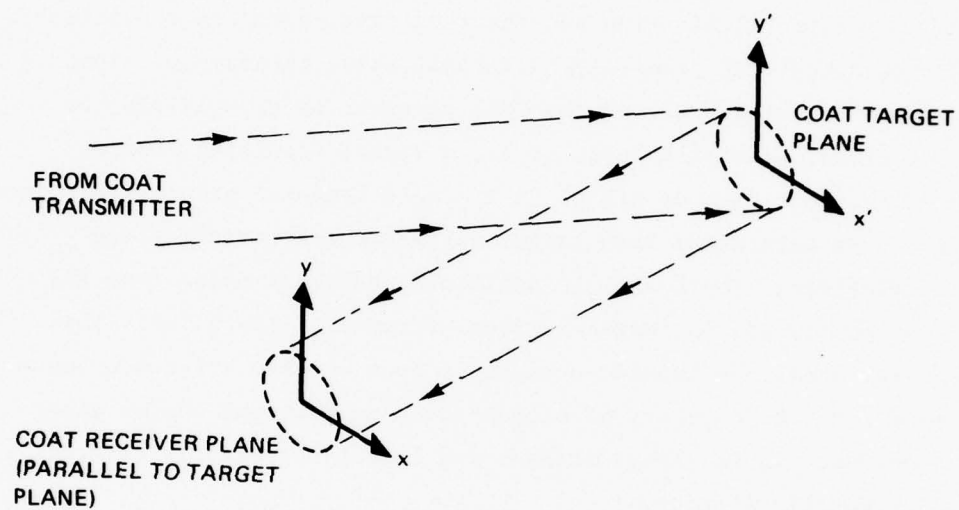
Figure 8. Definition of geometry.

amplitude in radians of wavelength, ω_n is the dither frequency, and α_n is an arbitrary phase. Thus, we can express the total field as

$$U_o(\vec{x},'t) = \sum_{n=1}^{N} V_{on}(\vec{x}') e^{i\left[\beta_n(\vec{x}',t) + \psi_n \sin(\omega_n t + \alpha_n)\right]} , \qquad (3.2)$$

where $V_{on}(\vec{x}')$ is a real-valued function representing the amplitude of the nth element field.

The target can be represented by a dimensionless complex reflectance function $\rho(\vec{x}')e^{i\phi(\vec{x}')}$ defined on the target plane, where $\phi(\vec{x}')$ and $\rho(\vec{x}')$ are real-valued functions with actual values or more conveniently, statistical properties that can be determined from the characteristics of the target surface. The field reflected from the target plane is just $U_o(\vec{x}',t)$ multiplied by the reflectance function. Assuming that the receiver plane is in the far field of the target plane, the reflected field can be propagated using the Frannhofer integral. The field at the receiver plane is given by

$$U_R(\vec{x},t) = \frac{e^{ikz} e^{i\frac{k}{2z} \vec{x} \cdot \vec{x}}}{i\lambda z} \int d^2x' \, U_o(\vec{x}',t)\rho(\vec{x}')e^{i\phi(\vec{x}')} e^{-i\frac{k}{z}(\vec{x} \cdot \vec{x}')},$$

$$(3.3)$$

where $\vec{x}$ is the two-dimensional position coordinate on the receiver plane, z is the distance from the target to the receiver, λ is the wavelength, and k is the wave number of the propagated light. The integral in Eq. 3.3 is easier to handle if we assume that the reflectance function is glint-like:

$$\rho(\vec{x}') \equiv \sum_{\ell} \delta (\vec{x}' - \vec{x}'_{\ell}) R_{\ell} , \qquad (3.4)$$

35

where R_ℓ is a real number with dimensions of area representing the reflectance of the infinitesimal area around the point $\vec{x}'_\ell$. This assumption is not a limitation because we can approximate any continuous distribution this way as accurately as we want. The receiver field becomes

$$U_R(\vec{x},t) =$$

$$\frac{e^{ikz} e^{i\frac{k}{2z}\vec{x}\cdot\vec{x}}}{i\lambda z} \sum_\ell R_\ell e^{i\phi(\vec{x}'_\ell)} \sum_{n=1}^{N} V_{on}(\vec{x}'_\ell) e^{i\left[\beta_n(\vec{x}_\ell,t)+ \psi_n \sin(\omega_n t+\alpha_n)\right]} e^{i\frac{k}{z}(\vec{x}\cdot\vec{x}'_\ell)} , \tag{3.5}$$

where $\phi(\vec{x}'_\ell)$ is referred to simply as ϕ_ℓ. The receiver intensity $I_R(\vec{x},t)$ is given by the absolute square of Eq. 3.5:

$$I_R(\vec{x},t) \equiv U_R(\vec{x},t)\ U_R^*(\vec{x},t)$$

$$= \frac{1}{(\lambda z)^2} \sum_\ell \sum_p R_\ell R_p\ e^{i\left[(\phi_\ell-\phi_p)\right]} e^{i\frac{k}{z}\vec{x}\cdot(\vec{x}'_p - \vec{x}'_\ell)} \tag{3.6}$$

$$\cdot \sum_{n=1}^{N} \sum_{m=1}^{N} V_{on}(\vec{x}'_\ell)\ V_{om}(\vec{x}'_p) e^{i\left[\beta_n(\vec{x}'_\ell,t) -\beta_m(\vec{x}'_p,t)\right]}$$

$$\cdot e^{i\left[\psi_n \sin(\omega_n t+\alpha_n) - \psi_m \sin(\omega_m t+\alpha_m)\right]}$$

Eq. 3.6 contains all the information needed to understand the effects of speckle on zonal multimode COAT systems. The information is very general, however, making most of its obscure. Therefore, some special cases are discussed in the following sections.

Eq. 3.6 can also be expressed in a form more compatible with Eq. 2.2 by separating the summations over n and m into three terms, one associated

36

with a specific channel (i.e., $n = m = \nu$), one associated with the double summation over the remaining channels (reduced array), and one containing the cross coupling terms between the two. Through a lengthy derivation, the COAT photo-detector current can be shown to be expressible as in Eq. 2.2. Rather than do this, however, it is easier to simply assume a reduced array field, formed from all channels except channel ν, beating against the single element field associated with channel ν. This approach is taken in Section 3.E.

B. CASE 1 — POINT SOURCE

In much of the early COAT work, before speckle was recognized as a problem, the target was idealized as a point source. With this assumption, Eq. 3.6 reduces to the same expression used in those early analyses. Since there is only one glint, the summations over ℓ and p reduce to a single term, and there is no need to explicitly show the spatial dependence of various functions of position in the target plane. The receiver intensity becomes

$$I_R(t) = \frac{R^2}{(\lambda z)^2} \sum_{n=1}^{N} \sum_{m=1}^{N} V_{on} V_{om} \, e^{i[\beta_n(t) - \beta_n(t)]}$$

$$e^{i[\psi_n \sin(\omega_n t + \alpha_n) - \psi_m \sin(\omega_m t + \alpha_m)]} \quad , \qquad (3.7)$$

where R is the single glint reflectance amplitude. With the additional assumptions that all the dither amplitudes ψ_n, were equal, and all the field amplitudes V_{om}, were equal, Eq. 3.7 has been the starting point in much of the earlier COAT servo analyses. Note that the receiver intensity is only a function of time and that there is no spatial variation in the receiver plane.

If we expand the second exponential in the summation of Eq. 3.7 into a Fourier-Bessel series, the receiver intensity can be expressed as the sum

37

of a mean value $I_M(t)$ plus spectral components at all the dither frequencies
and their sum and difference frequencies. This is done in Eq. 3.8, except
that only the dither components and those at twice the dither frequencies
are shown. Higher harmonics are neligible at the small values of ψ_n
(typically, about 0.3 to 0.4 rad) used in most COAT systems. Thus, the
receiver plane intensity $I_g(t)$ resulting from a single glint can be expressed
as:

$$
I_g(t) \equiv \frac{R^2}{(\lambda z)^2} \left\{ I_M(t) + \sum_{n=1}^{N} [A_n \sin(\omega_n t + \alpha_n) \right.
$$

$$
\left. + B_n \cos(2\omega_n t + 2\alpha_n)] + \text{higher harmonics} \right\} , \qquad (3.8)
$$

where

$$
I_m(t) \equiv \sum_{n=1}^{N} V_{on}^2 + \sum_{\substack{n=1 \\ n \neq m}}^{N} \sum_{m=1}^{N} J_o(\psi_n) J_o(\psi_m) \cos [\beta_n(t) - \beta_m(t)]
$$

$$
\qquad (3.9)
$$

$$
A_n \equiv -4 J_1(\psi_n) V_{on} \sum_{\substack{m=1 \\ m \neq n}}^{N} V_{om} J_o(\psi_m) \sin [\beta_n(t) - \beta_m(t)] \qquad (3.10)
$$

$$
B_n \equiv 4 J_2(\psi_n) V_{on} \sum_{\substack{m=1 \\ m \neq n}}^{N} V_{om} J_o(\psi_m) \cos [\beta_n(t) - \beta_m(t)] . \qquad (3.11)
$$

C. CASE 2 — SMALL CLUSTER OF GLINTS

We now consider a small cluster of glints located within an area that is small compared with the diffraction-limited spot size of the total COAT transmitter aperture. Therefore, it is reasonable to assume that the illumination field amplitude distribution $V_{on}(\vec{x}')$ and average phase distribution $\beta_n(\vec{x}',t)$ from a single element (with an area much smaller than the total transmitter aperture) are fairly constant over this target plane area. This assumption becomes more and more accurate as the number of elements increases and the aperture area in the transmitter plane associated with each decreases. Thus, we ignore the spatial dependence of these functions and write them as constants, allowing us to rewrite Eq. 3.6 as the product of a glint-like return multiplied by a spatial modulation function $M_s(\vec{x})$ due to speckle:

$$I_R(\vec{x},t) = \frac{1}{(\lambda z)^2} \left\{ \sum_\ell \sum_p R_\ell R_p e^{i\left[(\phi_\ell - \phi_p)\right]} e^{i\frac{k}{z}\vec{x}\cdot(\vec{x}_p' - \vec{x}_\ell')} \right\}$$

$$\cdot \left\{ \sum_{n=1}^{N} \sum_{m=1}^{N} V_{on} V_{om} e^{i[\beta_n(t)-\beta_m(t)]} \right\}$$

$$e^{i[\psi_n \sin(\omega_n t+\alpha_n) - \psi_m \sin(\omega_m t+\alpha_m)]}$$

$$= \sigma \, \overline{M}_s(\vec{x}) \, I_g(t), \tag{3.12}$$

where σ is the normalization constant $(\lambda z)^{-2}$ dependent on distance between the target and receiver, and $\overline{M}_s(\vec{x})$ is just the factor in the first brackets. This expression is the same as Eq. 3.8 in its time

dependence, but the spatial variation in the receiver plane is no longer constant. Since $\overline{M}_s(\vec{x})$ can be seen by inspection to be real, it can be expressed as

$$\overline{M}_s(\vec{x}) = \sum_{\ell} \sum_{p} R_{\ell} R_p \cos (K_{\ell p} \cdot \vec{x} + \phi_{\ell p}) , \tag{3.13}$$

where

$$\vec{K}_{\ell p} \equiv \frac{k}{z} (\vec{x}'_p - \vec{x}'_{\ell}), \tag{3.14}$$

$$\phi_{\ell p} \equiv \phi_{\ell} - \phi_p . \tag{3.15}$$

The spatial frequency distribution in this speckle pattern is directly proportional to the spacing between pairs of glints, and the amplitude at each frequency is proportional to the product of the reflectance at each glint. *The maximum spatial frequency for this case would be*

$$K_{max} = \frac{k}{z} \cdot \text{(largest glint separation)}.$$

Goldfischer,[7] Goodman,[8,9] George,[10] and Erdman and Gellert[11] have done extensive studies which characterize speckle patterns in much greater depth than these cursory comments.

As the target moves, the spatial modulations also move past the receiver, causing temporal modulation of the glint-like reflected intensity. Since the electric signal S_o from the photodetector receiver is proportional to the average intensity incident on it, we can write

$$S_o = K M_s(t) I_g(t), \tag{3.16}$$

40

where K is a proportionality constant, and $M_s(t)$ is the aperture averaged temporal modulation function resulting from the motion of $\overline{M}_s(\vec{x})$ past the receiver. If this temporal modulation contains a significant amount of energy at or near the COAT dither frequencies, then the resulting adaptive performance can be degraded.[1,2,12]

It is interesting to examine the effect of aperture averaging associated with this type of spatial frequency distribution. This can be done very simply if we asume a shared aperture of diameter D_{TX} for the COAT transmitter and receiver. A diffraction-limited spot size, therefore, has a null-to-null diameter D_s that is approximately given by

$$D_s \simeq 2 \frac{\lambda z}{D_{TX}} \quad . \tag{3.17}$$

In the case we have considered, the largest glint separation, $\Delta x = \left| \vec{x}'_p - \vec{x}'_\ell \right|$, is small compared to D_s. Therefore, the spatial wavelengths (i.e., $\Lambda \equiv \frac{2\pi}{K}$) associated with this speckle pattern are all much longer than the receiver diameter:

$$\Lambda = \frac{\lambda z}{\Delta x} >> \frac{\lambda z}{D_s} \simeq \frac{D_{TX}}{2} \tag{3.18}$$

Consequently, there will be very little aperture averaging.

As the glint spacing increases to a length comparable to a diffraction-limited spot diameter, higher frequencies or shorter spatial wavelengths appear in the speckle pattern.

The greater the spacing between two arbitrary glints located at $\vec{x}'_\ell$ and $\vec{x}'_p$, the higher the probability that the phases $\beta_n(\vec{x}'_\ell)$ and $\beta_n(\vec{x}'_p)$ associated with array element n are appreciably different. Since the equality of these phases was a crucial assumption in the derivation of Eq. 3.12, the validity of that equation becomes suspect. On the other hand, as the spacing increases, so does the amount of aperture averaging.

41

For spacings on the order of half a spot diameter and larger, the attenuation due to aperture averaging is virtually total. In addition, since the total amplitude at a given spatial frequency is proportional to the number of glint pairs having a separation corresponding to that frequency (as given by Eq. 3.14), the amplitudes at spatial frequencies associated with larger separations of glint pairs are smaller than with those associated with smaller separations because of the statistically smaller number of possible pairs. Thus, Eq. 3.12 may still be approximately correct even when the small cluster of glints is no longer confined to an area that is small compared with a diffraction-limited spot. This special case is discussed in more detail in Section 3.E.

D.   CASE 3 — SMALL CLUSTER OF STRONG GLINTS PLUS A DIFFUSE BACKGROUND

We now proceed to a very general case in a hypothetical COAT target scenario. Referring to Figure 9, let us represent the target by a reflectance function consisting of a small cluster of strong glints in an area that is small compared with a diffraction-limited spot size; the remaining area of the target plane is covered by a uniform distribution of weaker glints having random phases (i.e., a diffuse reflecting surface). To calculate receiver illumination, it is convenient to separate the summations over the target plane in Eq. 3.6 into the sum of two separate summations: one over the small cluster of strong glints (which we identify by a plain summation sign as before) and one over the remaining glints (which we identify by a prime over the summation sing). As done in the previous cases, we will drop the spatial references to the amplitude and phase distributions of the target illumination functions on the region where the strong glints are clustered. The receiver illumination from Eq. 3.6 becomes

WEAKER GLINTS OVER
REMAINING AREA
(PRIMED SUMMATION Σ')

STRONG GLINTS OVER AN AREA SMALL
COMPARED TO A DIFFRACTION
LIMITED SPOT (REGULAR
SUMMATION Σ)
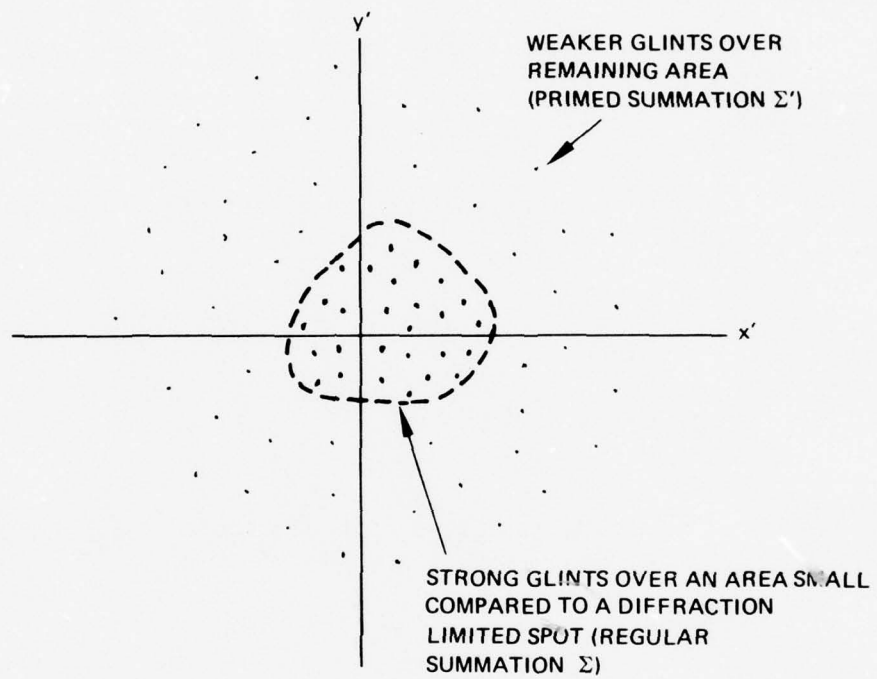
Figure 9. Glint distribution in target plane correspond-
ing to case 3.

$$
I_R(\vec{x},t) = \frac{1}{(\lambda z)^2} \left\{ \sum_\ell \sum_p R_\ell R_p e^{i[(\phi_\ell - \phi_p)]} e^{i\frac{k}{z}\vec{x}\cdot(\vec{x}_p' - \vec{x}_\ell')} \right\}
$$

$$
\cdot \left\{ \sum_{n=1}^{N} \sum_{m=1}^{N} V_{on} V_{om} e^{i[\beta_n(t) - \beta_m(t)]} e^{i[\psi_n \sin(\omega_n t + \alpha_n) - \psi_m \sin(\omega_m t + \alpha_m)]} \right\}
$$

$$
+ \left\{ \frac{1}{(\lambda z)^2} \sum_\ell {\sum_p}' R_\ell R_p e^{i[(\phi_\ell - \phi_p)]} e^{i\frac{k}{z}\vec{x}\cdot(\vec{x}_p' - \vec{x}_\ell')} \right.
$$

$$
\cdot \sum_{n=1}^{N} \sum_{m=1}^{N} V_{on} V_{om}(\vec{x}_p') e^{i[\beta_n(t) - \beta_m(\vec{x}_p',t)]} e^{i[\psi_n \sin(\omega_n t + \alpha_n) - \psi_m \sin(\omega_m t + \alpha_m)]} \left. \right\}
$$

$$
+ \left\{ \frac{1}{(\lambda z)^2} {\sum_\ell}' \sum_p R_\ell R_p e^{i[(\phi_\ell - \phi_p)]} e^{i\frac{k}{z}\vec{x}\cdot(\vec{x}_p' - \vec{x}_\ell')} \right.
$$

$$
\cdot \sum_{n=1}^{N} \sum_{m=1}^{N} V_{on}(\vec{x}') V_{om} e^{i[\beta_n(\vec{x}',t) - \beta_m(t)]} e^{i[\psi_n \sin(\omega_n t + \alpha_n) - \psi_m \sin(\omega_m t + \alpha_m)]} \left. \right\}
$$

$$
+ \left\{ \frac{1}{(\lambda z)^2} {\sum_\ell}' {\sum_p}' R_\ell R_p e^{i[(\phi_\ell - \phi_p)]} e^{i\frac{k}{z}\vec{x}\cdot(\vec{x}_p' - \vec{x}_\ell')} \right.
$$

$$
\cdot \sum_{n=1}^{N} \sum_{m=1}^{N} V_{on}(\vec{x}_\ell') V_{om}(\vec{x}_p') e^{i[\beta_n(\vec{x}_\ell',t) - \beta_m(\vec{x}_p',t)]}
$$

$$
e^{i[\psi_n \sin(\omega_n t + \alpha_n) - \psi_m \sin(\omega_m t + \alpha_m)]} \left. \right\}
$$

$$
= \sigma \overline{M}_s(\vec{x}) I_g(t) + \text{Addative Noise} . \tag{3.19}
$$

44

The first term in Eq. 3.19 is identical to Eq. 3.12. The remaining three terms may be regarded as additive noise. This noise may or may not be a problem depending on its relative strength compared to the first, or glint, term. For example, if the background noise is comparable in magnitude to the glint return, the COAT system could fail to converge, with or without the added complication of speckle interference. This kind of problem would generally be remedied by a restricted field of view or IMPACT[16] system. Such a remedy is completely compatible with the speckle problem because it eliminates the additive noise and again allows us to characterize the speckle interference as simply a multiplicative noise.

The distribution of spatial frequencies in the speckle terms of Eq. 3.19 is still dependent on spacing between individual glints (i.e., $\vec{x}_p - \vec{x}_\ell$). Thus, the arguments presented in Section 3.C, concerning aperture averaging still hold. Namely, the speckle pattern associated with glints spaced on the order of half a diffraction-limited array spot diameter or larger will be eliminated by aperture averaging. The critical case, which is considered in Section 3.E, occurs when there are strong glints that are spaced slightly closer than half a diffraction-limited spot diameter and thus are close enough together to avoid complete aperture averaging.

E.   CASE 4 — M GLINTS DISTRIBUTED OVER THE WIDTH OF AN ARRAY PATTERN

As shown by Eq. 3.6, the general result for an N-element array reflecting off of M scattering centers is quite complex. This section considers a simpler case, a system that is operating near convergence with small dither amplitudes ψ_o, that are the same in each channel. We consider the effect of speckle jamming on the dc terms and on the dither signals and show that the resultant speckle multipliers may be significantly different.

More specifically, we let all N-1 elements except for element n be reasonably well phased and consider the beat between the received field from this element and the ensemble receiver field from the remaining N-1 elements, which we call the reduced array. Such a viewpoint describes

45

the key behavior of multidither systems, even if the other elements are not well phased (for point targets).[13] Since we take N to be reasonably large (N > 20), the converged target plane field from the N-1 elements is very close to that of the full array. For example, with square arrays of square elements, the reduced-array target-plane field would be (nearly) a two-dimensional sinc-like function with amplitude and width that are being perturbed in time by a small percentage as a consequence of the small dithers. Explicitly, we take the field in the target plane $U_o(\vec{x}', t)$, decomposed into the two field components just discussed, which gives

$$U_o(\vec{x}', t) = U_{ra}(\vec{x}') + U_e(\vec{x}') \exp\left[i\,\beta_n + \psi_o \sin(\omega_n t) + \frac{k}{z}(\vec{x}_n'' \cdot \vec{x}')\right],$$

(3.20)

where $U_{ra}(\vec{x}')$ is the reduced array target plane field,

$$U_{ra}(\vec{x}') = \left|U_{ra}(\vec{x}')\right| \exp(i\beta_{ra}) \quad,$$

(3.21)

and β_{ra} is the average phase of the reduced array.* The parameter $U_e(\vec{x}')$ is the field pattern from the nth element and $\vec{x}_n''$ is the coordinate of the center of the nth element.

Each of the field components in Eq. 3.20 illuminates a (possibly) large number of scattering centers, which we have taken to be "glint-like" δ functions as described in Eq. 3.4. Each component generates a speckle field which we call

$$U_{Rra}(x) = \left|U_{Ra}(x)\right| e^{i(\phi_{ra} + \beta_{ra})}$$

(3.23a)

$$U_{Re}(x) = \left|U_{Re}(x)\right| e^{i(\phi_e + \beta_n + \psi_o \sin \omega_n t)}$$

(3.23b)

---

*It is easy to show that the dithers produce only extremely small perturbations in the average phase.

Each of these speckle patterns contains exactly the same spatial frequency components since the sources that created each one have exactly the same locations. However, each frequency component is in general weighted differently for two reasons: (1) the illumination fields from the reduced array and the nth element have appreciably different widths, and (2) the $\frac{k}{z}$ ($\vec{x}''_n \cdot \vec{x}'$) exponent in Eq. 3.20 produces a nonuniform phase in the element illumination fields (except for a central element).

If we sum these fields to generate the total field at the receiver plane, its squared magnitude is

$$I_R(\vec{x},t) = |U_{Rra} + U_{Re}|^2$$

$$= |U_{Rra}(\vec{x})|^2 + |U_{Re}(\vec{x})|^2$$

$$+ 2|U_{Rra}(\vec{x})| |U_{re}(\vec{x})| \cos [\phi_{ra}(\vec{x}) - \phi_e(\vec{x})$$

$$+ \beta_{ra} - \beta_n - \psi_o \sin \omega_n] \qquad (3.24)$$

The dither-modulation component becomes explicit if Eq. 3.24 is rewritten in the form

$$I_R(\vec{x},t) \doteq |U_{Rra}(\vec{x})|^2 + |U_{Re}(\vec{x})|^2$$

$$+ 2J_o(\psi_o) |U_{Rra}(\vec{x})| |U_{re}(\vec{x})| \cos [\phi_{ra}(\vec{x}) - \phi_e(\vec{x})$$

$$+ \beta_{ra} - \beta_n] - 2J_1(\psi_o) |U_{Rra}(\vec{x}')||U_{Re}(\vec{x}')|$$

$$\sin (\phi_{RA} - \phi_e + \beta_{ra} - \beta_m) \sin \omega_n t \qquad (3.25)$$

The "dc" (unmodulated) and ac (modulated) terms in Eq. 3.25 are given to an excellent approximation as

$$I_{dc}(\vec{x}) \doteq [|U_{Rra}(\vec{x})| + |U_{Re}(\vec{x})|]^2 \doteq |U_{Rra}(\vec{x})|^2 \qquad (3.26a)$$

$$I_{ac}(\vec{x},t) \doteq 2J_o(\psi_o) |U_{Rra}(\vec{x})| |U_{Re}(\vec{x})| \sin(\phi_{ra} - \phi_e + \beta_{ra} - \beta_n)$$

$$(3.26b)$$

Eq. 3.25 corresponds to a static target. As the target rotates, fields $|U_{Rra}(\vec{x})|$, $|U_{Re}(\vec{x})|$, and $\phi_{ra}(\vec{x}) - \phi_e(\vec{x})$ translate past the receiver aperture, thus generating a corresponding time varying output in the receiver detector. Since, in general, each of the coefficients in Eq. 3.25 has a different spatial frequency distribution, each term produces a different temporal frequency modulation in the dc and ac detector output terms of Eq. 3.26.

If the glint distribution is very tightly packed in comparison with the width of the reduced array pattern, then both $U_{ra}(\vec{x}')$ and $U_e(\vec{x}')$ essentially will illuminate the glints uniformly and therefore

$$|U_{Rra}(\vec{x}'')| = K |U_{Re}(\vec{x})| \quad . \qquad (3.27)$$

In other words, within a constant, K, the two multiplicative speckle patterns are essentially equal and as described in Section 3.C there exists a single speckle multiplier:

$$\overline{M}_s(\vec{x}) = |U_{Re}(\vec{x})|^2 \quad . \qquad (3.28)$$

On the other hand, if some of the major glints are located on the intermediate skirts of the reduced array pattern, the multipliers may be appreciably different. To explore these effects quantitatively, we will consider a specific example. The target will consist of three coplanar glints, one at the origin and two symmetrically displaced from it by a distance x'_g in the target plane. The glint magnitudes are 1, ρ, and ρ, as illustrated in Figure 10(a). The reduced-array and element field components in the receiver plane are thus

48

$$|U_{Rra}| = P[U_{ra}(0) + \rho U_{ra}(x_g') \cos(\frac{kx_g'x}{z})] \qquad (3.29a)$$

$$|U_{Re}| = P[U_e(0) + \rho U_e(x_g') \cos(\frac{kx_g'x}{z} + \Omega)], \qquad (3.29b)$$

where P is a propagation factor, and Ω is a phase factor stemming from the possible wavefront tilt in the element field illuminating the glints (after Eq. 3.20). Explicitly,

$$\Omega = \frac{k \vec{x}_{on}'' \cdot \vec{x}_g'}{z} \qquad , \qquad (3.29c)$$

where $\vec{x}_{on}''$ is the central position of the nth element in the array. From here on, we consider the most favorable case where $\vec{x}_{on}''$ is zero (a central element). Thus, the spatial frequency distribution in both components is a constant plus a single (cosine) frequency component. The spatial (fundamental) modulation coefficient in these two components are defined as

$$F_{Rra} \approx \frac{\rho U_{ra}(x_g')}{U_{ra}(0)} \qquad (3.30a)$$

$$F_{Re} \approx \frac{\rho U_e(x_g')}{U_e(0)} \qquad . \qquad (3.30b)$$

The spatial (fundamental) modulation coefficient in the dc and ac components of Eqs. 3.26a and 3.26b is thus (approximately) for moderate to small ρ,

$$F_{Rdc} \doteq \frac{2\rho U_{ra}(x_g')}{U_{ra}(0)} \qquad (3.31a)$$

$$F_{Rac} \doteq \rho \left[\frac{U_{ra}(x_g')}{U_{ra}(0)} + \frac{U_e(x_g')}{U_e(0)} \right] \qquad (3.31b)$$

49

The modulation coefficients of Eqs. 3.31a and 3.31b are not generally the same. To give a specific illustration, consider a square array of 25 square elements such that the reduced array patterns and element patterns are, for good convergence on all other elements,

$$U_{ra}(x') \doteq 4.8H \frac{\sin[5\theta(x')]}{\theta(x')} \tag{3.32a}$$

$$U_e(x') = H \frac{\sin[\theta(x')]}{\theta(x')} = H \text{sinc}[\theta(x')] , \tag{3.32b}$$

where

$$\theta(x') = \frac{1}{2} \frac{k}{z} (x''_e \cdot x') = \frac{\Pi}{5}(\frac{x'}{x_{ra}}) \tag{3.32c}$$

and where x''_e is the width of an element, and x'_{ra} is the reduced array beamwidth* in the target plane. The parameter H is another propagation constant, which we do not require in explicit form.

For this particular case, Eq. 3.31 gives

$$F_{Rdc} = 2\rho \text{ sinc}\left[\Pi(\frac{x'_g}{x_{ra}})\right] \tag{3.33a}$$

$$F_{Rac} = \rho \left\{ \text{sinc}\left[\Pi(\frac{x'_g}{x_{ra}})\right] + \text{sinc}\left[\frac{\Pi}{5}(\frac{x'_g}{x_{ra}})\right] \right\} . \tag{3.33b}$$

These spatial modulation coefficients are translated into temporal coefficients by the scan of the spatial pattern past the aperture. However, the filtering action of the aperture reduces the associated temporal modulation coefficients (as discussed in Section 3.E and 3.D), which become

---

* Defined as half the null-to-null spacing.

50

$$F_{Rdc} = 2W_a \, \rho \, \text{sinc}[\Pi(\frac{x_g'}{x_{ra}})] \qquad\qquad (3.34a)$$

$$F_{Rad} = W_a \, \rho \, \{\text{sinc}\,[\Pi(\frac{x_g'}{x_{ra}})] + \text{sinc}\,[\frac{\Pi}{5}(\frac{x_g'}{x_{ra}})]\}, \qquad (3.34b)$$

where W_a, the aperture weighting or filtering factor, is

$$W_a = \text{sinc}(k\,\frac{x_g'}{z}\,x_r) \quad , \qquad\qquad (3.35)$$

and $2x_r$ is width of the receive aperture (assuming a square aperture).

For the special (but typical) case where the receiver aperature matches the transmitting aperature ($2x_r = 5x_e''$), Eq. 3.35 becomes

$$W_a = \text{sinc}\,[\Pi(\frac{x_g'}{x_{ra}})] \quad . \qquad\qquad (3.36)$$

If we estimate the time-varying speckle modulation from the ac components (as given by an ASPECT I estimation system, for example) and divide through by this estimation, the residual (fundamental) modulation in the ASPECT-corrected dc term is given by the ratio

$$R = \frac{1 + 2W_a \, \rho \, \text{sinc}\,[\Pi(\frac{x_g'}{x_{ra}})]\,\sin(\omega_m t)}{1 + W_a \, \rho\,\{\text{sinc}\,[\Pi(\frac{x_g'}{x_{ra}})] + \text{sinc}[\frac{\Pi}{5}(\frac{x_g'}{x_{ra}})]\}\,\sin(\omega_m t)}$$

$$\doteq 1 + W_a \, \rho \, \{\text{sinc}[\Pi(\frac{x_g'}{x_{ra}})] - \text{sinc}[\frac{\Pi}{5}(\frac{x_g'}{x_{ra}})]\}\sin(\omega_m t), \qquad (3.37)$$

where the second form of Eq. 3.37 is valid for reasonably small values of $W_a \rho$. For the matched receive aperture of Eq. 3.36, the residual modulation becomes

$$M_{RESID} \doteq \rho \left\{ \text{sinc}^2[\Pi(\frac{x'_g}{x_{ra}})] - \text{sinc}[\Pi(\frac{x'_g}{x_{rs}})] \, \text{sinc}[\frac{\Pi}{5}(\frac{x'_g}{x_{ra}})] \right\} \sin(\omega_m t). \quad (3.38)$$

As illustrated in Figure 10(b), there is no residual modulation for small glint spacings since the two components in Eq. 3.38 nearly cancel; similarly, both components become small for widely spaced glints. The maximum problem occurs at a glint-spacing to beamwdith ratio of about 0.6.

Although the analysis up to this point has considered only array states near convergence, we have also examined a limited number of special cases for arrays in a general state of convergence and have found the same general conclusions to be true. There are the same three basic types of speckle interference previously discussed. Second, the multiplicative speckle noise is, in general, different for the dc and ac components in the detector output. Third, if the major target glints or reflectivity elements are concentrated within a region which is small compared to the overall (converged) beamwidth, the effect of the differences in speckle noise is negligible.
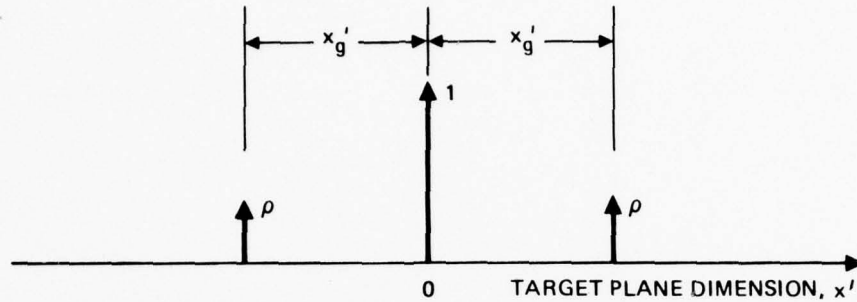
Figure 10(a).   Test case of three glints.   The array and
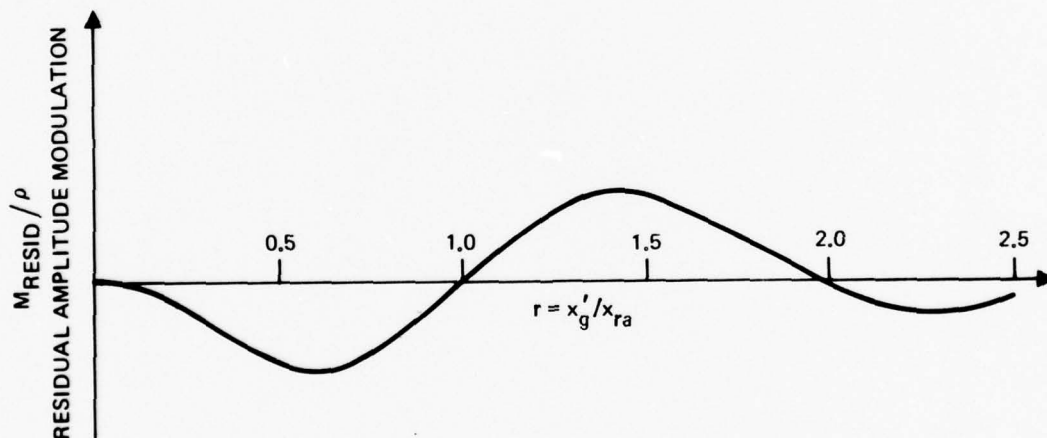element patterns center on x' = 0.

Figure 10(b).   Residual ASPECT speckle modulation (on dc term) for three
glint system above, as a function of glint spacing to
converged array beamwidth.

53

SECTION 4

AN ANALYSIS OF ASPECT II

A. GENERAL DESCRIPTION

This section describes how an ASPECT II system estimates the speckle modulation function $M_s(t)$ and cancels out the speckle interference. For the remainder of this section, we drop the designation "II" and simply refer to ASPECT. Consider the schematic of a COAT/ASPECT system in Figure 11. A small fraction* η_2 of the total field from a COAT laser beam is split off into a secondary beam and is combined with the remaining fraction η_1, in the principal beam, with the combined beam proceeding through the usual COAT optics. Each element or zone in the principal beam is tagged with a dither frequency, which is then synchronously detected and processed electronically to generate phase corrections at each zone for the entire beam.[4-6] The secondary beam is piston dithered at a frequency ω_A, which is substantially higher than the highest COAT dither frequency, and with an amplitude of ψ_A radians of wavelength. The beams are then combined in phase ** and propagated to the target. Following the development of the previous section, we write the incident field on the target plane as a sum of the N-element fields that make up each of these beams:

$$U_o(\vec{x}',t) \equiv \eta_1 \sum_{n=1}^{N} V_{on}(\vec{x}') e^{i\Gamma_n(\vec{x}',t)}$$

$$+ \eta_2 \sum_{n=1}^{N} V_{on}(\vec{x}') e^{i\bar{\Gamma}_n(\vec{x}',t)} . \qquad (4.1)$$

---

*
The power split in one of the beam splitters is thus in the ratio of η_2 to η_1, after the discussion in Section 2.

**
By "in phase" we mean the average path length of the two beams, excluding dither variations, differ by an integral number of path lengths.

ASPECT PISTON
DITHER MIRROR
ω_S

COAT
CORRECTOR
MIRROR

COAT
DITHER
MIRROR

η_2

COAT
LASER TX

η_1

TO
TARGET

PHASE
CORRECTION
SIGNALS

DITHER
SIGNALS

COAT
ELECTRONICS

LIMITER

LPF

ASPECT
ESTIMATOR

COAT
PHOTODETECTOR
RX

$K_1 M_s(t)$

AGC

÷

LPF

$S_0 = K_0 M_s(t) I_g(t)$

TARGET
RETURN

$$1 + \frac{\delta I(t)}{\langle I_g \rangle} + \left[\frac{\delta M_s(t)}{\langle M_s \rangle} + \epsilon(t) \right]$$
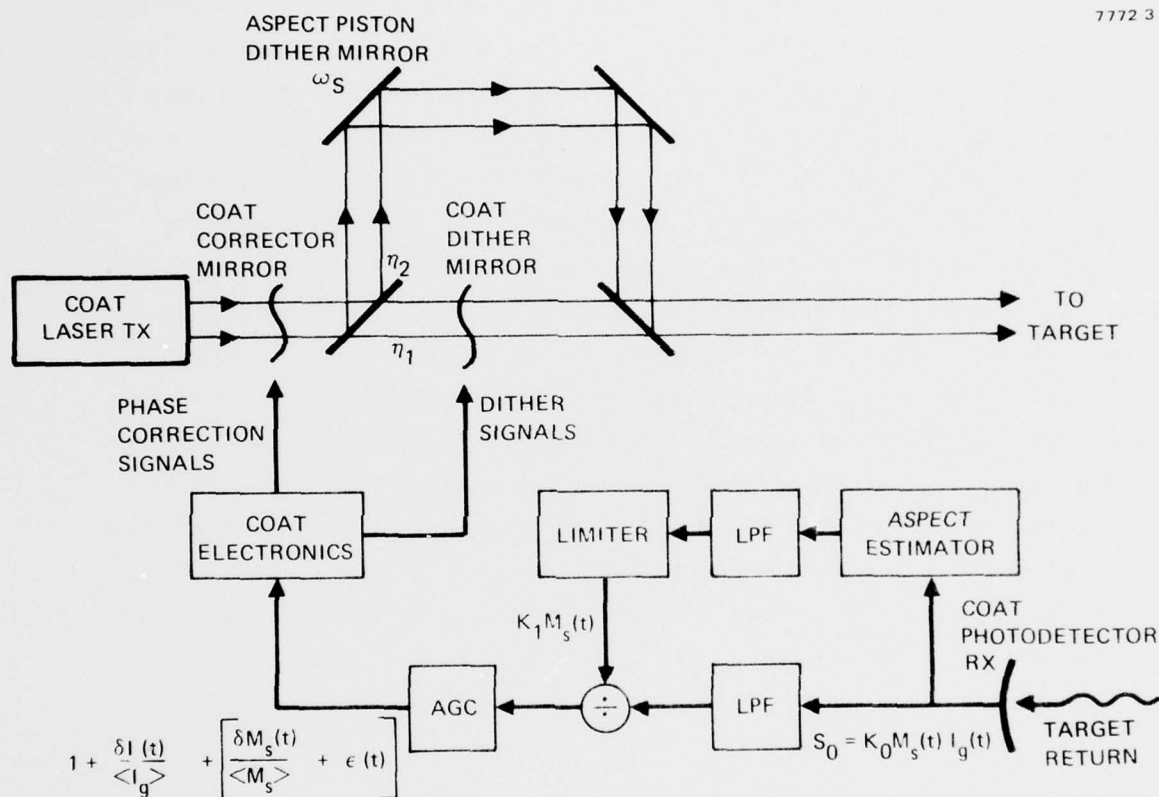
Figure 11.   Schematic of a COAT/ASPECT optical system.

56

The amplitude distribution $V_{on}(\vec{x}')$ associated with each element field is the same as in Section 3, but the phase distributions, $\Gamma_n(\vec{x}',t)$ and $\bar{\Gamma}_n(\vec{x}',t)$, have different dither components. In the principal beam, represented by the first summation in Eq. 4.1, the phase distribution is the same as the typical zonal multidither COAT system of Section 3:

$$\Gamma_n \equiv \beta_n(\vec{x},t) + \psi_o \sin(\omega_n t + \alpha_n), \qquad (4.2)$$

where, for simplicity, the dither amplitude ψ_o is the same for all COAT channels. The phase distributions in the secondary beam have the same mean values as the primary beam, but only one piston dither amplitude and phase, which is the same for each element. Thus,

$$\bar{\Gamma}_n \equiv \beta_n(\vec{x},t) + \psi_A \sin(\omega_A t + \alpha_A), \qquad (4.3)$$

where α_A is an arbitrary reference phase. As discussed in Section 2, Eq. 2.5, we require that

$$\eta_1 + \eta_2 \equiv 1. \qquad (4.4.)$$

Again, the reflected field on the target plane is obtained by multiplying the incident field by the glint-like reflectance function of Eq. 3.4. Propagating this field back to the COAT receiver plane using the Frannhofer integral gives the field at the receiver plane:

$$U_R(\vec{x},t) = \frac{e^{ikz\left(1 + \frac{\vec{x}\cdot\vec{x}}{2z^2}\right)}}{i\lambda z} \sum_\ell R_\ell \, e^{i\phi_\ell} \left\{ \eta_1 \sum_{n=1}^{N} V_{on}(\vec{x}'_\ell) e^{i\Gamma_n(\vec{x}'_\ell,t)} \right.$$

$$\left. + \eta_2 \sum_{n=1}^{N} V_{on}(\vec{x}'_\ell) \, e^{i\bar{\Gamma}_n(\vec{x}'_\ell,t)} \right\} e^{-i\frac{k}{z}(\vec{x}\cdot\vec{x}'_\ell)} \qquad (4.5)$$

The intensity distribution on the receiver plane, $I_R(\vec{x},t)$, is:

$$I_R(\vec{x},t) \equiv U_R(\vec{x},t)\, U_R^*(\vec{x},t)$$

$$= \frac{1}{(\lambda z)^2} \sum_\ell \sum_p R_\ell R_p\, e^{i(\phi_\ell - \phi_p)}\, e^{-i\frac{k}{z}\vec{x}o(\vec{x}_\ell' - \vec{x}_p')}$$

$$\cdot \left\{ \eta_1^2 \sum_{n=1}^{N} \sum_{m=1}^{N} V_{on}(\vec{x}_\ell')\, V_{om}(\vec{x}_p')\, e^{i[\Gamma_n(\vec{x}_\ell',t) - \Gamma_m(\vec{x}_p',t)]} \right.$$

$$+ \eta_1\eta_2 \sum_{n=1}^{N} \sum_{m=1}^{N} V_{on}(\vec{x}_\ell')\, V_{om}(\vec{x}_p')\, e^{i[\Gamma_n(\vec{x}_\ell',t) - \bar{\Gamma}_m(\vec{x}_p',t)]}$$

$$+ \eta_2\,\eta_1 \sum_{n=1}^{N} \sum_{m=1}^{N} V_{on}(\vec{x}_\ell')\, V_{om}(\vec{x}_p')\, e^{i[\Gamma_n(\vec{x}_\ell',t) - \Gamma_m(\vec{x}_p',t)]}$$

$$\left. + \eta_2^2 \sum_{n=1}^{N} \sum_{m=1}^{N} V_{on}(\vec{x}_\ell')\, V_{om}(\vec{x}_p')\, e^{i[\bar{\Gamma}_n(\vec{x}_\ell',t) - \bar{\Gamma}_m(\vec{x}_p',t)]} \right\}.$$

$$(4.6)$$

This is similar to Eq. 3.9; it is a very general expression that contains
all the information needed to understand the fundamental operating princi-
ples of a COAT/ASPECT system. We again consider the special case of a
small number of target glints clustered within an area that is small in
comparison with a diffraction-limited spot size of the total COAT trans-
mitter aperture. Therefore, following the same procedure as we did for
Case 2 in Section 3, we ignore the small spatial variation of the ampli-
tude and phase distributions of the N-element fields over this area.
This allows the receiving plane intensity distribution to again be
expressed as a product of a point-source-type return multiplied by a
speckle-caused amplitude modulation. Eq. 4.6 becomes

$$I_R(\vec{x},t) = \frac{1}{(\lambda z)^2} \left\{ \sum_{\ell}\sum_{p} R_\ell R_p \, e^{i(\phi_\ell - \phi_p)} \, e^{-i\frac{k}{z}\vec{x}\cdot(\vec{x}_\ell' - \vec{x}_p')} \right\}$$

$$\cdot \left\{ \eta_1^2 \sum_{n=1}^{N}\sum_{m=1}^{N} V_{on}V_{om}\, e^{i[\beta_n(t)-\beta_m(t)]} \, e^{i\psi_o[\sin(\omega_n t + \alpha_n) - \sin(\omega_m t + \alpha_m)]} \right.$$

$$+ \eta_1\eta_2 \sum_{n=1}^{N}\sum_{m=1}^{N} V_{on}V_{om}\, e^{i[\beta_n(t)-\beta_m(t)]} \, e^{i[\psi_o \sin(\omega_n t + \alpha_n) - \psi_A \sin(\omega_A t + \alpha_A)]}$$

$$+ \eta_2\eta_1 \sum_{n=1}^{N}\sum_{m=1}^{N} V_{on}V_{om}\, e^{i[\beta_n(t)-\beta_m(t)]} \, e^{i[\psi_A \sin(\omega_A t + \alpha_A) - \psi_o \sin(\omega_m t + \alpha_m)]}$$

$$\left. + \eta_2^2 \sum_{n=1}^{N}\sum_{m=1}^{N} V_{on}V_{om}\, e^{i[\beta_n(t)-\beta_m(t)]} \right\} \quad . \tag{4.7}$$

Expanding the dither phases in Eq. 4.3 into a Fourier-Bessel series allows the entire dither spectrum to be expressed explicitly. Thus, Eq. 4.7 can be rewritten conveniently as

$$I_R(\vec{x},t) = \overline{M}_S(\vec{x}) \left[I_M' + B_A' \cos(2\omega_A t + 2\alpha_A) \right.$$

$$+ \sum_{n=1}^{N} A_n' \sin(\omega_n t + \alpha_n) + B_n' \cos(2\omega_n t + 2\alpha_n)$$

$$\left. + \text{higher harmonics} \right] \quad , \tag{4.8}$$

59

where $M_s(\vec{x})$ is the same speckle modulation function as that of Eq. 3.2, and

$$I_M' \equiv [\eta_1^2 + 2\eta_1\eta_2 J_o(\psi_o) J_o(\psi_A) + \eta_2^2] \sum_{n=1}^{N} V_{on}^2$$

$$+ [\eta_1^2 J_o^2(\psi_o) + 2\eta_1\eta_2 J_o(\psi_o)J_o(\psi_A) + \eta_2^2] \sum_{\substack{n=1 \\ n \neq m}}^{N} \sum_{m=1}^{N} V_{on} V_{om} \cos[\beta_n(t) - \beta_m(t)] ,$$

$$(4.9)$$

$$B_A' \equiv 4\eta_1\eta_2 \left\{ J_o(\psi_o) J_2(\psi_A) \sum_{n=1}^{N} \sum_{m=1}^{N} V_{on}V_{om}\cos[\beta_n(t)-\beta_m(t)] \right.$$

$$\left. -2J_1(\psi_o)J_2(\psi_A) \sum_{n=1}^{N} \sum_{m=1}^{N} V_{on}V_{om} \sin[\beta_n(t)-\beta_m(t)] \ \sin(\omega_n t + \alpha_n) \right\} \quad (4.10)$$

$$A_n' \equiv -4 J_1(\psi_o)V_{on}[\eta_1^2 J_o(\psi_o) + \eta_1\eta_2 J_o(\psi_A)] \sum_{\substack{m=1 \\ m \neq n}}^{N} V_{om} \sin[\beta_n(t)-\beta_m(t)]$$

$$(4.11)$$

$$B_n' \equiv 4\eta_1\eta_2 J_2(\psi_o)J_o(\psi_A) \ V_{on}^2$$

$$+ 4J_2(\psi_o) \ V_{on}[\eta_1^2 J_o(\psi_o) + \eta_1\eta_2 J_o(\psi_A)] \sum_{\substack{m=1 \\ m \neq n}}^{N} V_{om} \cos[\beta_n(t)-\beta_m(t)] \quad (4.12)$$

The higher harmonics of Eq. 4.8 have amplitudes proportional to the corresponding products of higher-order Bessel functions of ψ_o and ψ_A which make them negligible compared to the above coefficients. Equation 4.9 permits estimating the additional loss in the Strehl ratio incurred as a result of adding the ASPECT dither. For even a modest number of elements, the second term in Eq. 4.9 dominates the first near-convergence and thus controls the Strehl ratio. Under this assumption, the multiplicative Strehl factor which the ASPECT dither introduces is

60

$$S_A = 1 - 2\eta_1 (1-\eta_1) \left\{ 1 - \left[\frac{J_o(\psi_s)}{J_o(\psi_o)} \right] \right\}. \tag{4.13}$$

If we choose ψ_A near the zero of $J_o(\psi_A \doteq 2.4$ rad) and small η_1, then Eq. 4.13 becomes

$$S_A \doteq 1 - 2\eta_1 . \tag{4.14}$$

Thus for 2% of the power split off into the ASPECT encoding systems, we have an $S_A \doteq 0.96$. When the target moves the spatial speckle modulation function $M_s(\vec{x})$ produces the same temporal modulation function $M_s(t)$ as discussed in Section 3.C. The signal S_o from the photodetector becomes

$$S_o = K M_s(t) I'g(t) , \tag{4.15}$$

where $I'g(t)$ is the expression in brackets in Eq. 4.8. We can estimate the modulation function multiplied by the coefficient B'_A if we synchronously detect the signal S_o ot the carrier $2\omega_A$.

To ensure a high-quality estimate of the spectral content of $M_s(t)$ in the region of the COAT dither band, it is desirable to allow an ample frequency interval around the carrier. Ideally, the carrier should be close to an order of magnitude higher than the highest COAT dither frequency. To have a strong signal at the carrier frequency it is also desirable to have a rather large ASPECT dither amplitude, ψ_A. As much as π rad of wavelength might be used. But since the amplitude of the COAT dither signals are reduced by such a choice, as is the mean convergence level, I_M, some optimum compromise value must ultimately be selected. This is readily apparent from Eqs. 4.9 through 4.14, which define the amplitudes of the mean level and the modulations at the dither frequencies in terms of the COAT/ASPECT system parameters.

The speckle estimator signal of Eq. 4.10 also contains the basic dither signals (as a multiplicative factor), and thus the process of dividing (or subtracting) this estimator from the basic dither channel signals has the potential to wholly or partly cancel the basic dither information

and the speckle noise introduced by $\overline{M}_s(\overline{x})$. This potential is quantified below. Combining the results of Eqs. 4.9 and 4.11 yields the amplitude modulation index for the basic n^{th} dither signal, which is for large N,

$$\mathcal{M}_n = \frac{-4J_1(\psi_o)\, V_{on}\, [\eta_1^2 J_o(\psi_o) + \eta_1\eta_2 J_o(\psi_A)]\, \sum_{m=1}^{N} V_{om}\, \sin(\beta_n(t)-\beta_m(t))}{[\eta_1^2 J_o^2(\psi_o) + 2\eta_1\eta_2 J_o(\psi_o)J_o(\psi_A) + \eta_2^2]\, \sum_{n=1}^{N} \sum_{\substack{m=1 \\ n \neq m}}^{N} V_{on}V_{om}\cos(\beta_n(t)-\beta_m(t))}\, ,$$

(4.16a)

while the corresponding modulation index in the ASPECT estimator output is obtained from Eq. 4.10 as

$$\mathcal{M}_n = \frac{-2J_1(\psi_o)\, \sum_{m=1}^{N} V_{on}V_{om}\, \sin(\beta_n(t) - \beta_m(t))}{J_o(\psi_o)\, \sum_{n=1}^{N} \sum_{\substack{m=1 \\ n \neq m}}^{N} V_{on}V_{om}\, \cos(\beta_n(t) - \beta_m(t))}\, .$$

(4.16b)

If we consider the case (which we expect to be typical in application) in which

$$\eta_1 \gg \eta_2\, ,$$

then Eq. 4.16a becomes, to an excellent approximation,

$$\mathcal{M}_n \doteq \frac{-4J_1(\psi_o)V_{on} \displaystyle\sum_{m=1}^{N} V_{om} \sin(\beta_n(t) - \beta_m(t))}{J_o(\psi_o) \displaystyle\sum_{\substack{n=1 \\ n \neq m}}^{N} \sum_{m=1}^{N} V_{om} \cos(\beta_n(t) - \beta_m(t))} \qquad . \qquad (4.16c)$$

Comparing Eq 4.16b to Eq. 4.16c shows that the modulation index of the estimator channel is nearly 0.5, the basic channel modulation index, for all possible phase error states of the system.

Consequently, a system that divides or subtracts the estimated signal will cancel about one-half of the dither signal component. This becomes important if thermal or shot noise components dominate speckle noise.

Note, however, that if one attempts to use a probe beam with comparable power to the basic dither encoded beam (that is, with $\eta_1 = \eta_2 = 1/2$), then nearly complete dither cancellation will result and the cancellation of speckle noise will prove to be a hollow victory. For example, take the case of $\eta_1 = \eta_2$ and an ASPECT index* $\psi_A = 2.4$ such that

$$J_o(\psi_A) \doteq 0.$$

Eq. 4.16a then becomes

$$\mathcal{M}_n = \frac{-4J_1(\psi_o) J_o(\psi_o) V_{on} \displaystyle\sum_{m=1}^{N} V_{om} \sin(\beta_n(t) - \beta_m(t))}{[1 + J_o^2(\psi_o)] \displaystyle\sum_{\substack{n=1 \\ n \neq m}}^{N} \sum_{m=1}^{N} V_{on}V_{om} \cos(\beta_n(t) - \beta_m(t))} \qquad .$$

$$(4.16d)$$

---

*This is an excellent choice for most system applications.

63

For low values of ψ_o (such as those typically employed), Eqs. 4.16 and 4.16b are nearly identical, yielding a system with substantial cancellation.

For the special case discussed in Section 3.E, Eq. 4.6 can again be separated into terms associated with a given element or channel and a reduced array composed of the remaining elements or channels. Such an analysis would again show a different speckle multiplier for the ac and dc terms. As discussed in Section 2.A, however, the ASPECT-II scheme estimates the dc multiplier, which is the principal source of degradation. Partial cancellation of the ac multiplier will also occur since the two are similar although not identical. In any event, the ac multiplier seems to produce negligible performance degradation, as demonstrated by computer simulation results. We discuss this point in greater depth in Section 4.B. To show that we indeed do estimate the dc multiplier by synchronously detecting at ω_A, we will examine Eq. 4.6 for the general case of an arbitrary distribution of glints in the target plane, but this time we will ignore the COAT dithers. This simplifies the result without obscuring the central issue of the speckle multipliers. Under these conditions, Eq. 4.6 becomes

$$
\begin{aligned}
I_R(\vec{x},t) = & \frac{1}{(\lambda z)^2} \sum_\ell \sum_p R_\ell R_p \cos[\phi_\ell - \phi_p + \frac{k}{z}\vec{x}\cdot(\vec{x}_\ell' - \vec{x}_p')] \\
& \cdot \left\{ (\eta_1^2 + \eta_2^2) \sum_{n=1}^N \sum_{m=1}^N V_{on}(\vec{x}_\ell')V_{om}(\vec{x}_p')\cos[\beta_n(\vec{x}_\ell',t)-\beta_m(\vec{x}_p',t)] \right. \\
& + 2\eta_1\eta_2 \cos[\psi_A \sin(\omega_A t + \alpha_A)] \sum_{n=1}^N \sum_{m=1}^N V_{on}(\vec{x}_\ell') \\
& \left. V_{om}(\vec{x}_p') \cos[\beta_n(\vec{x}_\ell',t)-\beta_m(\vec{x}_p',t)] \right\} .
\end{aligned}
\tag{4.17}
$$

Expanding $\cos[\psi_A \sin(\omega_A t + \alpha_A)]$ into a Bessel series and retaining the two lowest order terms gives

$$I_R(\vec{x},t) = \frac{1}{(\lambda z)^2} \sum_\ell \sum_p R_\ell R_p \cos\left[\phi_\ell - \phi_p + \frac{k}{z}\,\vec{x}\cdot(\vec{x}_\ell' - \vec{x}_p')\right]$$

$$\cdot\left[(\eta_1^2 + 2\eta_1\eta_2\,J_o(\psi_A) + \eta_2^2) + 4\eta_1\eta_2\,J_2(\psi_A)\cos(2\omega_A t + 2\alpha_A)\right]$$

$$\cdot \sum_{n=1}^{N}\sum_{m=1}^{N} V_{on}(\vec{x}_\ell')\,V_{om}(\vec{x}_p')\cos[\beta_n(\vec{x}_\ell',t) - \beta_m(\vec{x}_p',t)] \quad . \quad (4.18)$$

It is obvious by inspecting Eq. 4.18 that the temporal modulation produced by the sweep of the above speckle pattern past the COAT receiver will generate a detector current of the form

$$S_o = M_{S2}(t) + CM_{S2}(t)\cos(2\omega_A t + \alpha_A). \qquad (4.19)$$
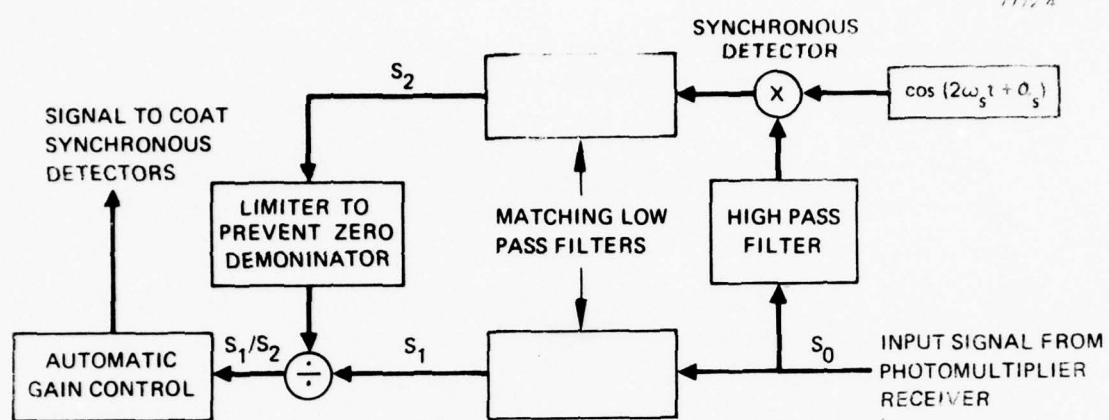
Had we included the dither terms, the general result would be essentially the same as Eq. 2.2 of Section 2.A.1.

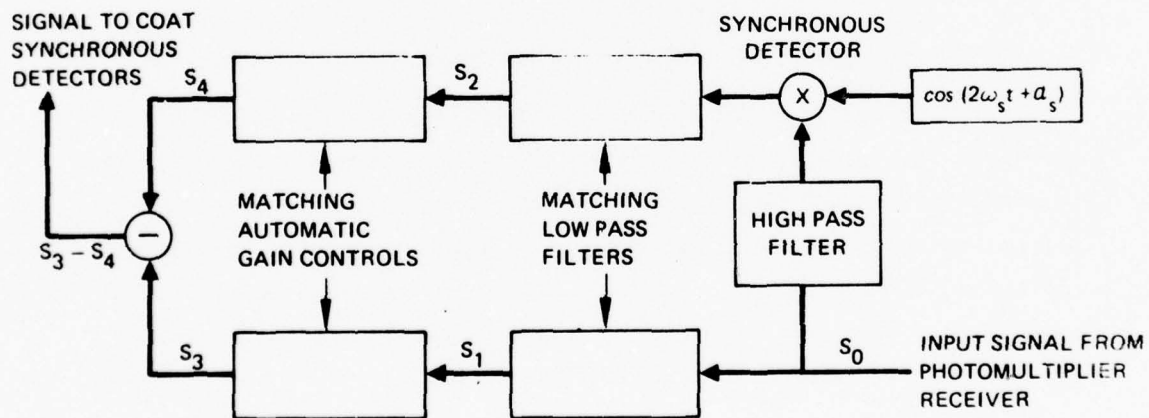## B.   ESTIMATION AND CALCULATION OF THE SPECKLE MODULATION FUNCTION

Consider the diagrams of the two ASPECT speckle cancellation schemes in Figure 12. The electric signal S_o from the photomultiplier receiver is conducted through two separate channels, one containing a low-pass filter and the other a high-pass filter. The low-pass filter passes all signals with frequencies in the COAT dither band and below, attenuating the ASPECT carrier signal, which is significantly higher than the highest COAT dither. Therefore, the filter output S_1 can be written approximately as

$$S_1 \simeq K\,M_s(t)\,(I_M' + I_D') \quad . \qquad (4.20)$$

This is essentially equivalent to the usual COAT signal (i.e., without ASPECT), where I_D' contains the modulations at the dither frequencies.

65

(a) DIVISION SCHEME

SYNCHRONOUS DETECTOR

$\cos(2\omega_s t + \theta_s)$

SIGNAL TO COAT SYNCHRONOUS DETECTORS

S_2

MATCHING LOW PASS FILTERS

HIGH PASS FILTER

LIMITER TO PREVENT ZERO DEMONINATOR

AUTOMATIC GAIN CONTROL

S_1/S_2

S_1

S_0

INPUT SIGNAL FROM PHOTOMULTIPLIER RECEIVER

(a) DIVISION SCHEME

(b) SUBTRACTION SCHEME

SIGNAL TO COAT SYNCHRONOUS DETECTORS

SYNCHRONOUS DETECTOR

$\cos(2\omega_s t + a_s)$

S_4

S_2

$S_3 - S_4$

MATCHING AUTOMATIC GAIN CONTROLS

MATCHING LOW PASS FILTERS

HIGH PASS FILTER

S_3

S_1

S_0

INPUT SIGNAL FROM PHOTOMULTIPLIER RECEIVER

(b) SUBTRACTION SCHEME

Figure 12.   Schematic diagram of ASPECT speckle cancellation systems.

66

$$I_D' \equiv \sum_{n=1}^{N} A_n' \sin (\omega_n t + \alpha_n), \qquad (4.21)$$

and I_M' is defined in Eq. 4.9.

The portion of the signal S_o emerging from the high-pass filter, on the other hand, only contains signals at frequencies well beyond the dither band, in particular, the signal at the ASPECT carrier frequency $2\omega_A$. This signal is synchronously detected and low-pass filtered by a filter identical to the one in the other channel, giving the output signal S_2. This signal can be expressed approximately as

$$S_2 \simeq \frac{1}{2} K M_s(t) B_S', \qquad (4.22)$$

where the factor of one-half comes from the synchronous detection process. Inspection of Eqs. 4.9 and 4.10 shows, for a large number of channels, that the coefficient B_S' is related to the mean convergence level I_M' and the dither modulations I_D', as follows:

$$B_S' = K_1 I_M' + K_2 I_D', \qquad (4.23)$$

where K_1 and K_2 are easily calculated constants. Electronically dividing the signal S_1 by S_2 in accordance with the division scheme in Figure 12(a) yields

$$\frac{S_1}{S_2} \simeq \frac{2}{K_1} \left[1 + \left(1 - \frac{K_2}{K_1} \right) \frac{I_D'}{I_M'} \right], \qquad (4.24)$$

where we assume $I_M' \gg I_D'$. The speckle modulation function $M_s(t)$ has been cancelled by the division process. By processing this quotient signal by an automatic gain control (AGC) which normalizes the signal by its low-frequency component (the first term in Eq. 4.24), we get

67

$$\frac{S_1}{S_2} \xrightarrow{AGC} 1 + \frac{1}{2} (K_1 - K_2) \ \frac{I'_D}{I'_M} \ , \tag{4.25}$$

which is very similar to the usual COAT correction signal containing the dither modulations normalized to the mean or low-frequency level. However, the dither signals are reduced or illuminated, depending on the relative values of K_1 and K_2, as discussed in Section 4.A. For typical cases, where $\eta_1 \gg \eta_2$, this signal is reduced by a factor of 0.5. This signal loss can then be simply restored by increasing the loop gain electronically.

An alternate way to cancel out the speckle interference is shown in the substration scheme of Figure 12(b). There, signals S_1 and S_2 are channeled through identical AGCs. To give a simple illustration of how this process works, we separate the modulation function $M_s(t)$ into the sum of two components, one containing the low frequency variations (M_M) and the other containing the remaining high frequency variations (M_D). Then, using Eq. 4.20, we can write

$$S_1 = K(M_M + M_D) \ (I'_M + I'_D) \ = \ K \ (M_M I'_M + M_M I'_D + M_D I'_M + M_D I'_D). \tag{4.26}$$

When this signal is normalized by its low-frequency component, which consists primarily of $M_M I_M$, we get

$$S_1 \xrightarrow{AGC} S_3 = 1 + \frac{M_D}{M_M} + \frac{I_D}{I_M} \left(1 + \frac{M_D}{M_M}\right) \ , \tag{4.27}$$

where $\dfrac{M_D}{M_M}$ is identified as the undesirable speckle interference in the COAT dither band. Similarly, when the signal S_2 is processed by an AGC, we get

$$S_2 \xrightarrow{AGC} = S_4 = 1 + \frac{M_D}{M_M} + \frac{K_2}{K_1} \frac{I_D}{I_M} \left(1 + \frac{M_D}{M_M}\right), \tag{4.28}$$

68

Electronically subtracting these two signals leaves us with

$$S_3 - S_4 = \left(1 - \frac{K_2}{K_1}\right)\left(1 + \frac{M_D}{M_M}\right)\frac{I_D}{I_M} = \left(1 - \frac{K_2}{K_1}\right)\frac{I_D M_S}{I_M M_M} \cdot (4.29)$$

Notice that this process only cancels the speckle multiplier of the dc term, I_M in this case, and leaves it as a factor in the ac term, except for normalization terms. In previous sections, we have maintained that the ac multiplier has negligible effects on COAT performance. The viability of this subtraction scheme is crucially dependent on the validity of this claim. Thus, in demonstrating its good performance (see Section 4.c), we also verify that an ASPECT-II system that can only cancel the dc multiplier for the case where the two multiplier are different is a reliable technique for counseling speckle interference for all cases.

C.   COMPUTER SIMULATION RESULTS

A computer simulation program modeling an 18-element COAT servo and the ASPECT speckle cancellation electronics has been developed. It is a modification of a code used in previous studies of multidither COAT systems.[1,2,12] Figure 13, a schematic of the modified program, includes all of the electronic servo parameters, but no propagation effects. The receiver is ideal in the sense that it detects the return from a point source (i.e., a target glint). Speckle is then introduced as an amplitude modulation of the normal receiver signal. The speckle modulations themselves are calculated functions of time, generated by computer at the General Research Corporation and discussed in more detail in Ref. 1. They represent the aperture averaged intensity fluctuations at a COAT receiver caused by the motion of a speckle pattern from a rotating target sphere. The surface of the sphere was assumed to be optically rough, thus causing a speckle pattern with a unit contrast ratio, or, equivalently, very severe modulation depths. Three different target rotation rates were considered: 0.4 rad/sec (which contained most of its spectral energy below the COAT dither band), 2.0 rad/sec (which concentrated most of its
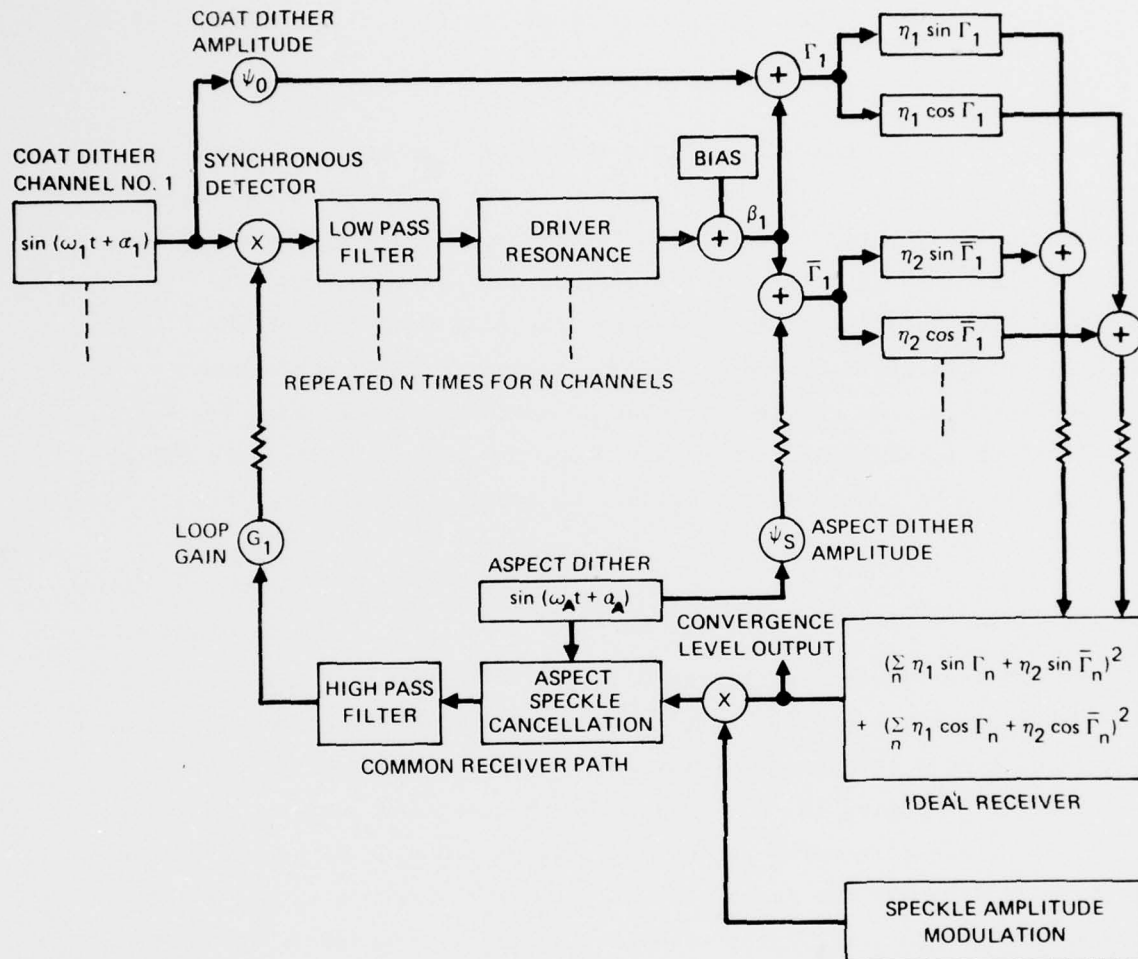
69

Figure 13. Schematic diagram of COAT/ASPECT computer simulation model.

spectral energy inside the COAT dither band), and 10.0 rad/sec (which had its spectral energy spread well beyond the COAT dither band). Our simulations show that COAT performance is noticeably degraded by this multiplicative noise, but that the performance degradation can be almost completely illuminated by ASPECT.

For reference, the ideal COAT performance is shown in Figure 14. The normalized target glint irradiance, or Strehl ratio, is shown as a function of time. The 18 channels are initiated with a random static error, which is quickly removed by the COAT servo. Even though there is no speckle modulation, the ASPECT dither (at one-half a wave) is included in this simulation to illustrate how peak Strehl ratio is reduced. Without the ASPECT dither, we normally achieve optimum average Strehl ratios at the target of about 0.94 for such a COAT simulation, but, with the additional dither, this is reduced to slightly over 0.80. No attempt has been made to optimize this value, and higher levels can be achieved at the expense of reduced signal strength in the ASPECT estimation channel. Figures 15, 16, and 17 show how this ideal performance is degraded by speckle modulations from a rotating target sphere. In each simulation, the target irradiance was initialized near its optimum value. Normally, the COAT servo would maintain this level through the entire simulation, but this was prevented in these runs by speckle interference. In Figure 15, which is the case of the slowest target rotation rate (0.4 rad/sec), where most of the speckle modulation power is below the COAT dither band, degradation is much greater. Using the same modulation functions, results similar to these but with slightly better performance were reported in Ref. 1. The performance here is generally poorer for two reasons. First, the incorporation of an ASPECT system with a multidither COAT system reduces the strength of the dither correction signals. This can be seen by comparing Eq. 4.11 with Eq. 3.10. These lower strength signals are more easily overcome by interference. Second, no attempt was made to optimize servo parameters (e.g., bandwidth, dither amplitude, clipping levels), which reduce speckle interference. This was done intentionally so that the total burden of speckle cancellation could be registered to the ASPECT system.
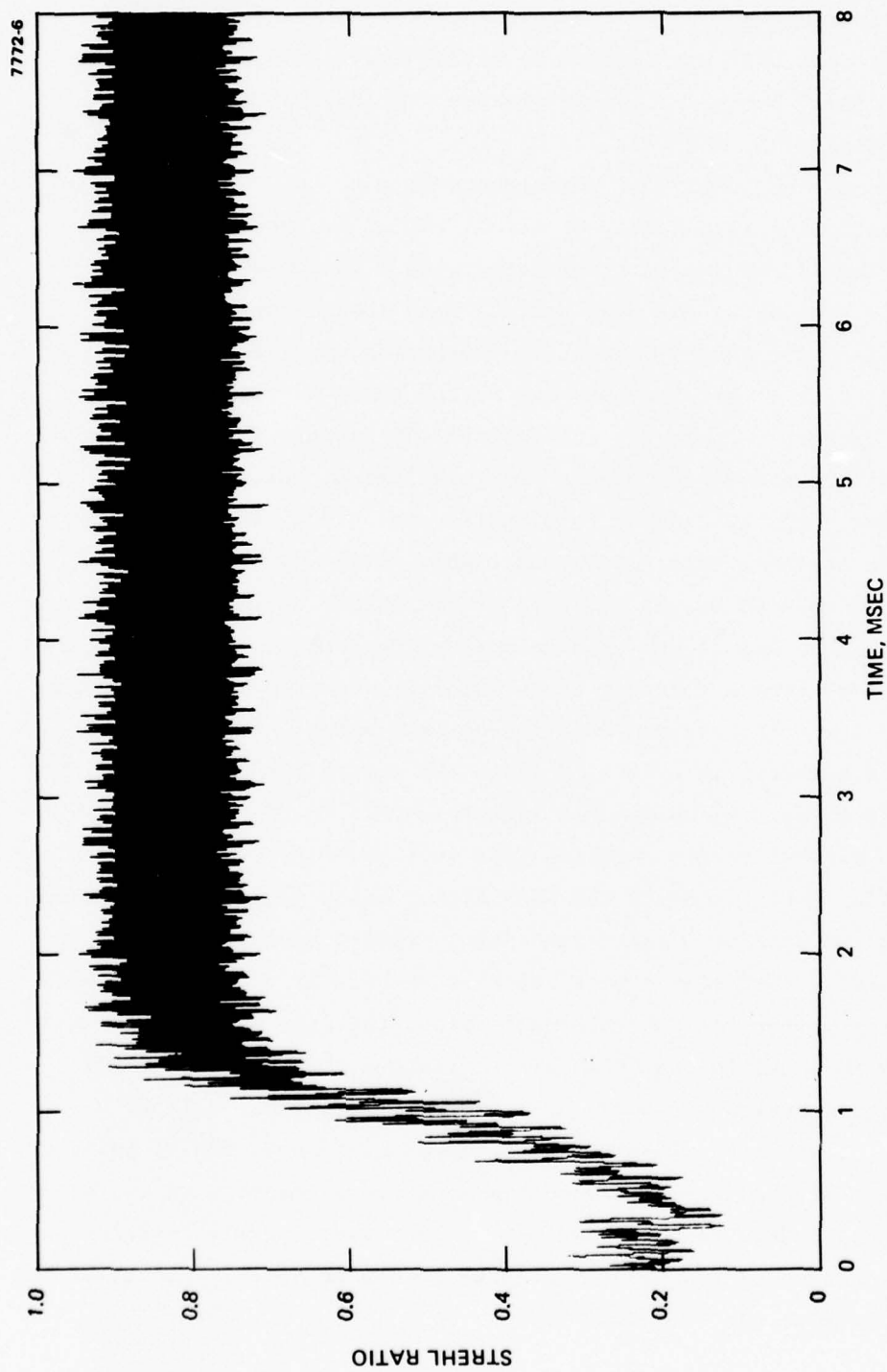
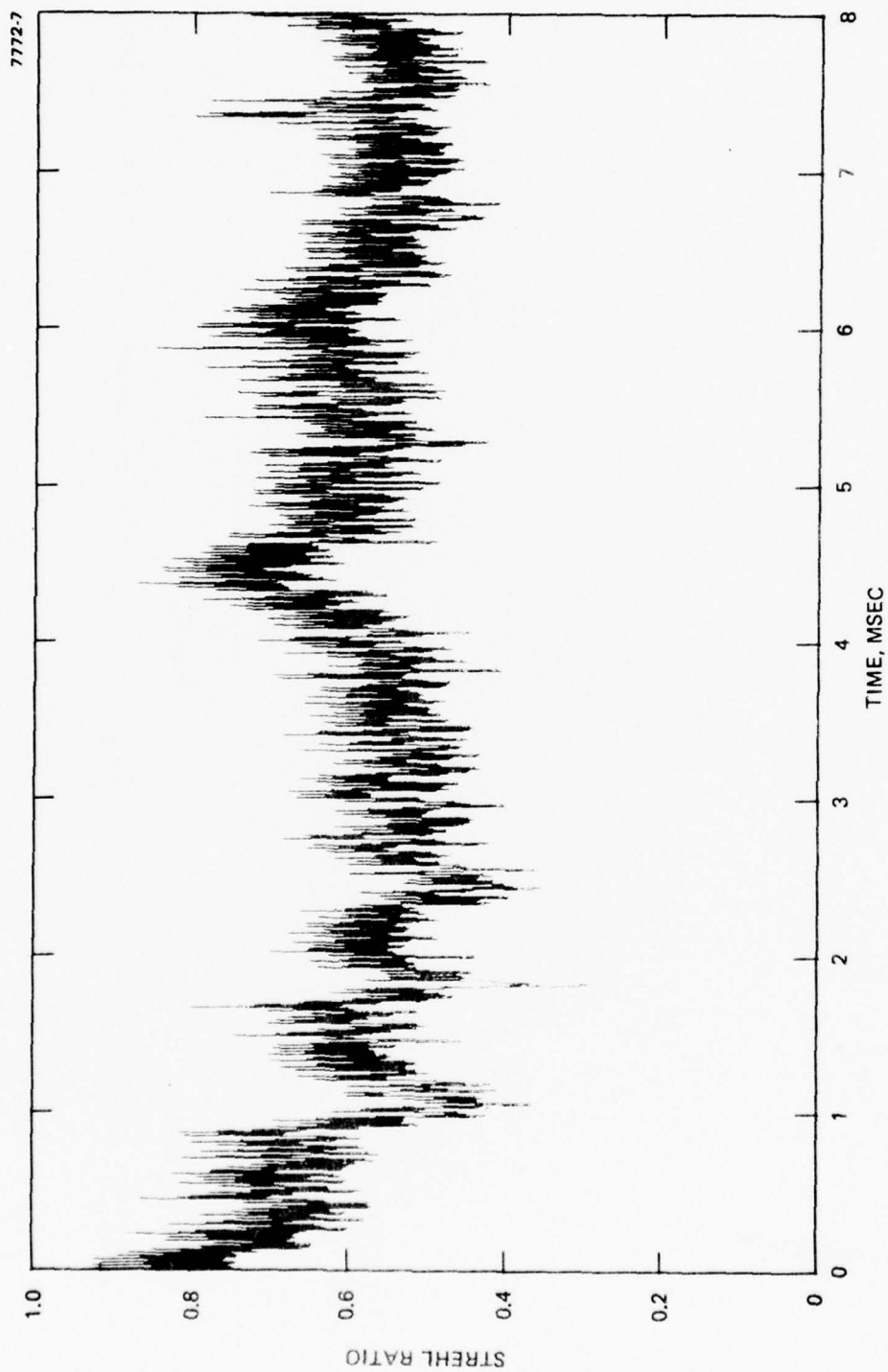Figure 14. Ideal COAT/ASPECT performance — no speckle.

72

Figure 15. Speckle degraded COAT performance ASPECT open loop target rotation rate 0.4 rad/sec.
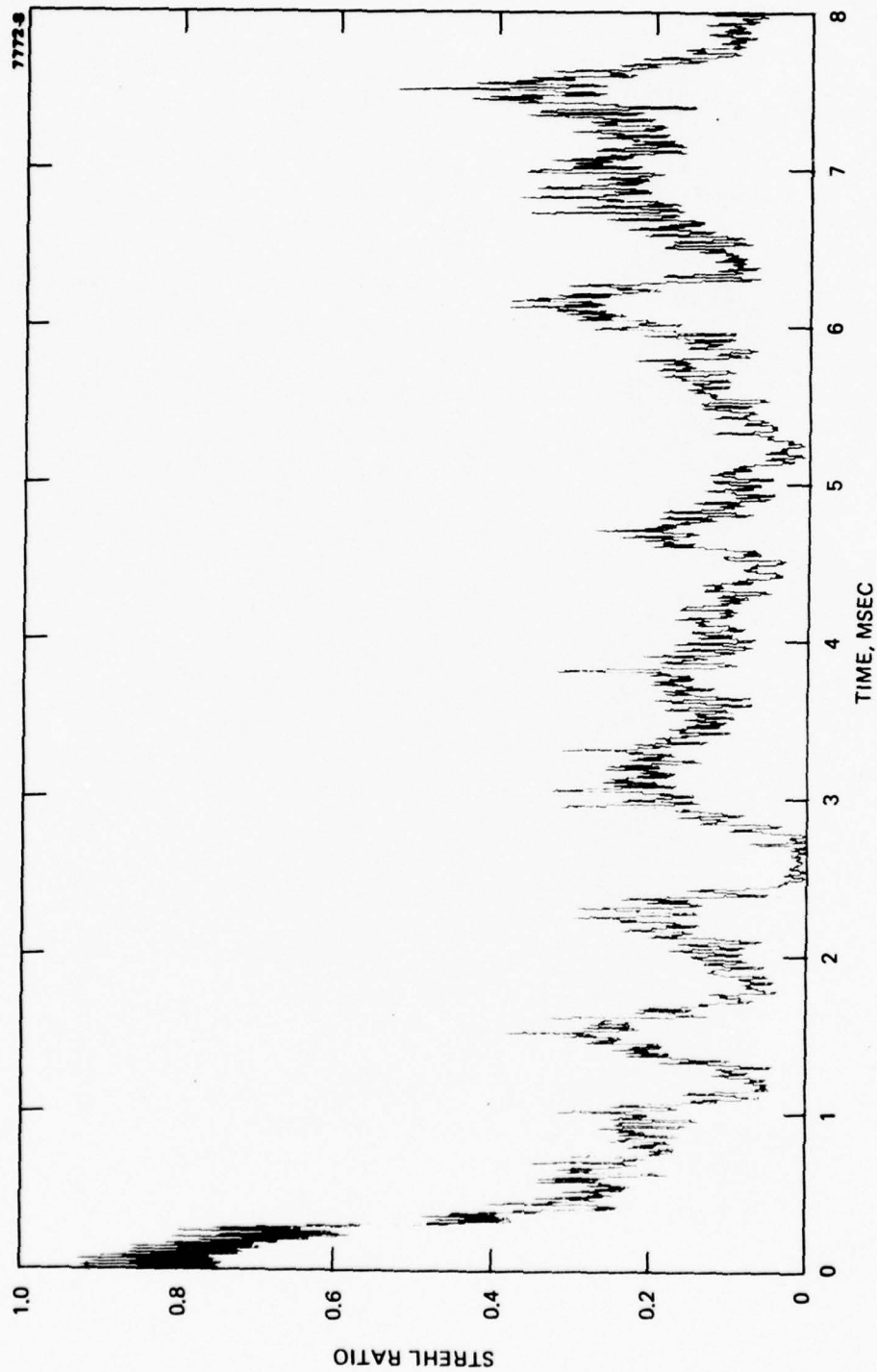
73

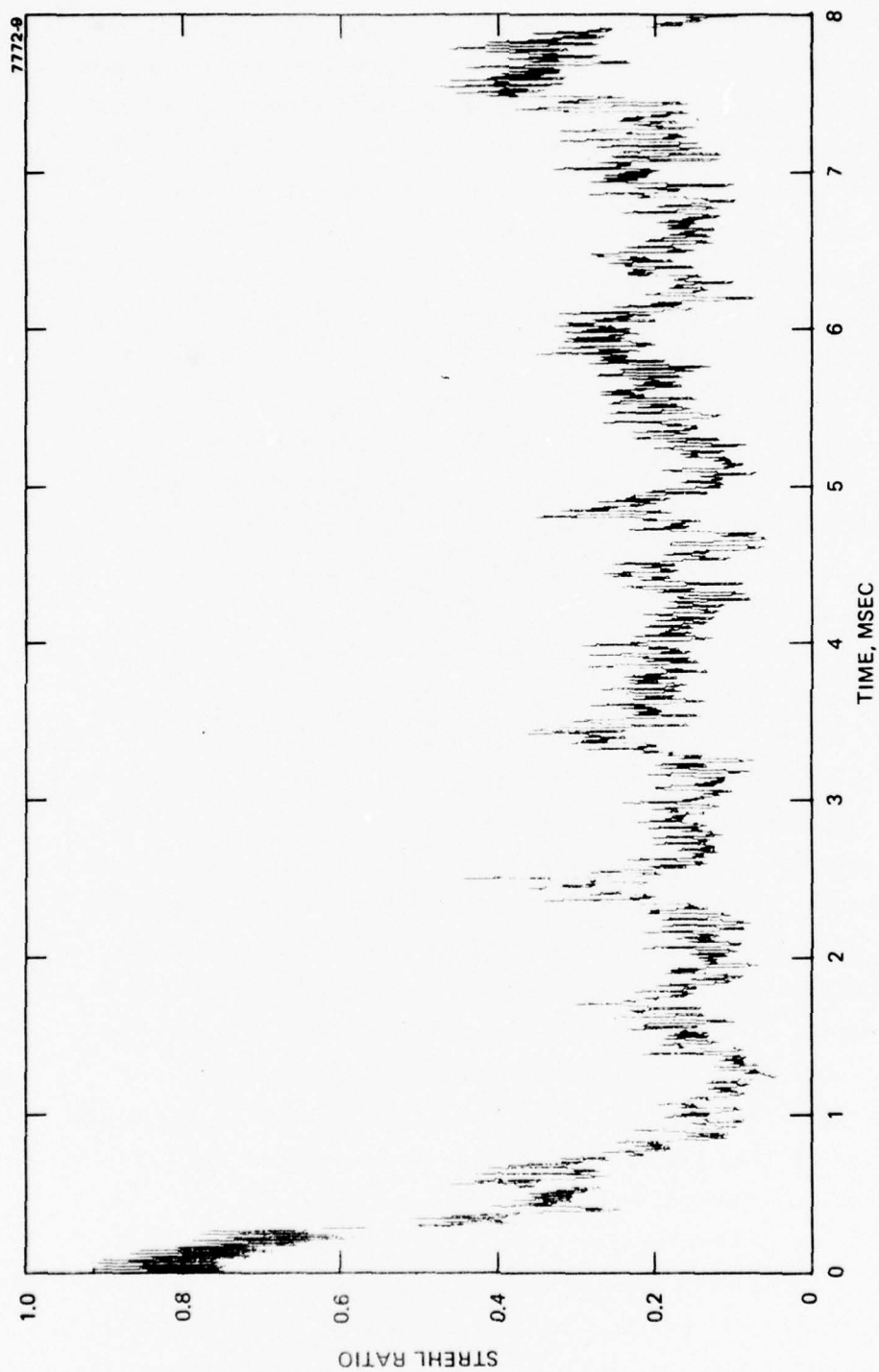Figure 16. Speckel degraded COAT performance ASPECT open loop target rotation rate 2.0 rad/sec.

Figure 17. Speckle degraded COAT performance ASPECT open loop target rotation rate 10 rad/sec.

Figures 18, 19, and 20 (which correspond to Figures 15, 16, and 17, respectively) show how the ASPECT system restores the speckle degraded COAT performance. After a transient response to the initialization parameters, the optimum Strehl ratio is restored and maintained. Since the ASPECT dither frequency used in all three of these simulations was 400 kHz, the synchronously detected signal, which provided the estimate of the speckle modulation function, had a carrier frequency of 800 kHz. This is well above the dither band with its 18 channels extending from 8.2 kHz to 32.0 kHz incremented by 1.4 kHz. The particular configurations shown in these simulations consisted of the division scheme from Figure 12.

The quality of the ASPECT-generated estimate of the speckle modulation function can be seen by comparing Figures 21 and 22. Figure 21 shows the time history of one of the three speckle-modulation functions used in these simulations (the one corresponding to a 0.4 target rotation rate). Figure 22 shows the ASPECT-generated estimate. Recall from Eqs. 4.8 and 4.10 that the estimate is modulated by a coefficient B_A' whose value varies with convergence level. The effect of this coefficient can be seen in the estimate, where the amplitude profile for the first few milliseconds differs from the actual modulation function itself. This difference has no effect on performance, however, because it is filtered out by the AGC (as discussed in Section 4.B).

These simulations were part of a parallel effort of analytical and experimental studies. As is typical of such studies, the experiments are usually subject to greater constraints than the computer simulations. One of these constraints was the inability of the experimental hardware to generate an ASPECT dither freuency greater than 50 kHz. To support the experimental work, we also ran simulations at progressively lower ASPECT dither frequencies. Anticipating poorer performance in the division scheme for cancelling the speckle interference, we also explored the alternate subtraction scheme discussed in Section 4.B.

Figures 23 and 24 show the simulation results for the respective schemes working to cancel the modulation function of Figure 21 using an ASPECT dither frequency of 200 kHz. At this frequency, the performance of both schemes is still very good, achieving essentially full speckle interference cancellation. Figures 25 and 26 show the respective performance
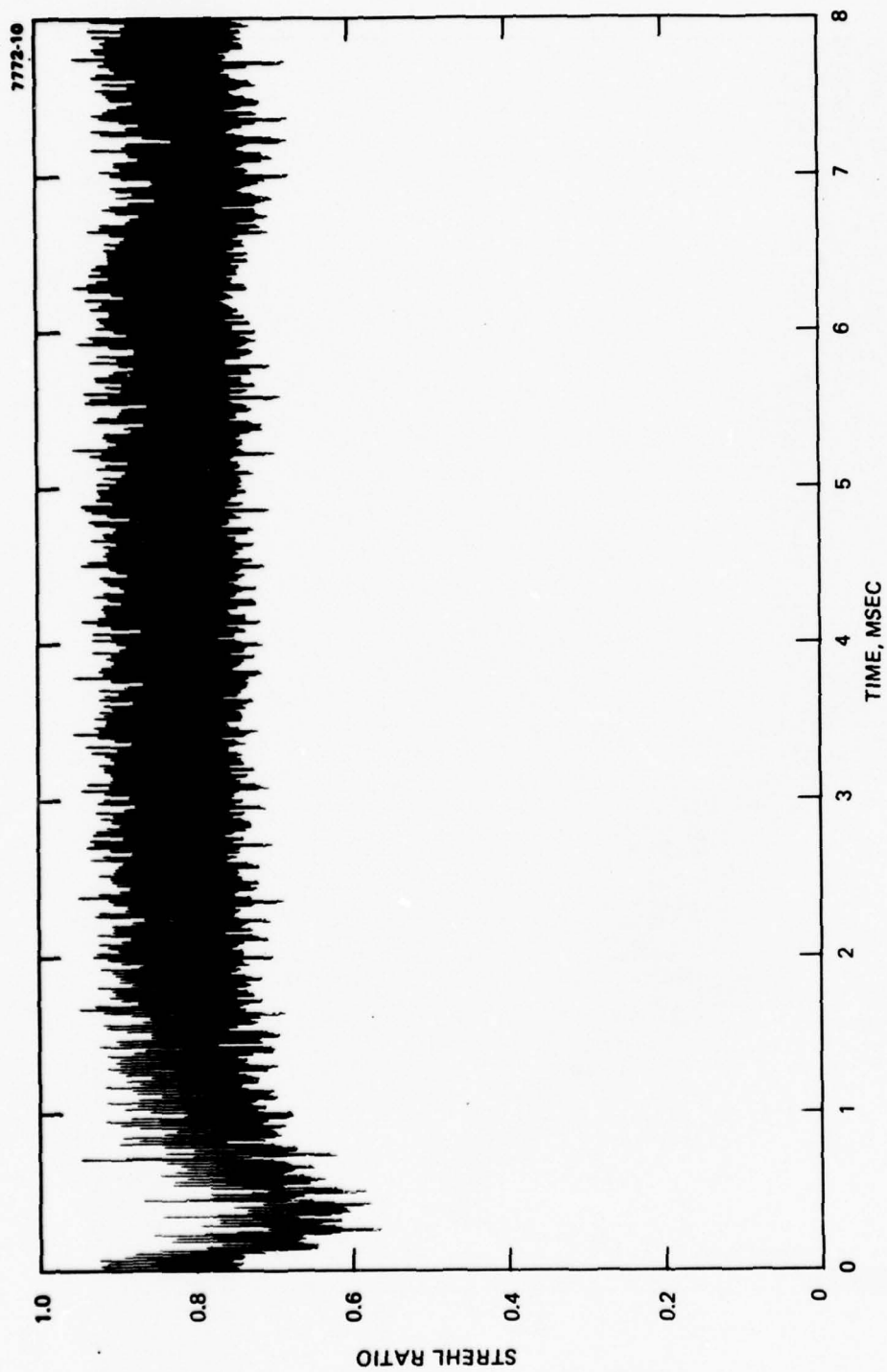
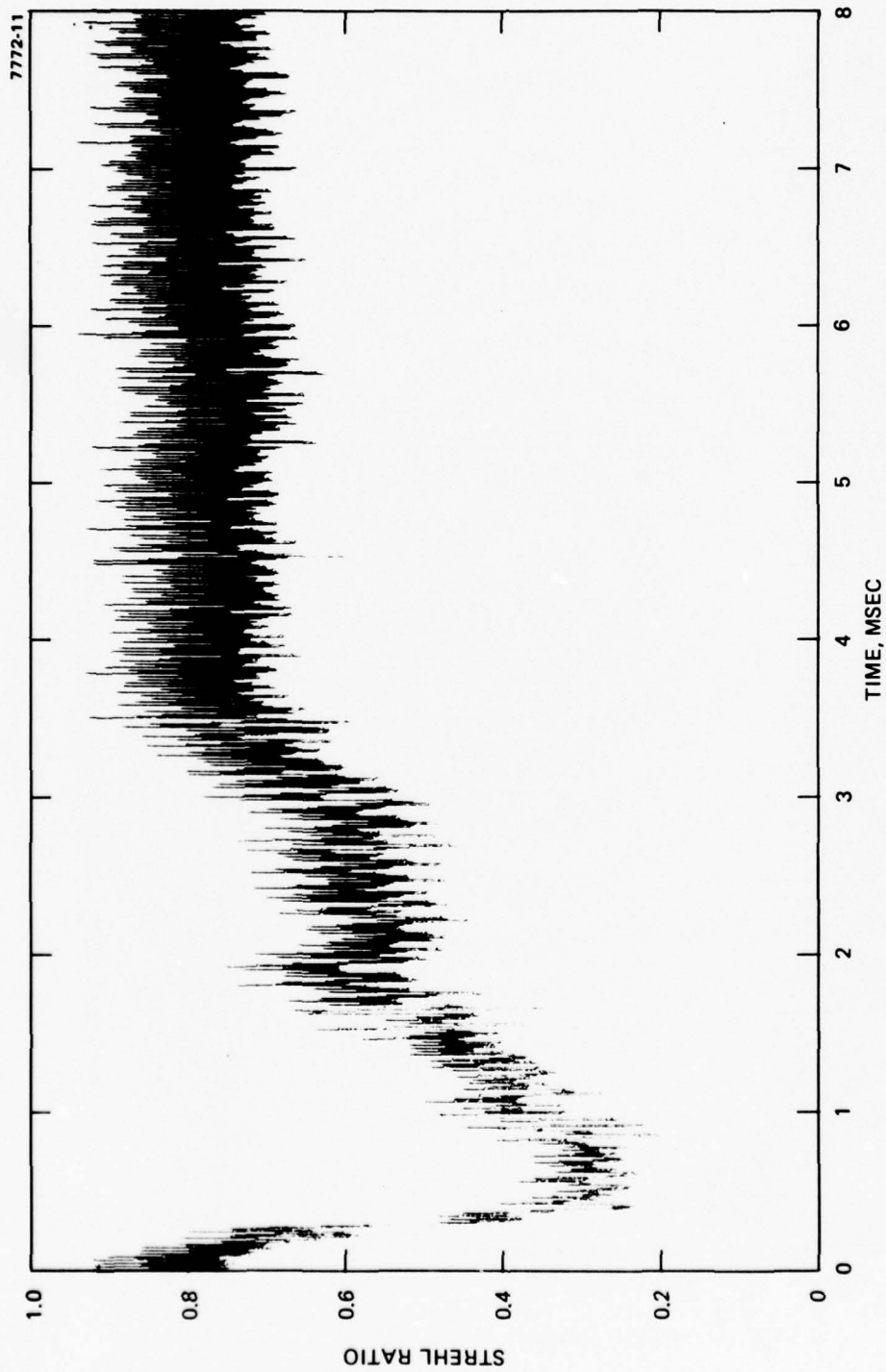Figure 18. Restored COAT performance ASPECT closed loop target rotation rate 0.4 rad/sec.

77

Figure 19. Restored COAT performance ASPECT closed loop target rotation rate 2.0 rad/sec.
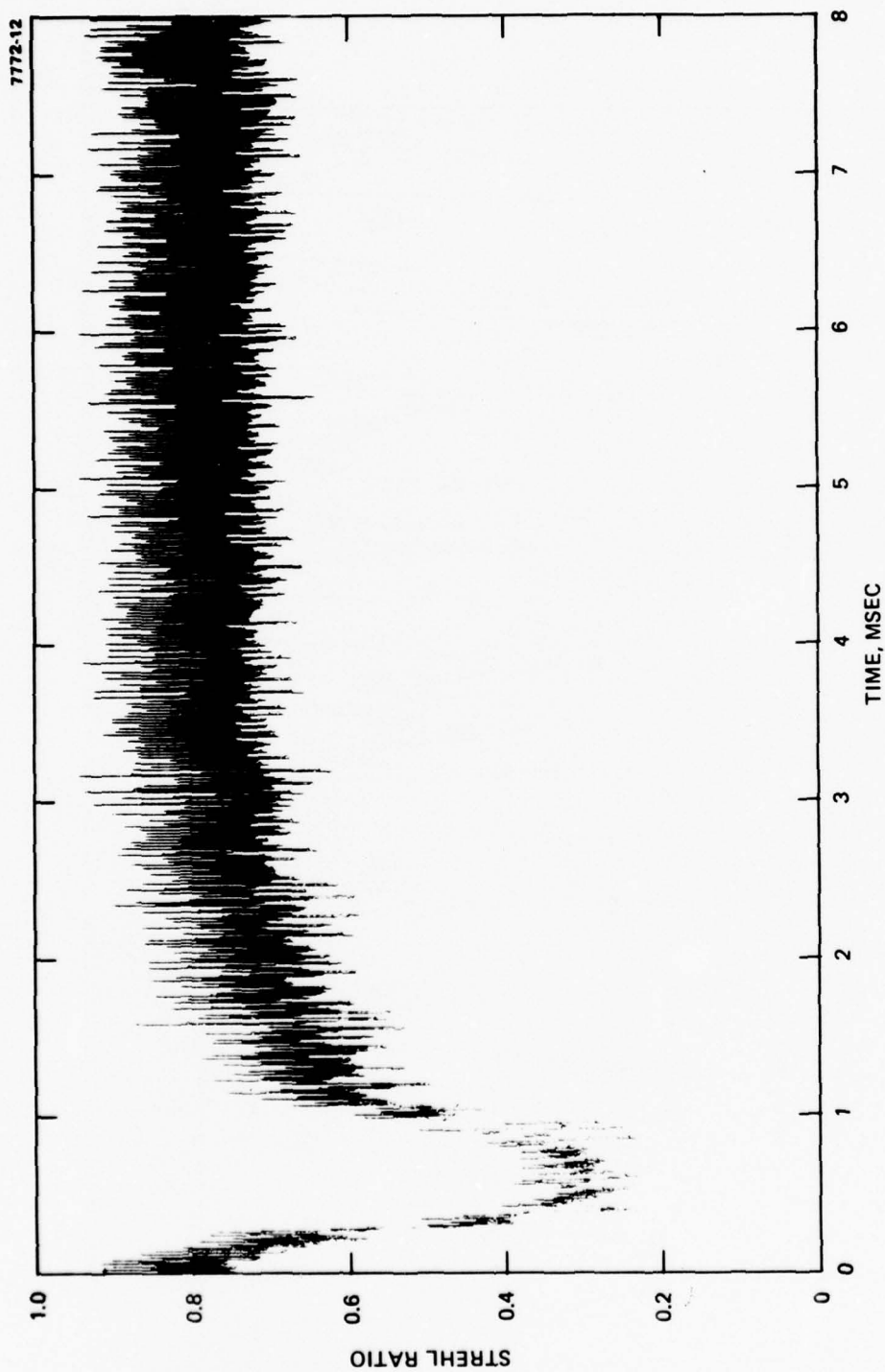
78

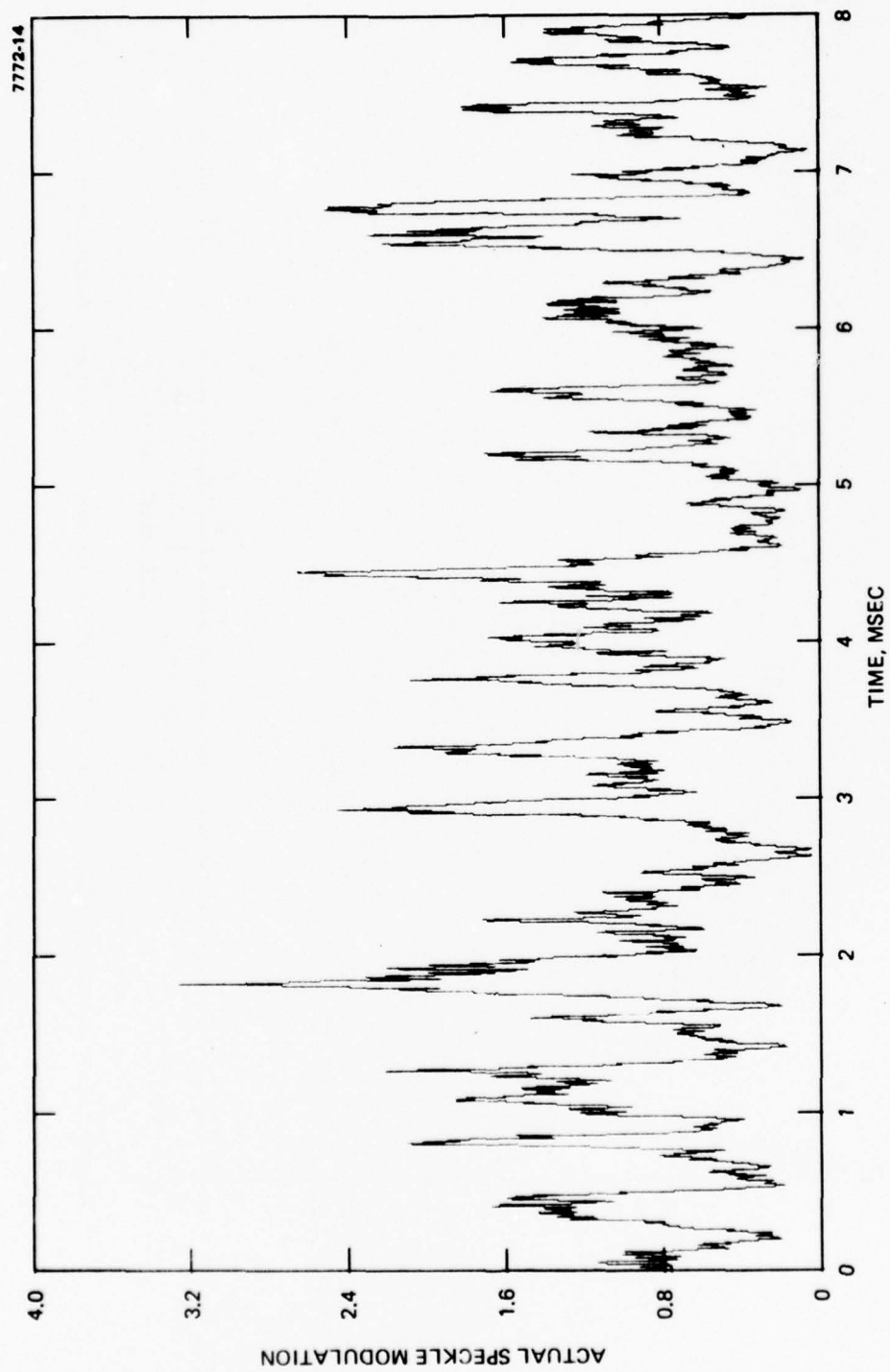Figure 20. Restored COAT performance ASPECT closed loop target rotation rate 10.0 rad/sec.

79

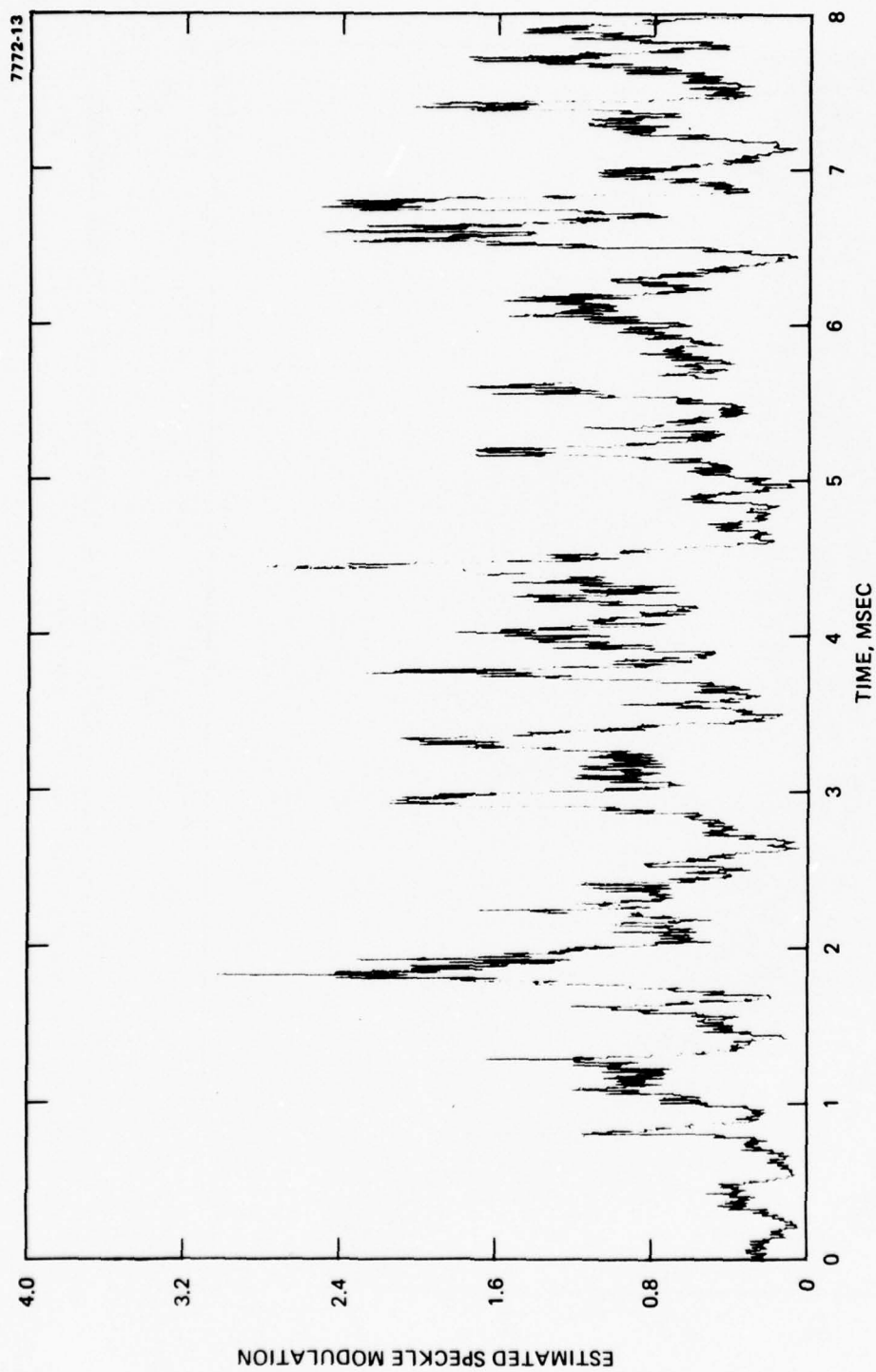Figure 21. Speckle modulation function used in computer simulations. Target rotation rate, 0.4 rad/sec.

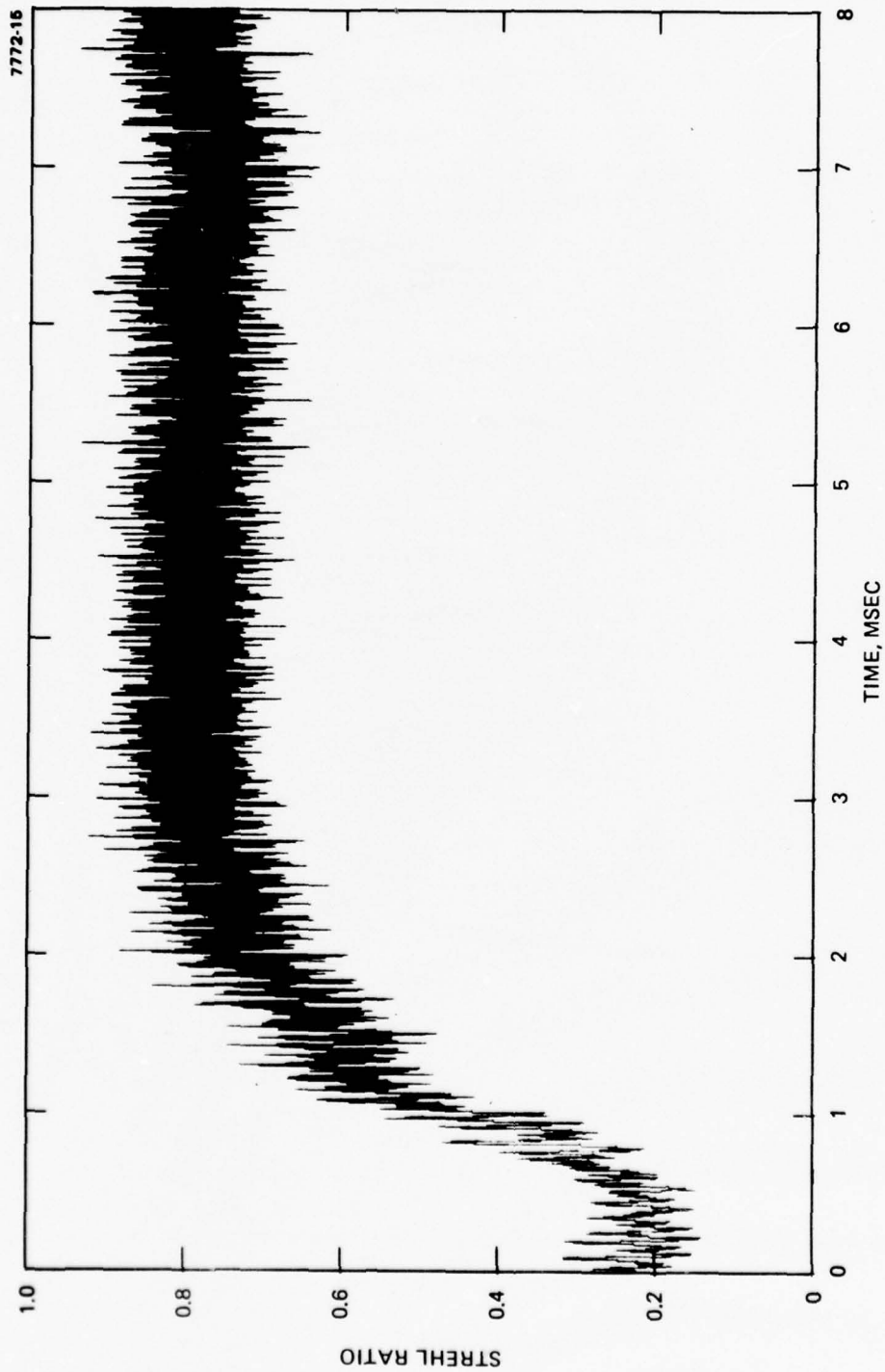Figure 22. Estimate of speckle modulation function of Figure 21.

81

Figure 23. COAT/ASPECT performance with speckle ASPECT dither frequency, 200 kHz division scheme. Target rotation rate 0.4 rad/sec.
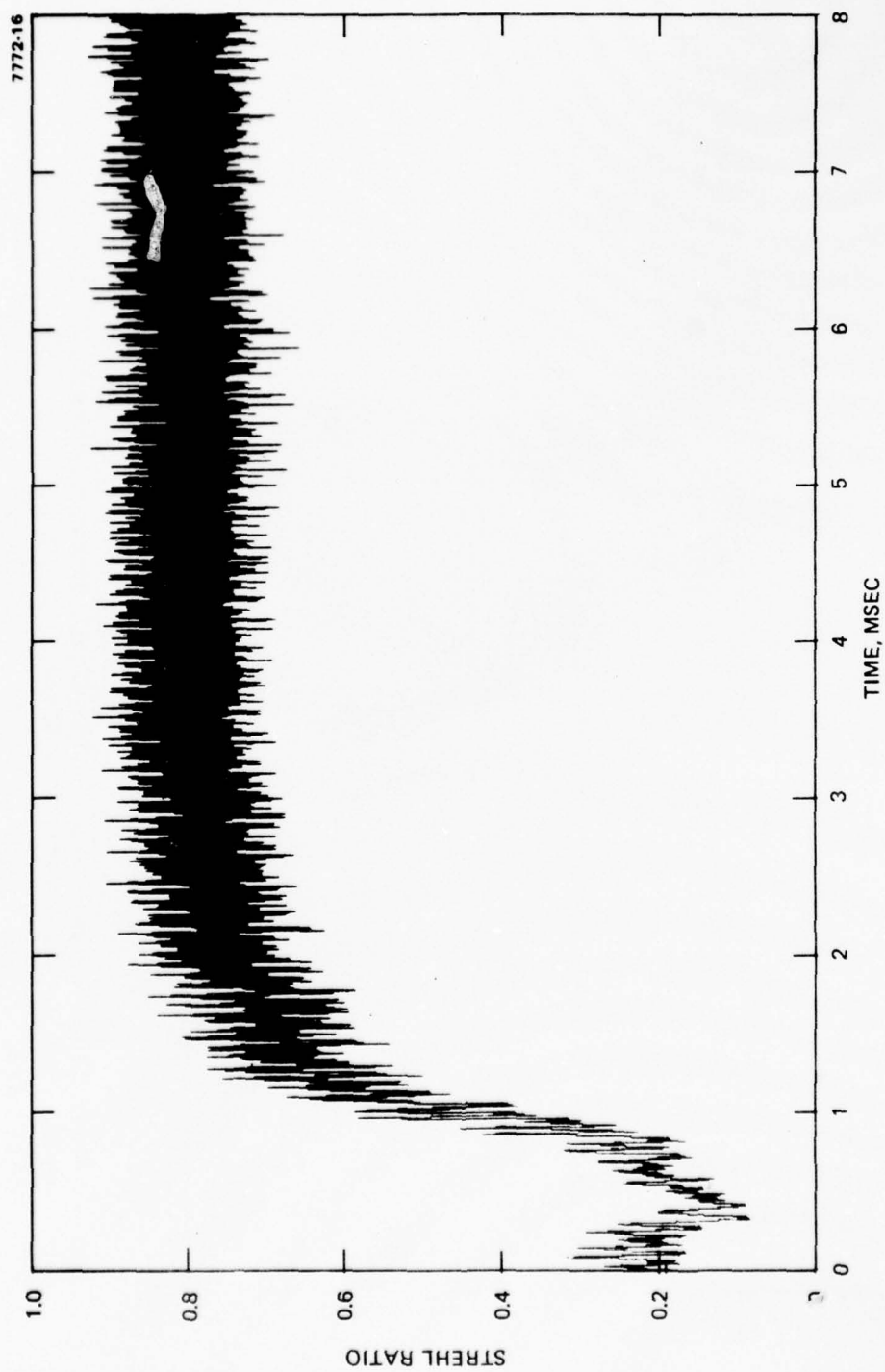
Figure 24. COAT/ASPECT performance with speckle ASPECT dither frequency, 200 kHz. Subtraction scheme target rotation rate 0.4 rad/sec.
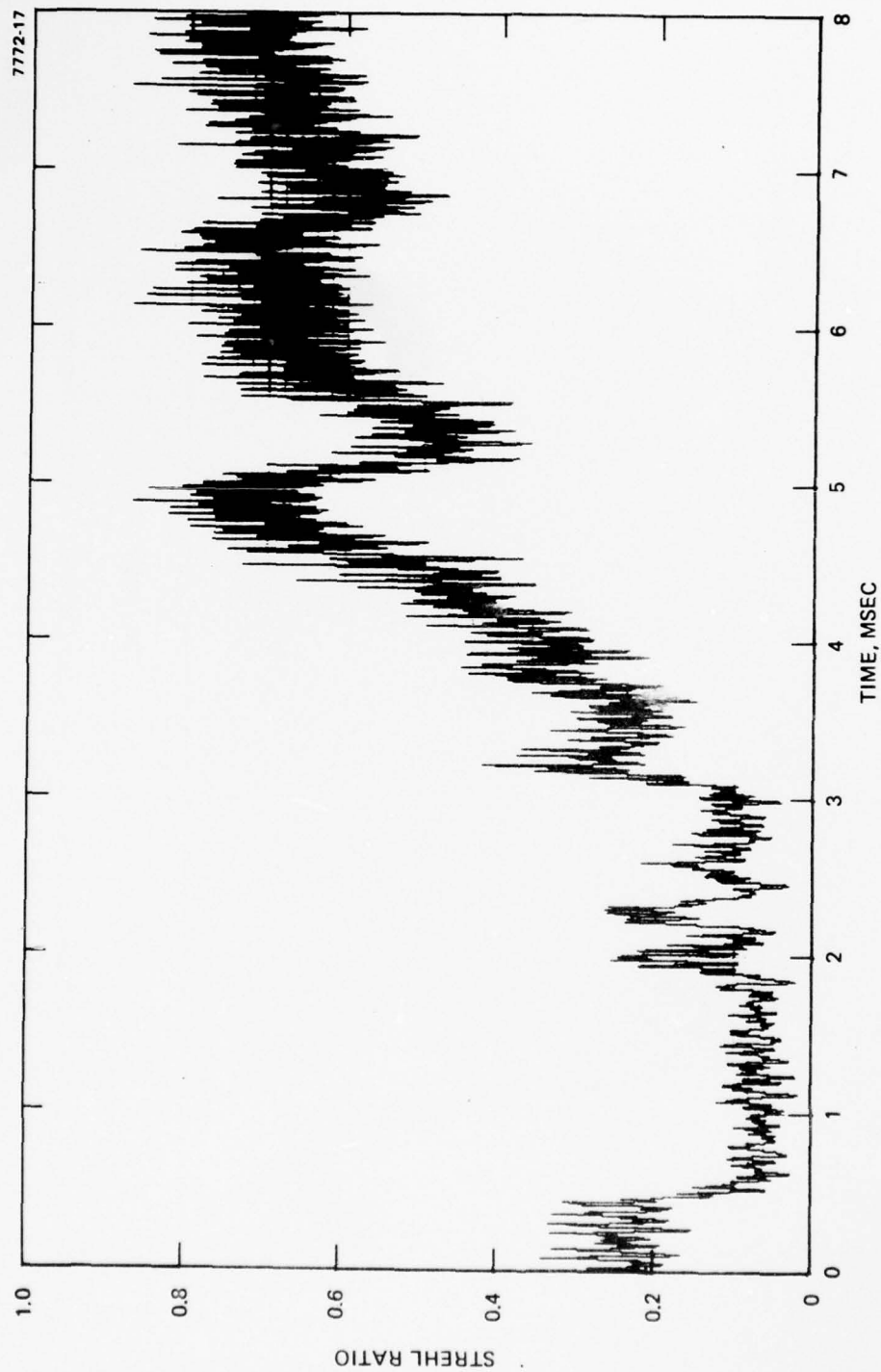
83

Figure 25.   COAT/ASPECT performance with speckle ASPECT dither frequency, 100 kHz. Division scheme target rotation rate 0.4 rad/sec.
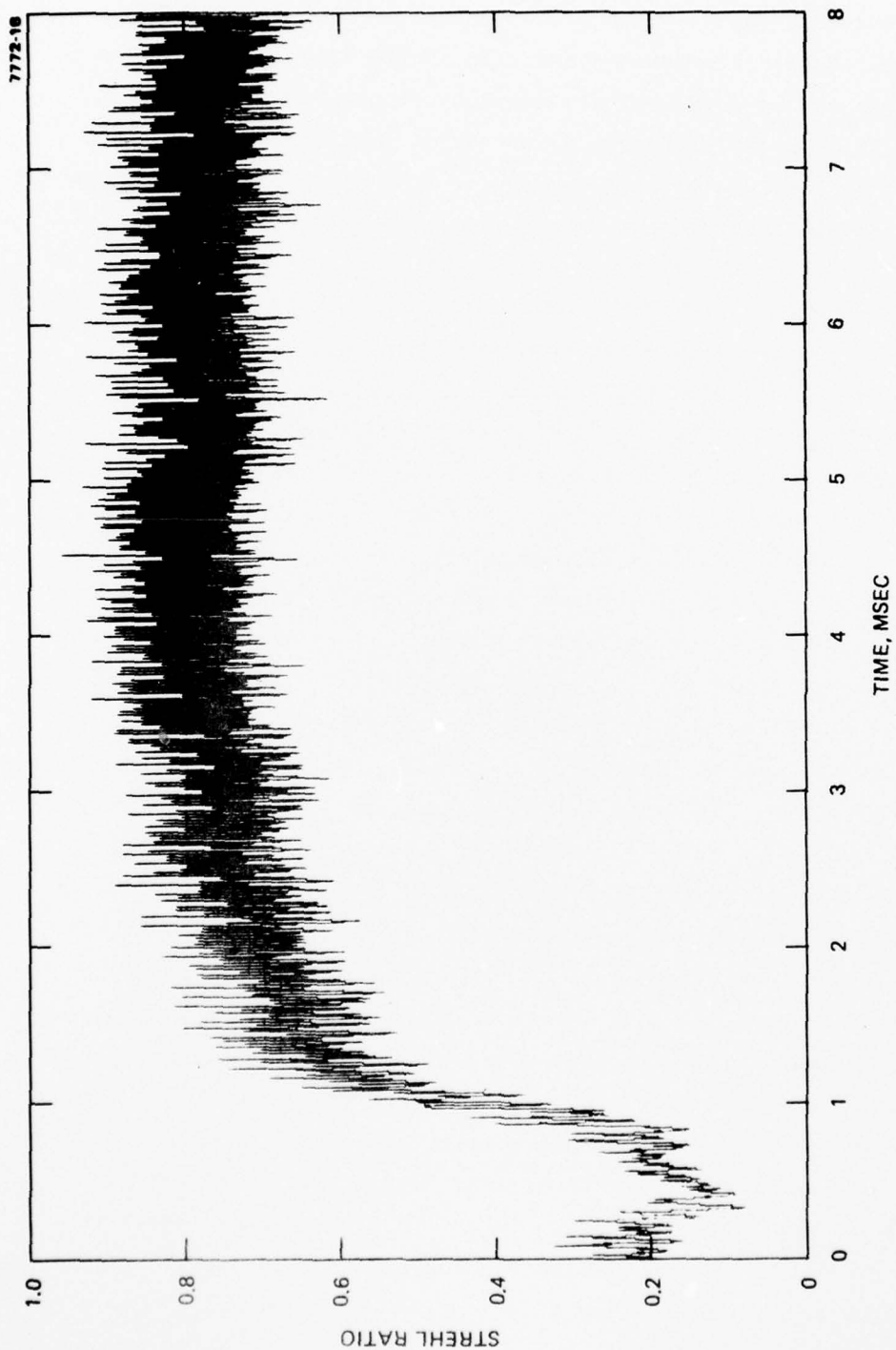
84

Figure 26. COAT/ASPECT performance with speckle ASPECT dither frequency, 100 kHz. Subtraction scheme target rotation rate 0.4 rad/sec.

of both schemes at 100 kHz. The average Strehl ratio for the division scheme is noticeably lower, but for the subtraction scheme it remains quite close to ideal. Simulations using an ASPECT dither of 50 kHz were also run. They showed a further degradation of performance of both schemes. In fact, at this frequency the ASPECT system actually caused more degradation than was originally present from the speckle modulations alone. The explanation for this behavior is presented below.

Consider the simplified hypothetical power spectrum (based on Eq. 4.8 and shown in Figure 27(a)) of a COAT receiver signal coming from a glint-like target return. There is a strong mean level at zero frequency, discrete dither signals, and additional signals at twice the dither frequencies displayed on an arbitrary frequency scale. There must, of course, be signals at all possible sums and differences of dither frequencies, but their amplitudes are very small compared to those shown. In addition to this, there is a discrete signal at twice the ASPECT dither frequency. Figure 27(b) shows a hypothetical speckle modulation spectrum. Since the receiver signal is the product of the speckle modulation function and the usual glint-like return, its power spectrum must, by the convolution theorem, be just the convolution of the former two spectra. This is shown in Figure 27(c). Notice that as long as the value of ASPECT carrier freuency $2\omega_A$ is significantly beyond the discrete signals associated with the glint return, the convolution process will reproduce the speckle modulation spectrum up to a multiplicative coefficient centered around the carrier frequency. The synchronous detection process then produces a signal that is instantaneously directly proportional to the speckle modulation function and also produces high frequency noise, which can easily be filtered. As the ASPECT dither frequency and therefore the carrier frquency are reduced, there will be more and more overlap between the frequency-shifted speckle modulation spectrum centered at the carrier frequency and the remaining lower frequency convolved spectrum. Therefore, the synchronous detection process will detect the erroneous overlap spectrum as well as the desired one, leading to a poorer estimate of the speckle modulation function.

(a) GLINT RETURN SPECTRUM

TWICE ASPECT DITHER FREQUENCY $2\omega_s$

TWICE THE DITHER FREQUENCIES $(2\omega_n)$

DITHER FREQUENCIES (ω_n)

(b) SPECKLE MODULATION SPECTRUM
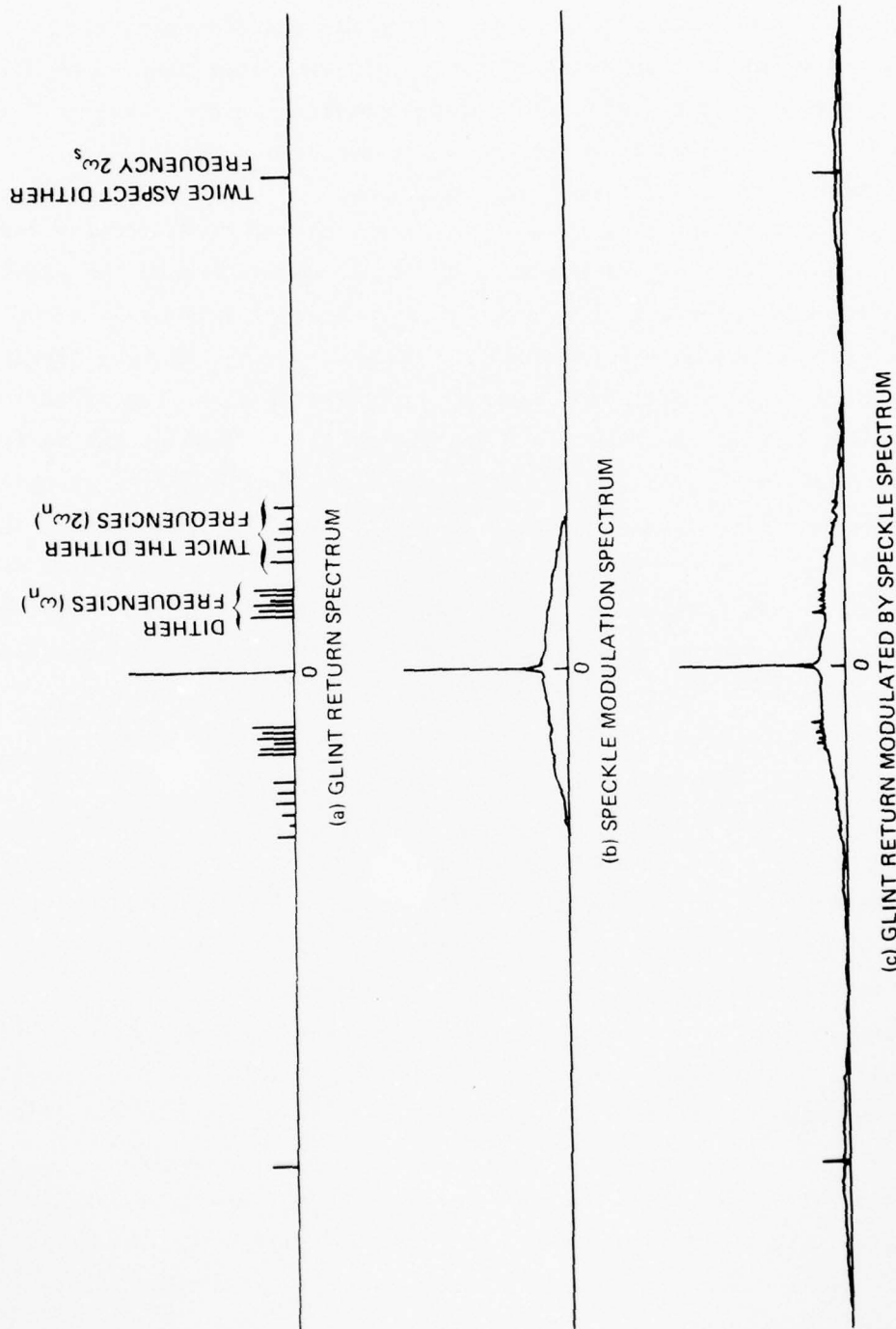
(c) GLINT RETURN MODULATED BY SPECKLE SPECTRUM

Figure 27. Hypothetical frequency spectrums of COAT receiver signal.

87

This also suggests why the subtraction scheme works better than the division scheme. A careful comparison of the two schemes will show that, if a perfect estimate of the speckle modulation function were available, the division scheme would cancel it completely while the subtraction scheme would leave residual uncancelled noise. On the other hand, when the estimate is not perfect, there will be some residual error using either method. Since the subtraction scheme is far less sensitive to error, it performs better under such circumstances.

To allow for a direct comparison between the experimental results and the computer simulation runs, we adjusted the input parameters to the simulation code to represent the actual laboratory system as closely as possible. The number of COAT channels was reduced from 18 to 7 having the same dither frequencies as the laboratory model described in Section 5.A. The ASPECT dither frequency was set at 50 kHz, and the corner frequencies of the various high- and low-pass filters in the ASPECT electronics where adjusted to the appropriate values. The division scheme of Figure 12(a) was used, since that was also the experimental configuration. The high-pass filter consisted of four poles with corner frequencies of 19.3 kHz each, while the two matching low pass filters had two poles each, and each pole had a corner frequency of 15.0 kHz. The COAT dither amplitude was 0.349 rad of wavelength in each channel, while the ASPECT piston dither amplitude was one-half a wave. A fraction $\eta_2 = 0.13$ of the optical field was used in the ASPECT beam; the remainder, $\eta_1 = 0.87$, was channeled through the usual COAT optics. Simulations were run using a single sine wave speckle modulation function at two different frequencies, one at 6.5 kHz and one at 13.4 kHz. In each case, the amplitude of the sine wave was 0.8 and the mean value was 1.0. Both of these modulations significantly degraded the COAT convergence level, or target Strehl ratio. In Figure 28 we show the ideal, no speckle, COAT target Strehl radio for this configuration. In Figures 29 and 30 we show how this ideal performance is degraded by the respective sine wave modulations. With the ASPECT loop opened, the average Strehl ratio at 6.5-kHz modulation is reduced to 0.36 of the ideal value; at 13.4 kHz, it is reduced to 0.51 of the ideal value. These two numbers can be directly compared to the experimental results in Section 5.B, where we observed a degradation to 0.39 of the ideal value at both of these frequencies.
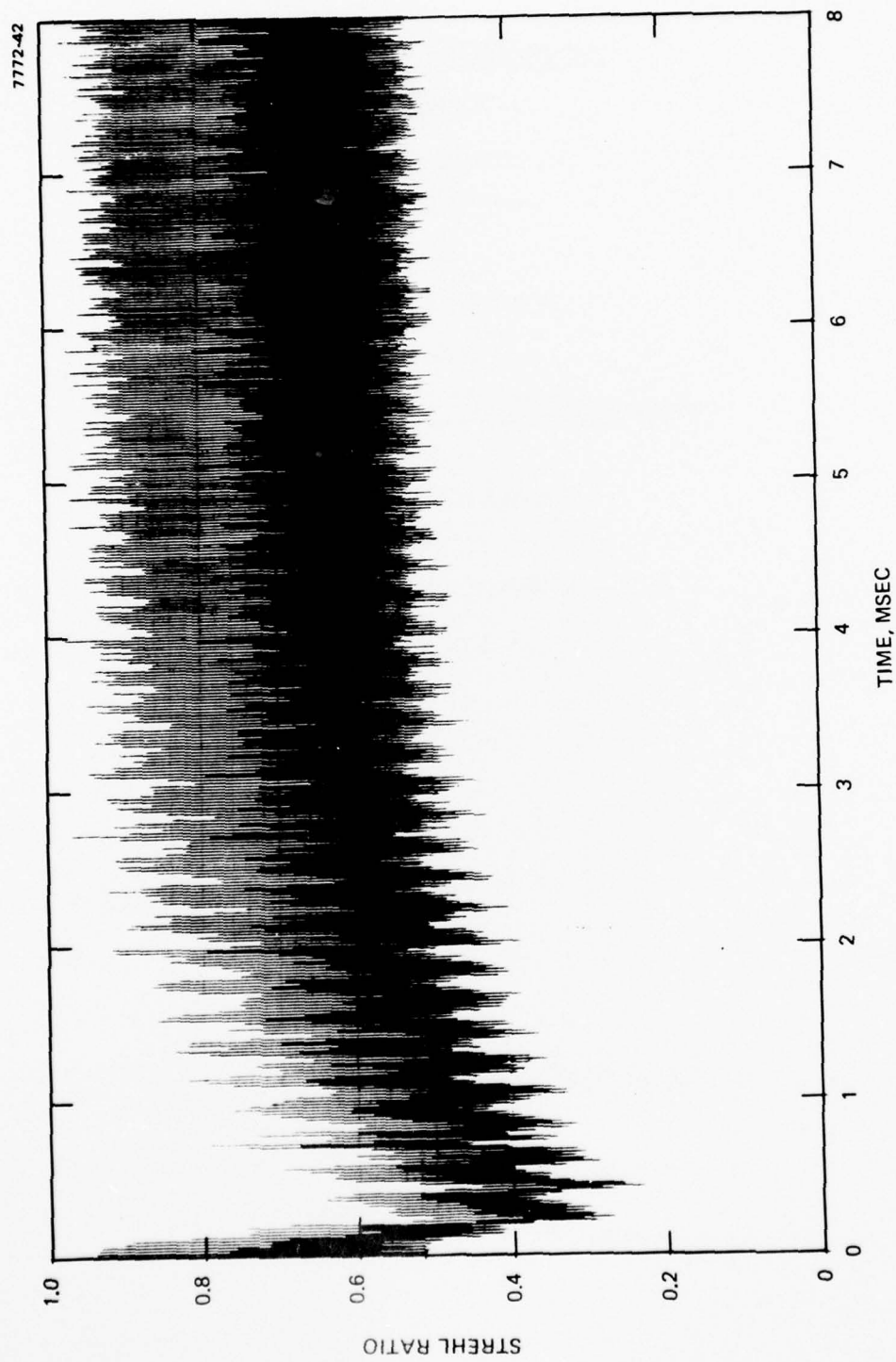
88

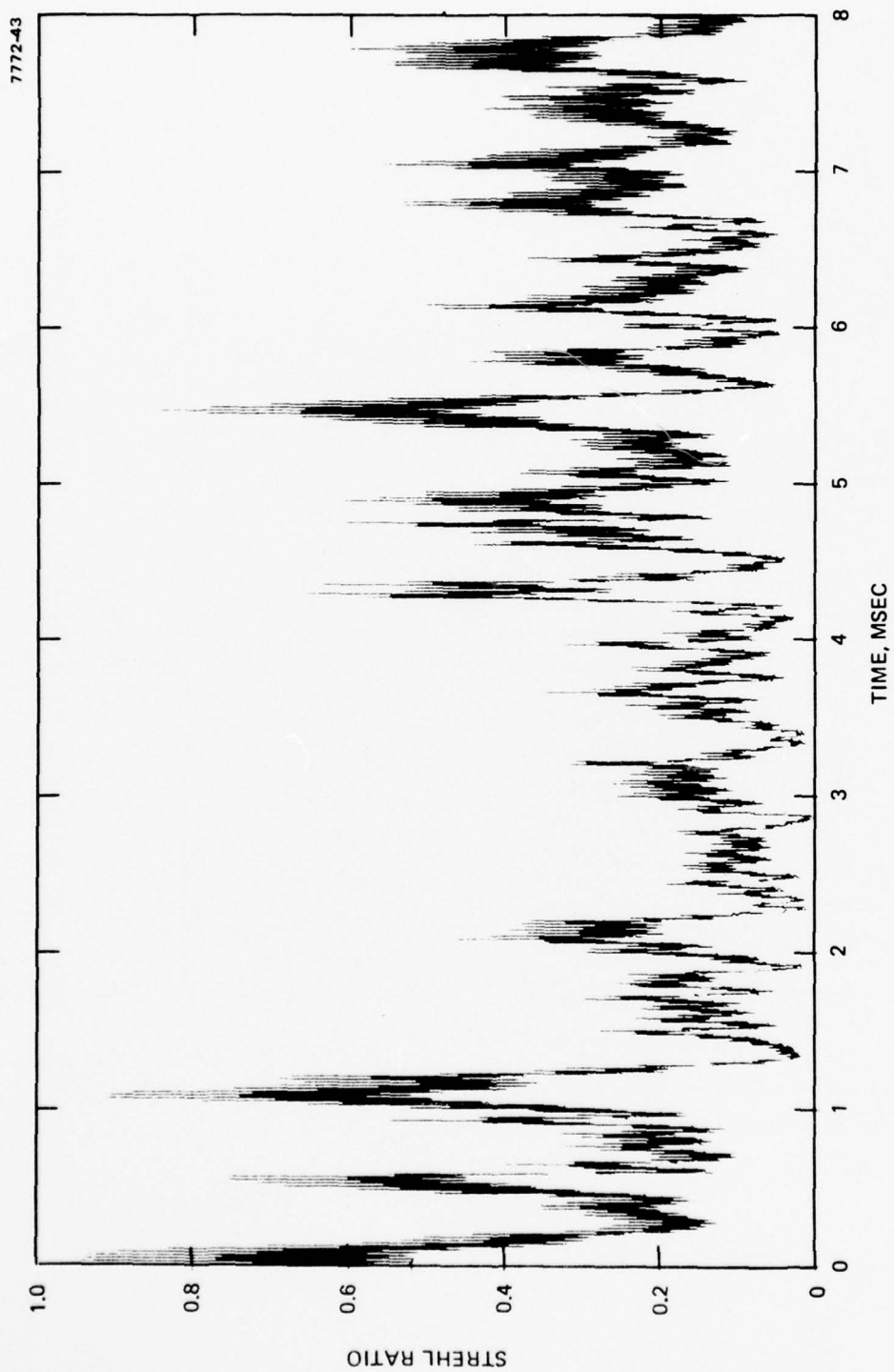Figure 28. Ideal, no speckle, COAT performance for laboratory configuration.

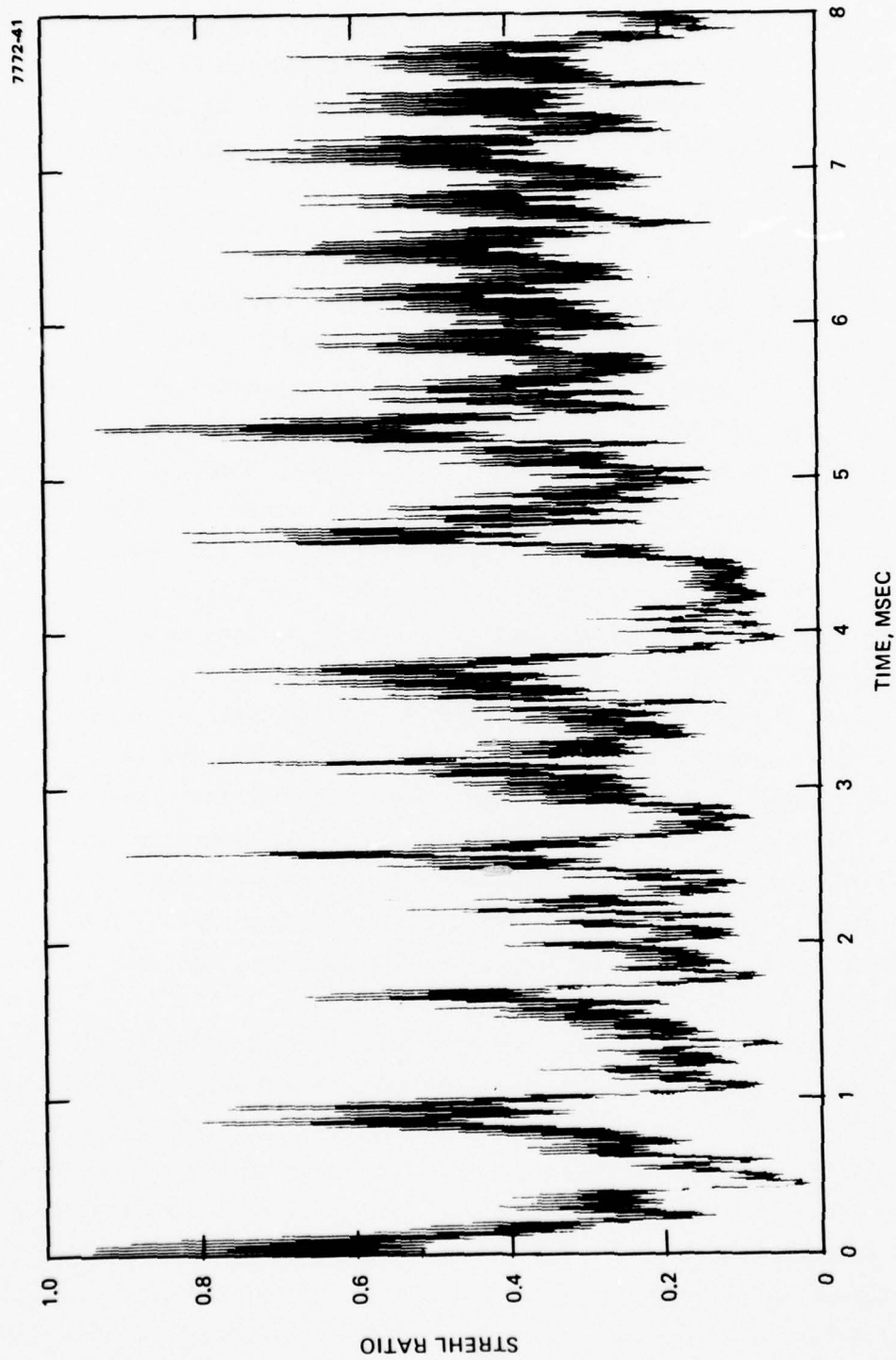Figure 29. Degraded COAT performance caused by sinewave modulation at 6.5 kHz.

90

Figure 30. Degraded COAT performance caused by sinewave modulation at 13.4 kHz.

Figures 31 and 32 show the ASPECT closed-loop results for the same two modulation functions. At 6.5 kHz, performance is almost fully restored, reaching 0.93 of the ideal level. At 13.4 kHz, the restoration is to 0.88 of ideal. This can be compared to 0.91 of ideal at 6.5 kHz, and 0.65 of ideal at 13.4 kHz, which are the corresponding experimental values from Section 5.B.

D.   CONCLUSIONS

The computer simulation results clearly demonstrate that it is possible to restore speckle-degraded performance of multidither COAT systems using an ASPECT cancellation scheme. High-quality estimates of the speckle modulation function can be generated if the ASPECT carrier frequency is substantially higher than the highest COAT dither frequency. If the ASPECT dither frequency is too close to the COAT dither band, then poorer estimates and consequently poorer cancellation will be achieved. As a general rule, our data indicate that the frequency interval between the highest COAT dither and the ASPECT carrier should be no less than 6 and prefereably about 10 times the highest COAT dither frequency. This will ensure that the available bandwidth around the carrier will be broad enough to faithfully reproduce the true spectrum of the speckle modulation function up through the entire COAT dither band. Beyond that frequency range it is no longer necessary to cancel any of the speckle modulations because they do not produce any significant interference. The spectral range of the speckle modulation function is also important. But since it depend on such parameters as target motion, geometry, and surface characteristics, it cannot be anticipated a priori.

There are several other important system parameters besides dither frequency that will influence the quality of the ASPECT estimates. The amount of energy in the secondary beam and the amplitude of the ASPECT dither are both very important in determining the strength of the carrier signal. To achieve a strong, easily detectable carrier it is desirable to dither with an amplitude of about half a wave. If the percentage power in the probe beam is large, it would have the effect of reducing the mean Strehl ratio or convergence level as well as the strength of the normal COAT error-correction signals at the dither frequencies.
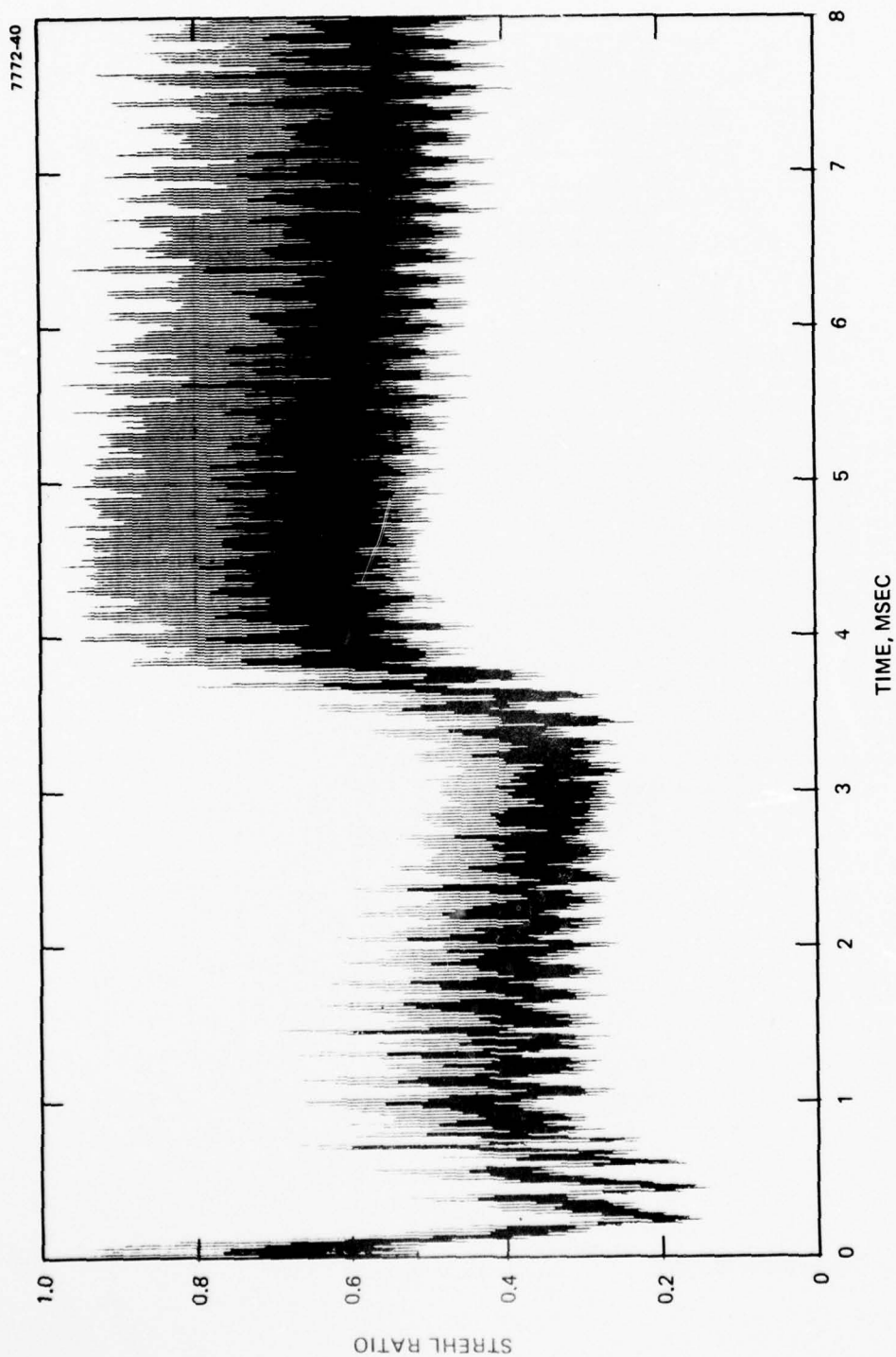
Figure 31. ASPECT restored COAT performance with 6.5 kHz sinewave modulation.
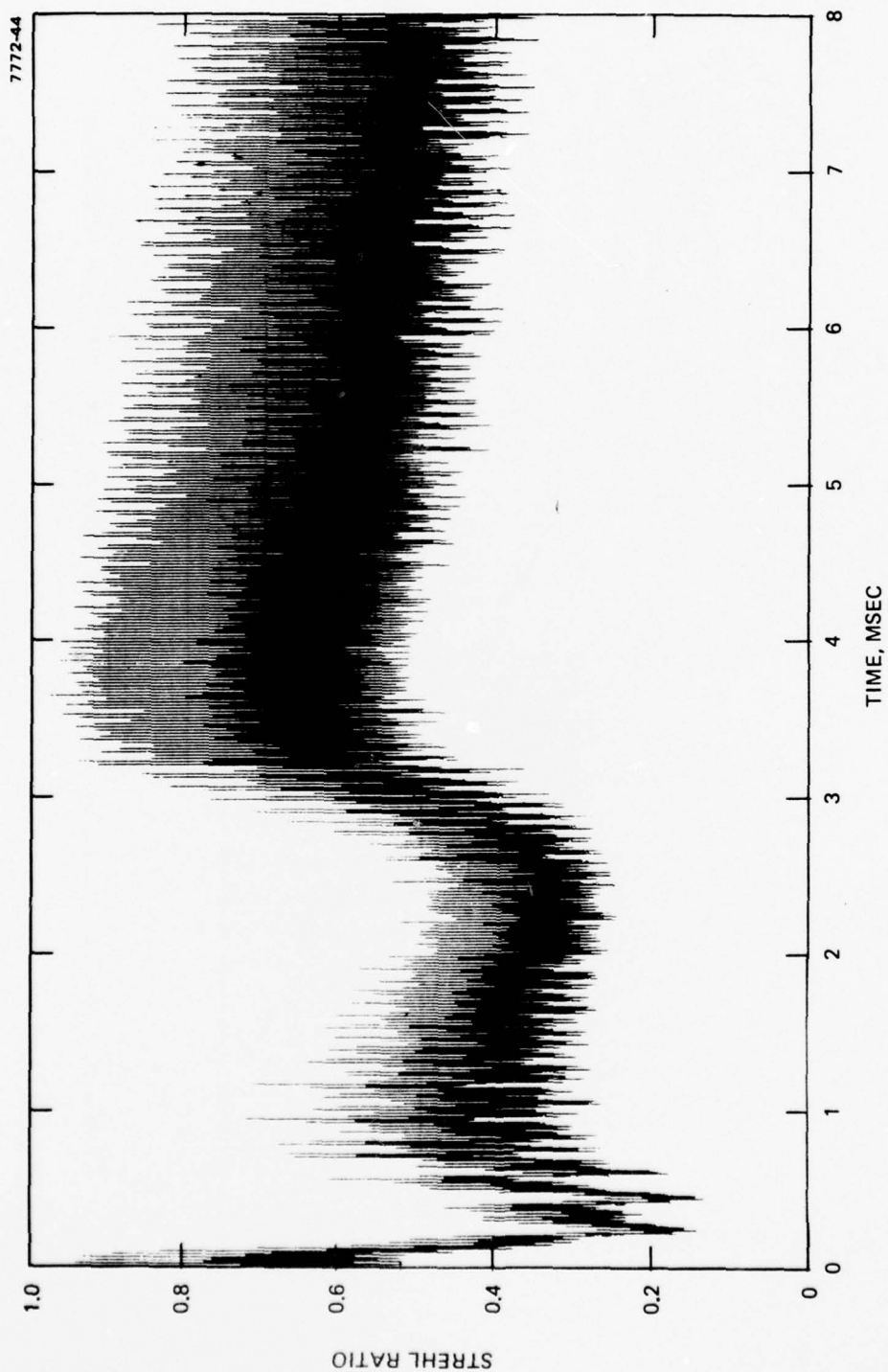
7772-44

STREHL RATIO

TIME, MSEC

Figure 32. ASPECT restored COAT performance with 13.4 kHz sinewave modulation.

94

Similarly, increasing the energy in the ASPECT probe beam would increase the strength of the carrier at the expense of the convergence level and dither signals. Since we were primarily interested in demonstrating the ASPECT concept and supporting the experimental effort, no attempt was made to optimize these parameters.

We also found that the subtraction scheme for canceling speckle interference is generally better than the division scheme. The division scheme is a mathematically more precise scheme in the sense that, given a perfect estimate of the speckle modulation, it would achieve perfect cancellation. The subtraction scheme on the other hand would leave residual uncanceled interference, even with a perfect estimate. But since the estimates are never perfect, the subtraction scheme usually performs better because it is less sensitive to errors.

The success of the subtraction scheme also demonstrates that, for the special case discussed in Section 3.E, in which the speckle interference cannot be characterized by a single multiplier, cancellation of the dc multiplier is all that is really ncessary because the ac multiplier will produce negligible interference in the COAT convergence process.

SECTION 5

ASPECT EXPERIMENTAL STUDIES

A. EXPERIMENTAL HARDWARE AND ELECTRONICS

The ASPECT system used in our experimental studies is an add-on system intended to "piggyback" the present laboratory COAT electronics thereby forming a complete adaptive optics speckle cancelling system. In the optical arrangement, the existing optics and light paths surrounding the operation of the present COAT deformable mirror remain unchanged except for the inclusion of two beam splitters, which are used in the ASPECT optical channel (see Figure 33 for the ASPECT optical layout).

The light source for the experiment was an argon laser tuned to 4880 $\overset{\circ}{A}$ and equipped with a rotatable $1/2$ λ plate and etalon. The beam coming from the laser goes to a spatial filter and lens (L1) where it is expanded and collimated and directed to the first beam splitter (BS1). This is the point of origin for the ASPECT probe path, which is marked by the broken line in Figure 33. The alternate COAT path is marked in Figure 33 by a solid line. Starting at the beam splitter and following along that path, we first come to lenses L2 and L3. These lenses form an expanding telescope to fill the deformable mirror with collimated light. After leaving the telescope, the beam passes through another telescope, consisting of lenses L3 and L4, which reduces the beam to its original size. After the light passes through lens L4, it is again collimated and directed to the second beam splitter BS2, after which it enters lenses L5 and L6, forming the final telescope. After leaving lens L6, the beam illuminates the target (a small piece of Scotchlite in a field of black velvet), and the spectral return from Scotchlite is received by photomultiplier (PMT1).

The ASPECT light path begins at beam splitter BS1, where the light is directed to mirror M3 and into lens L7 (the first lens of a 1 to 1 telescope). Since the dither actuator mirror (PZT1) is smaller than the beam entering lens L7, it is positioned just before the focal point of
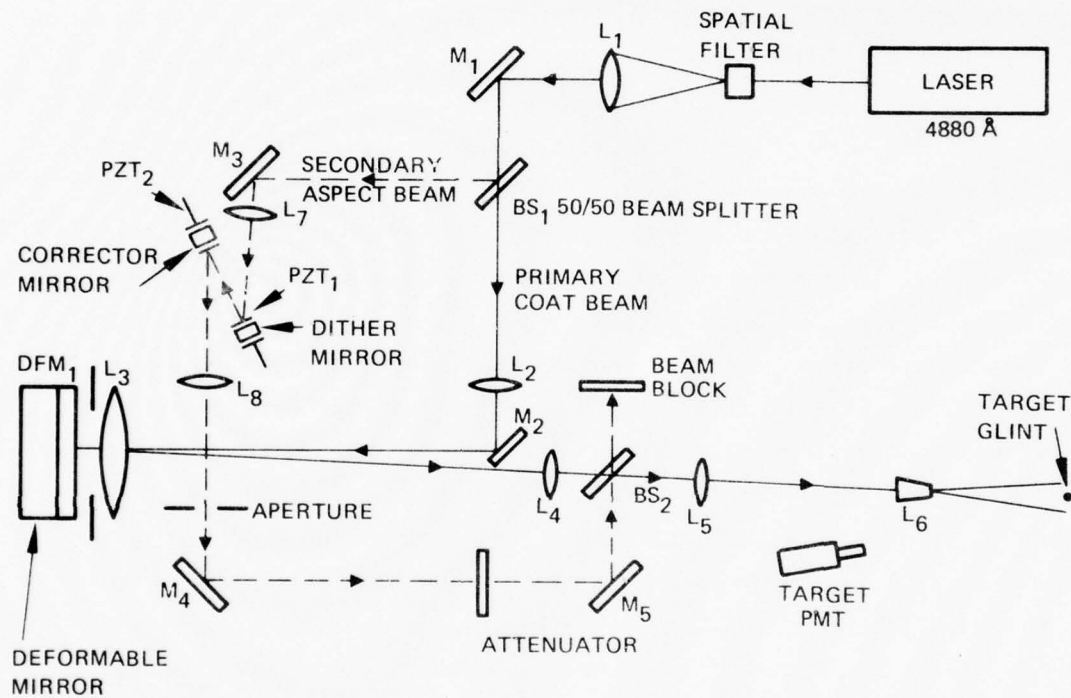
Figure 33. ASPECT optical layout.
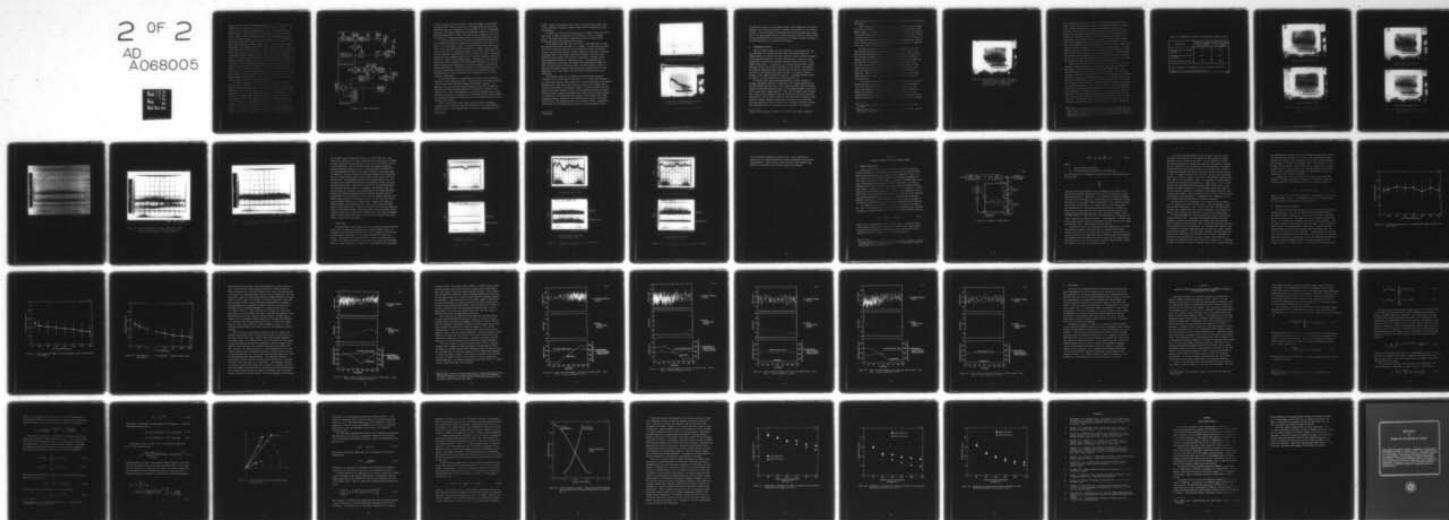
that lens and directed with minimum angle toward the corrector mirror (PZT2), which is positioned just after the focal point of lens L7. The light is then propagated through L8, the output lens of the telescope. Actuator mirror (PZT1) encodes the ASPECT beam with a 50-kHz dither signal, which is then synchronously detected in the same manner as the usual COAT dither signals. The resultant signal from the synchronous detection process then becomes the error signal which is applied to the path balancing corrector mirror, PZT2, which performs the path length adjustments, ensuring that the ASPECT beam is properly phased relative to the COAT beam at the target glint. After leaving lens L8, the encoded ASPECT beam passes through an aperture, where its size is adjusted to accommodate a proper overlay with the COAT beam at the beam splitter (BS2). In the far field, mirrors (M4) and (M5) provide the position and angle adjustments needed to control the interference pattern between the two beams. Before the beam leaving mirror (M5) reaches beam splitter (BS2), it passes through attenuator (AT1), where the intensity ratio between the two beams may be adjusted. In the experiments described in Section 5.B, we typically measured power levels of approximately 0.15 mW in the ASPECT beam and 7.0 mW in the COAT beam. These measurements were made following lens L5 in the optical layout, one beam being totally blocked while the power in the other was measured.

As shown in Figure 34, the ASPECT electronics system consists of three separate components: (1) a local loop subsystem, (2) a speckle simulation subsystem, and (3) a speckle detection loop. The local loop subsystem is essentially a copy of any one of the COAT channels.[5] With the exception of its higher dither frequency, all other parameters remain the same. A 50-kHz master oscillator supplies the input to the local loop's dither driver, which in turn tags the ASPECT optical beam with a $\pm \lambda/2$ phase dither via the ASPECT dither mirror. This oscillator also supplies the input to the adjustable phase shifter, which compensates for the phase delay in the dither driver electronics, PZT actuators, and preamps. The output of the phase shifter is the reference input to the local loop's synchronous detector, and the output of the detector drives
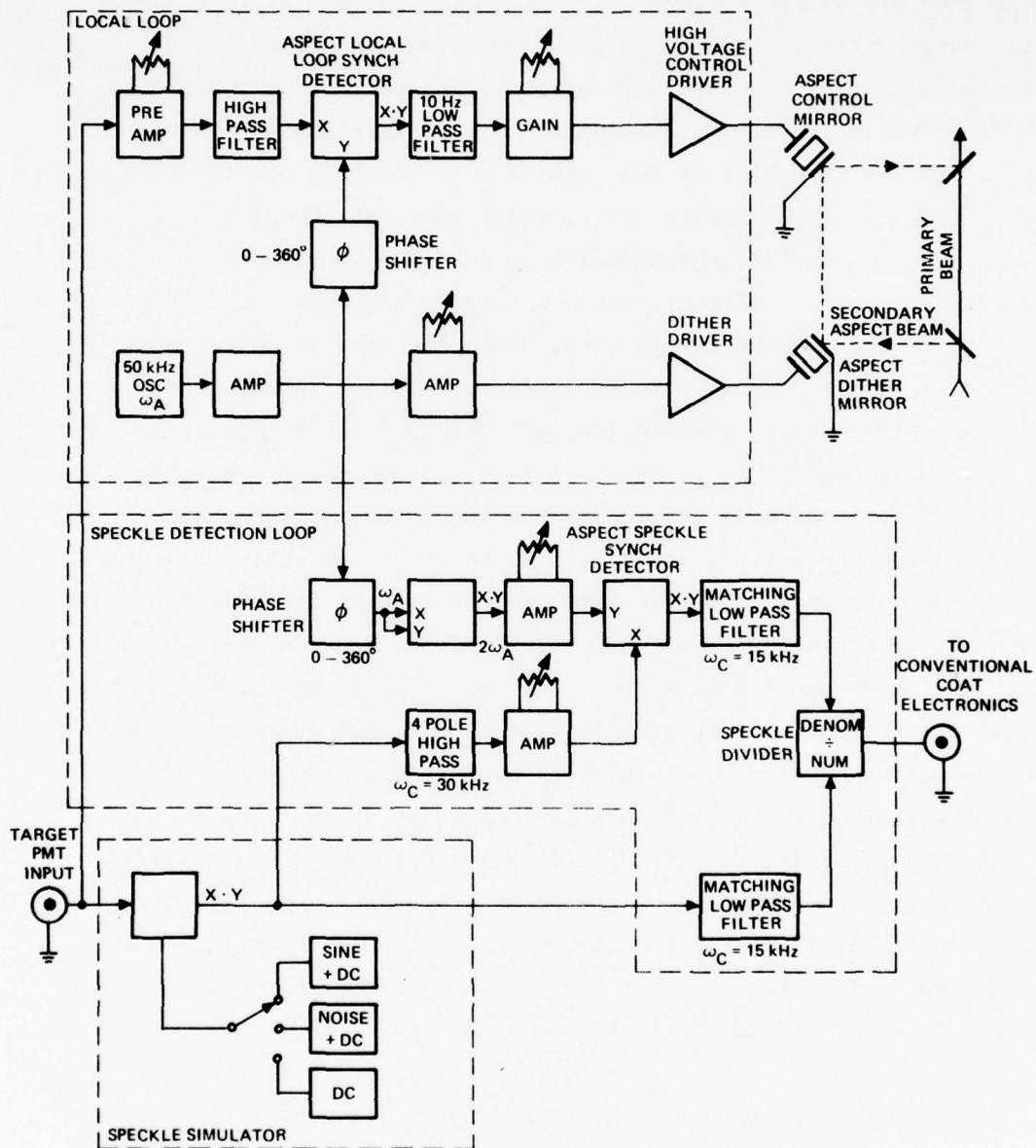
Figure 34. ASPECT electronics.

100

a 10-Hz[*] low-pass filter to provide a correction signal for the ASPECT corrector mirror (PZT2 of Figure 33). The signal input the local loop synchronous detector originates at the target PMT. Prior to synchronous detection, this signal is amplified and high-pass filtered to remove the undesired signals below 50 kHz. Two controls are provided in the local loop system: a preamp gain control and a correction signal gain control.

The speckle simulator shown in Figure 34 represents the multiplicative speckle interference discussed in varying detail in Sections 2, 3, and 4. It was necessary to use an artificial multiplicative noise source rather than a true speckle pattern because of a signal to noise problem in the target PMT and associated preamps. Even at full laser power, the receiver aperture of the PMT had to be quite large (an order of magnitude larger than the transmitter aperture mm) in order to operate in the shot-noise-limit range of the photomultiplier. Although this large aperture provided a very good signal to the COAT/ASPECT electronics, it also produced enough aperture averaging of the speckle pattern to preclude any speckle interference. Therefore, we chose the following scheme for electronically generating a multiplicative noise that would have a power spectrum similar to that observed from the backscatter of a rotating, optically rough sphere.

We used noise diode as a broad-band noise source and an adjustable amplifier to give amplitude control. This noise has a zero mean value and a flat spectrum well beyond the highest COAT dither frequency. To generate a strictly positive speckle modulation function, the noise was then passed through an analog multiplier to produce the square of the original noise. This was followed by a selectable low-pass filter, which allowed for modeling the frequency roll off characteristics always present in any speckle pattern, and in particular those patterns associated with a rotating target sphere.

Since a true speckle noise always contains effects of apreture averaging, which prevent it from ever reaching zero, we also introduce a small dc offset in the simulated noise to ensure a consistently positive

---

[*] 3 dB point.

101

signal. Figure 35(a) shows a scope trace of a typical noise signal used in the laboratory experiments; Figure 35(b) shows its spectrum on a spectrum analyzer.

In addition to the noise described above, the speckle simulator could also inject a single sine wave with a dc offset, or just a dc signal alone. The latter was used for comparative purposes to show how the systems operated without speckle interference.

In the speckle detection loop, the output of the target PMT is first multiplied by the noise, sine wave, or dc signal. It then takes two paths, one to the 15-kHz* low-pass filter in the numerator leg of the speckle divider, and the other through a 30-kHz* high-pass filter where it becomes the signal input of the speckle synchronous detector. With the interferometer loop converged, this signal is essentially a 100-kHz carrier whose modulation envelope is the speckle noise. The numerator path is almost identical to the usual COAT signal processing without ASPECT, the only difference being the low-pass filter that was inserted to match or duplicate the signal distortion introduced by an identical filter in the denominator leg. This assures that the division process will be time synchronous.

The reference signal to the ASPECT speckle synchronous detector originates at the 50 kHz master oscillator. It is first passed through a 0 to 360° phase shifter, which adjusts for the total phase lag in the speckle detection loop. The output from this phase shifter goes directly into a multiplier configured as a frequency doubler, creating a 100-kHz sine wave which is the actual reference input. On synchronous detection, the multiplicative noise is recovered and additional high-frequency product signals are introduced. The matching 15 kHz low-pass filter removes these high-frequency products, leaving only the multiplicative speckle noise, which then serves as the denominator input to the speckle divider. Depending on the fidelity of the synchronously detected and filtered speckle noise

_____

*3 dB point.

ARBITRARY
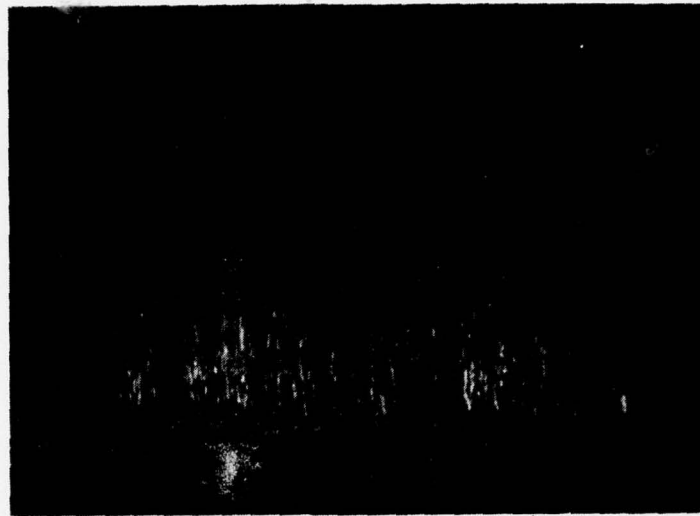
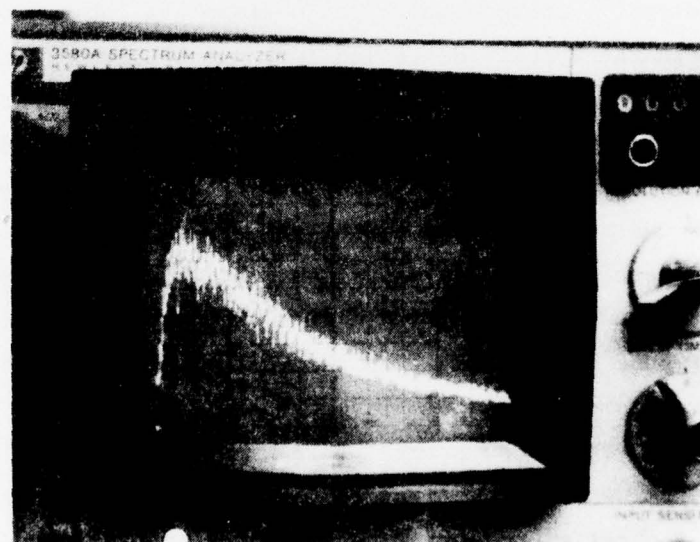0.5 MSEC

(a) TYPICAL NOISE SIGNAL AS A FUNCTION OF TIME

(b) SPECTRUM OF (a). HORIZONTAL SCALE IS 2 kHz/DIV.
VERTICAL SCALE LINEARLY NORMALIZED.

Figure 35. Simulated speckle interference.

estimate with respect to the original speckle noise coming from the speckle simulator, we can achieve partial or complete cancellation by the division process. Since introducing the matching low-pass filters generated a phase lag in the output signal from the speckle detection loop, the relative phase in the synchronous detector oscillators of the higher frequency channgles of the COAT system had to be adjusted accordingly.

B. EXPERIMENTAL RESULTS

When the ASPECT system was first attached to the existing COAT system, and before any attempt was made to get experimental data, the limitations of the hardware were made evident by limited frequency response in the available amplifiers, drivers, and actuators. Because of these limitations, 50 kHz was the maximum achievable dither frequency for the ASPECT dither mirror. Consequently, the maximum available probe carrier frequency used in the speckle detection loop was 100 kHz. According to the computer simulation results discussed in Section 4.C, this would be too close to the highest COAT dither (32 kHz) to provide an adequate estimate of the speckle modulation function. A minimum frequency ratio* of about 6 or 7 was required; the actual value was 3.13.

To verify these conclusions experimentally, several attempts to produce reasonable estimates of single sine wave speckle modulations in the COAT dither band were made. Even though the signal from the speckle simulator always had positive polarity, the estimated signals would often drop to zero and/or change polarity. This type of signal could obviously not be used as the denominator input to the divider without introducing large errors. The estimator output was also very noisy, containing large amounts of higher frequency modulations in addition to the particular sine wave being replicated, in spite of the low-pass filtering following the synchronous detector that generates the estimates. An attempt to

---

*Probe carrier frequency divided by the highest COAT dither frequency.

104

close the loop revealed unstable oscillations or fluctuations in the receiver PMT signal.

The separation of the 100-kHz probe carrier frequency from the highest COAT dither (32-kHz) was not large enough to generate a good speckle estimation signal. To achieve the necessary frequency separation, the number of active COAT channels had to be reduced from 18 to 7 with the highest dither frequency being 15 kHz.* This gave a frequency ratio of 6.67, which was in the range that should allow a reasonable estimate and appreciable cancellation. However, the computer simulation data still suggested that complete cancellation was not to be expected.

The above modifications required extensive adjustments in the COAT servo parameters that are too numerous to detail here.** Suffice it to say that the COAT/ASPECT system, including optical paths and electronics, was once again optimized to the point where the systems performed well without speckle interference and the speckle estimator could be monitored and observed. On introducing a totally positive polarity and single sine wave plus dc offset disturbance having a frequency inside the COAT dither band, the speckle estimator reproduced that same sine wave combined with appreciably reduced high-frequency noise (intermodulation products). With the improved electronics, the polarity of the estimate remained positive, indicating that the divider would work much better than previously.

In our initial experiments, we observed the performance of the entire system open and closed loop for two particular sine wave disturbances: at 6.5 kHz (the second lowest COAT dither frequency) and at 13.4 kHz (the second highest COAT dither frequency). Some results are shown in Figures 36 through 41. Figure 36 shows the Fourier spectrum of the signal from the target PMT under normal COAT operating conditions without speckle interference. Under these conditions, the beam is well converged

---

*
The new dither frequencies were 5.0, 6.5, 8.0, 9.5, 12.0, 13,4, and 15.0 kHz.
**
Unless otherwise specified, all parameters given in this report reflect this final configuration.
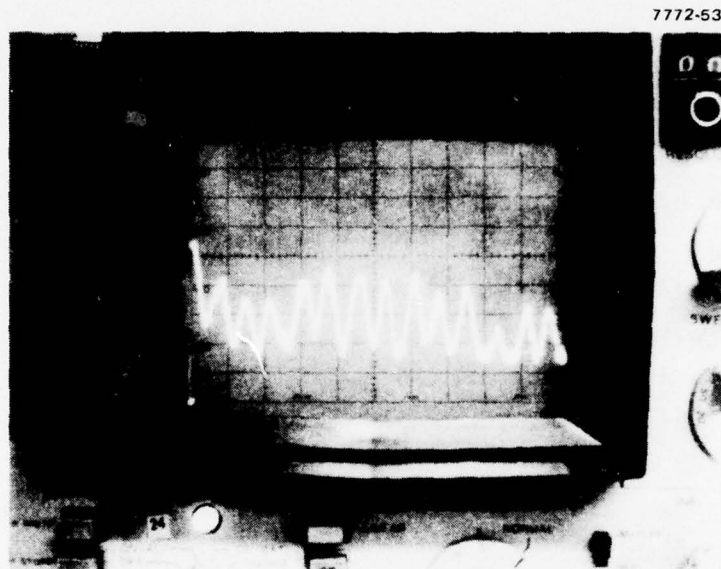
7772-53

Figure 36. Fourier spectrum of target PMT signal
for normal COAT operating conditions.
Horizontal scale: 2 kHz/division.
Vertical scale: 10 dB/division.

on the target and the spectral power at each dither frequency is quite small. These signals consist largely of noise, small amounts of energy at the dither frequencies, and various intermodulation produce frequencies. When we inject the single-frequency sine wave plus dc offset speckle multiplier via the speckle simulator and at the same time effectively open the speckle detector loop by channeling dc voltage* to the denominator of the speckle divider, we disable the COAT channel having that same frequency and to some extent the remaining channels as well. This is evidenced by the increased power at 6.5 kHz (shown in Figure 37(a)) and by the increased power at 13.5 kHz (shown in Figure 38(a)). In both figures, there is a slight increase in spectral power throughout the COAT dither band, which indicates lower overall convergence. When the ASPECT speckle detection and estimation loop is activated, most of the disturbing sine wave is cancelled and the power spectrum of the target PMT signal is returned to normal, as shown in Figures 37(b) and 38(b).

Figures 39, 40, and 41 show the effects of the above sine wave disturbances on the PMT signal as a function of time. The mean value of this signal is directly proportional to target illumination and is therefore indicative of the degree of COAT convergence. The top trace in Figure 39 shows the reference ideal signal with no speckle interference. The middle trace shows the degraded signal that results when the 6.5-kHz sine wave is introduced and there is no ASPECT cancellation. The bottom trace is just the reference zero voltage resulting from totally blocking the target PMT aperture. The top trace in Figure 40 shows the improved signal level resulting from the ASPECT cancellation of the 6.5-kHz sine wave modulation. The middle and bottom traces are the same as those in Figure 39. Finally, Figure 41 shows the improved signal level and the zero reference that result from the ASPECT cancellation of the 13.4-kHz sine wave. The degraded signal for this case is not shown, but it was virtually indistinguishable from the 6.5-kHz case. Table 1 summarizes

---

*This is done by adjusting the corner frequency on the usual 15-kHz low-pass filter to a much lower value making the divider a simple gain control in the COAT servo loop. Since there is an automatic gain control immediately following the divider, this modified gain does not change the normal COAT servo behavior.

Table 1. Comparison of Experiment and Computer Simulation Data

Disturbance	Normalized Target Glint Irradiance[a] without ASPECT	Normalized Target Glint Irradiance[a] with ASPECT
Sinewave plus dc offset[b] 6.5 kHz	0.39	0.91
Sinewave plus dc offset[b] 13.4 kHz	0.39	0.65
Speckle noise of figure	0.48	0.92

[a]The irradiance is normalized to the no speckle noise level.

[b]Ratio of ac to dc was approximately 0.8.

6352

108
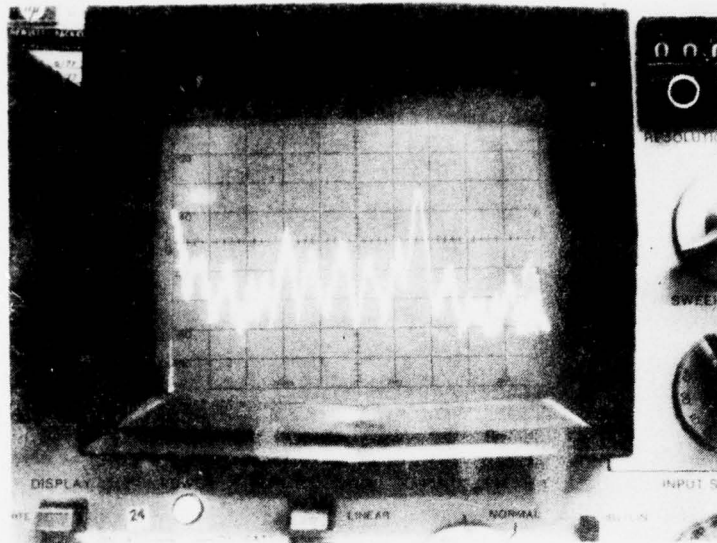
(a) WITHOUT ASPECT CANCELLATION
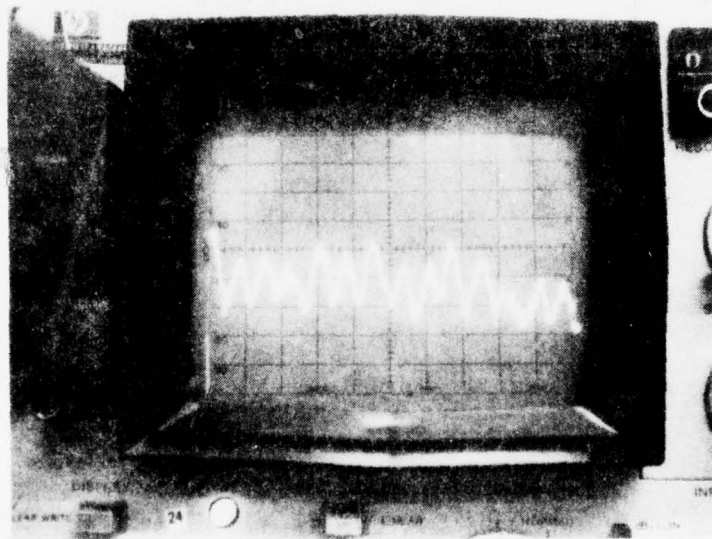
(b) WITH ASPECT CANCELLATION

Figure 37. Fourier spectrum of target PMT signal
with 6.5 kHz simulated speckle
modulation.

109

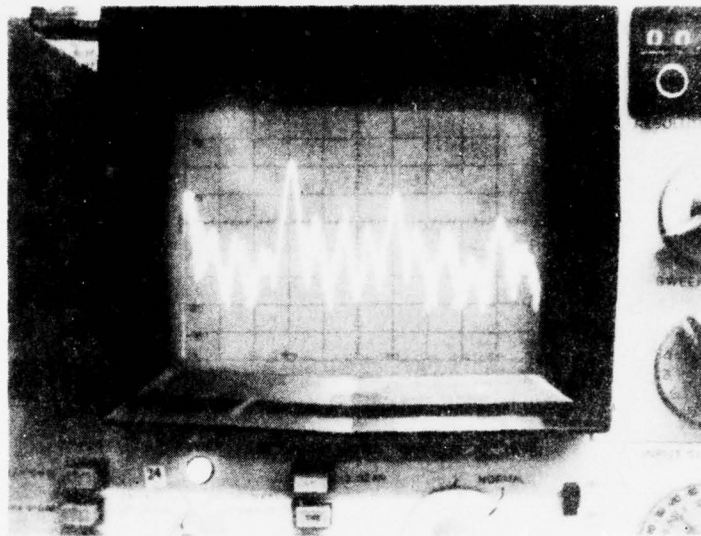(a) WITHOUT ASPECT CANCELLATION

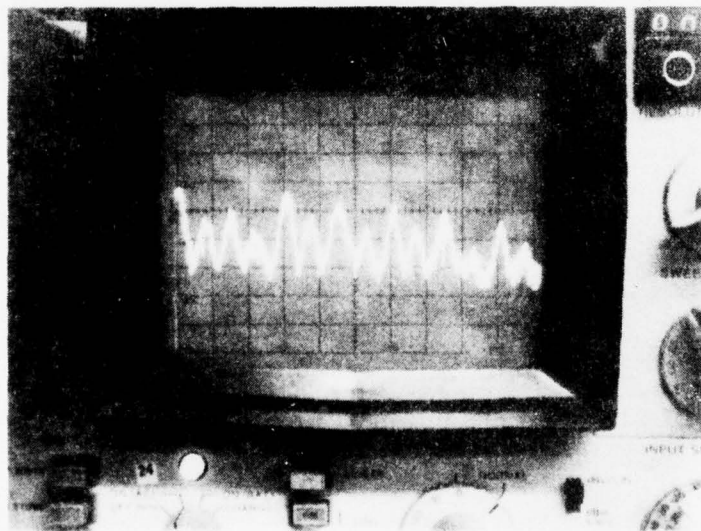

(b) WITH ASPECT CANCELLATION

Figure 38. Fourier spectrum of target PMT signal
with 13.4 kHz simulated speckle
modulation.
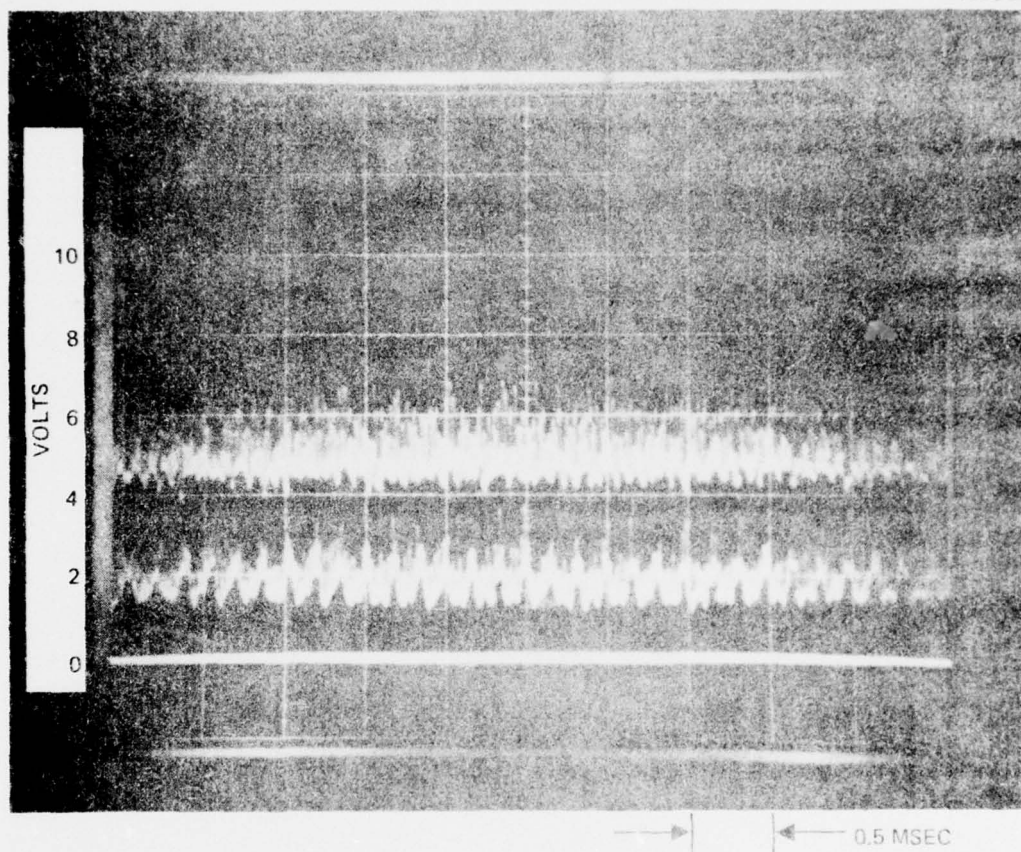
Figure 39. Target PMT signal versus time. Top trace: Ideal, no speckle level. Middle trace: degraded level resulting from 6.5 kHz sinewave modulation. Bottom trace: zero reference.

VOLTS

10
8
6
4
2
0

0.5 MSEC

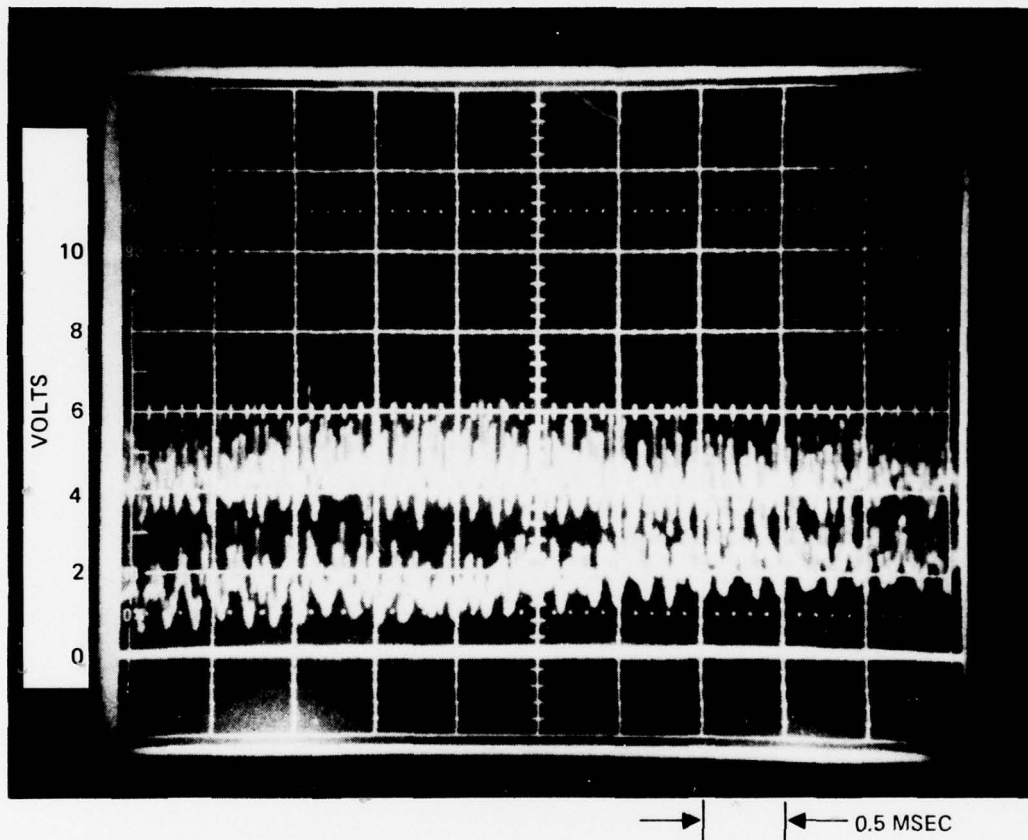Figure 40. Target PMT signal versus time. Top trace: ASPECT
restored level with 6.5 kHz sinewave modulation.
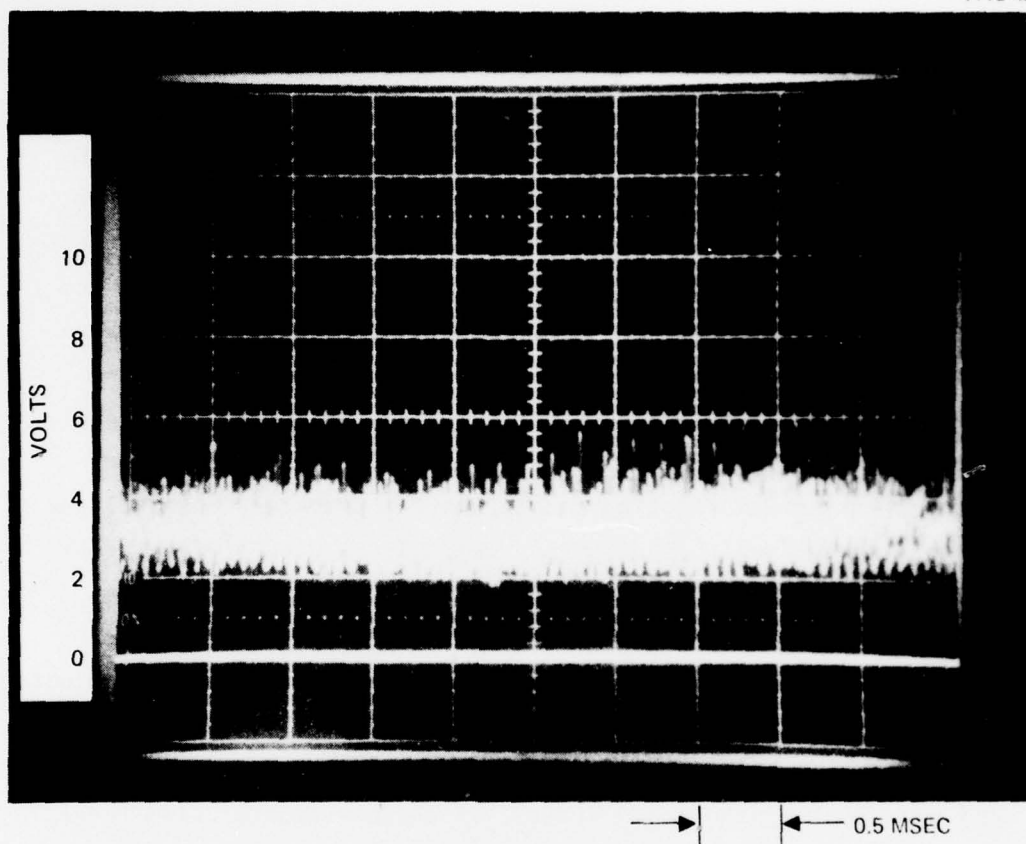Middle and bottom traces: same as Figure 39.

7772-48

Figure 41. Target PMT signal versus time. Top trace: ASPECT restored
level with 13.4 kHz sinewave modulation. Bottom trace:
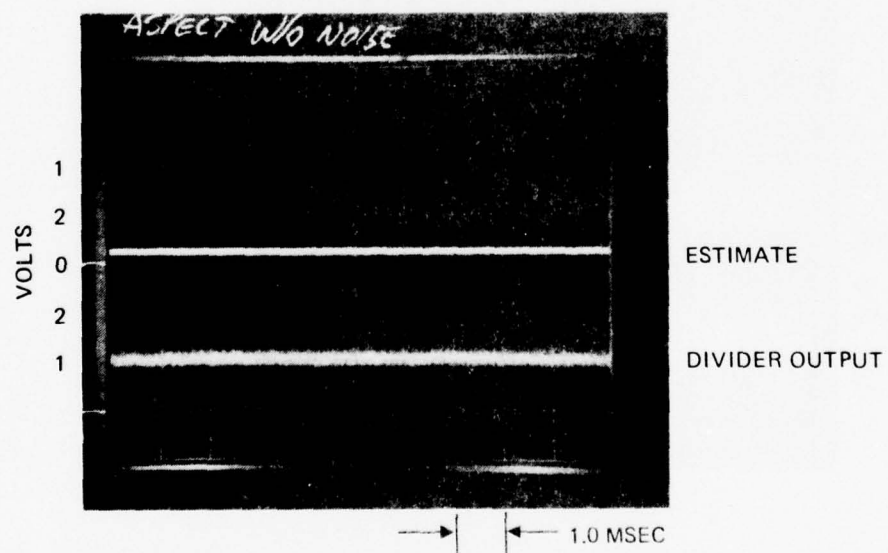zero reference.

113

the observed target illumination values. In the 6.5-kHz case, very
nearly full restoration of target illumination was achieved by the ASPECT
speckle cancellation system; in the 13.4-kHz case, only partial restora-
tion was observed. This is consistent with our computer simulation
results (discussed in Section 4.C). We also observed the behavior of
the seven-channel COAT/ASPECT system when subjected to the noise shown
in Figure 35. With no noise from the speckle simulator, the target PMT
output of Figure 42(a), which is proportional to the target irradiance,
was recorded. The denominator input to the speckle divider (i.e., the
estimate of the speckle modulation function) and the divider output are
shown in Figure 42(b). Since there was no noise, the estimated modula-
tion function (the top trace) is a constant. The divider output (the
bottom trace) is, therefore, just proportional to the target PMT signal.
Figure 43(a) shows the degraded target irradiance resulting from the
introduction of the multiplicative noise from the speckle simulator, the
ASPECT speckle detection loop being inactive. It is 0.48 of the refer-
ence no speckle noise level of Figure 42(a). Figure 43(b) shows the
ASPECT estimate of the speckle noise in the top trace and the divider
output in the bottom trace. When this esimtate is fed into the denominator
input of the speckle divider closing the ASPECT loop, the divider output
changes to that of the bottom trace, Figure 44(b). The target irradiance,
shown in Figure 44(a) is restored to 0.92 of the no speckle noise level,
about a factor of two improvement.

C.   CONCLUSIONS

The experimental study reported here clearly shows that multiplicative
noise can be estimated and cancelled by a hardware ASPECT system. In
retrospect, the laboratory hardware could have been improved if provisions
had been made to accommodate a much higher ASPECT probe carrier fre-
quency. But despite this shortcoming, the evidence is still quite con-
clusive. The laboratory hardware performed as well as we had anticipated,
based on computer simulation results (which had indicated that reasonable

7772-47
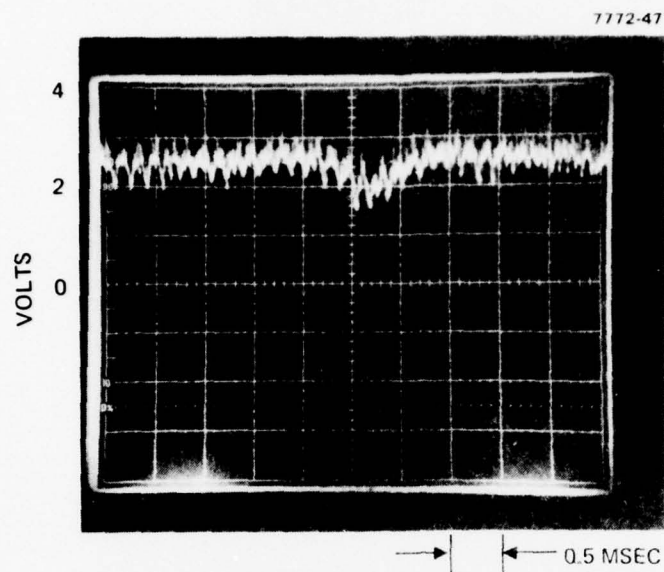
(a) TARGET PMT SIGNAL VS. TIME

(b) ESTIMATED SPECKLE NOISE AND
DIVIDER OUTPUT VS. TIME

Figure 42. Reference ideal COAT performance.

7772-46

VOLTS

4

2

0

→| |← 0.5 MSEC

(a) TARGET PMT SIGNAL VS. TIME

ASPECT OFF, NOISE ON

VOLTS

2
1
0

2
1
0

ESTIMATE

DIVIDER OUTPUT

→| |← 1.0 MSEC
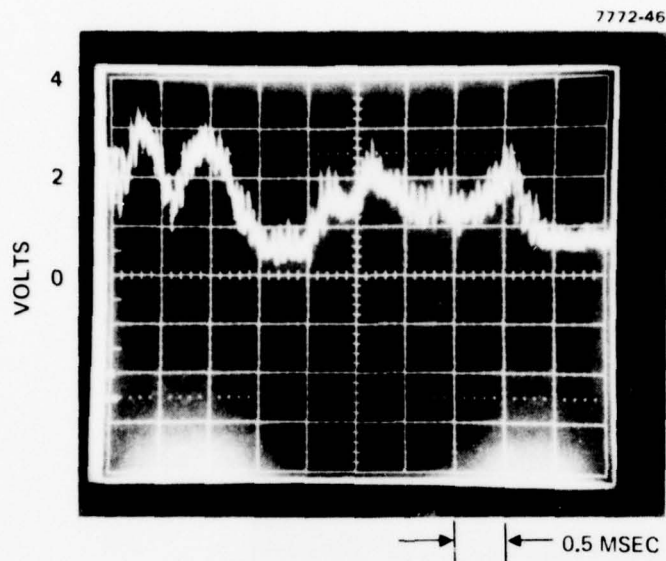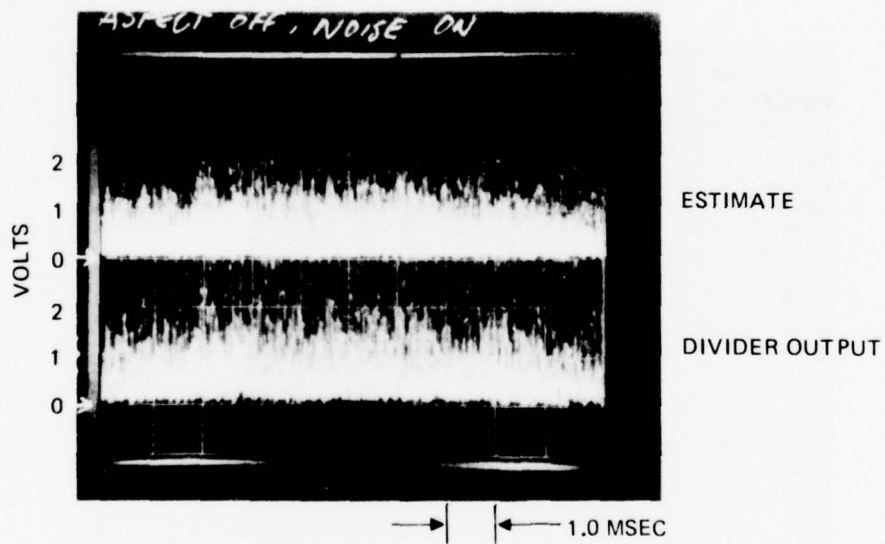
(b) ESTIMATED SPECKLE NOISE AND
DIVIDER OUTPUT VS. TIME

Figure 43. Degraded COAT performance with the modulation
formation of Figure 35.

116

7772-45
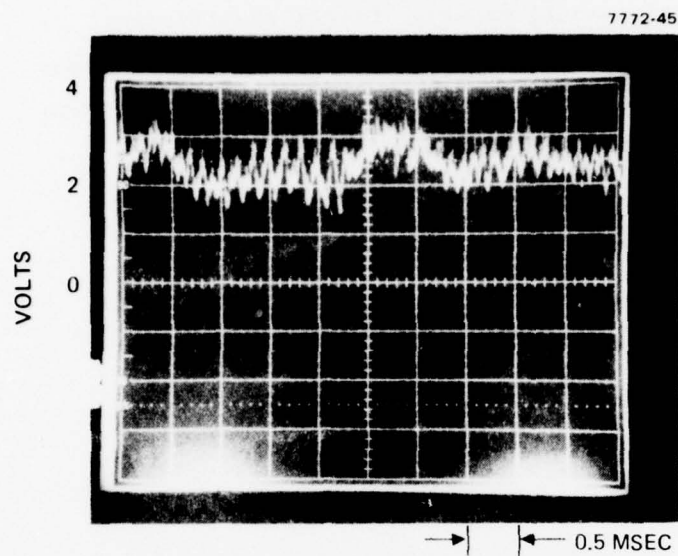
(a) TARGET PMT SIGNAL VS. TIME
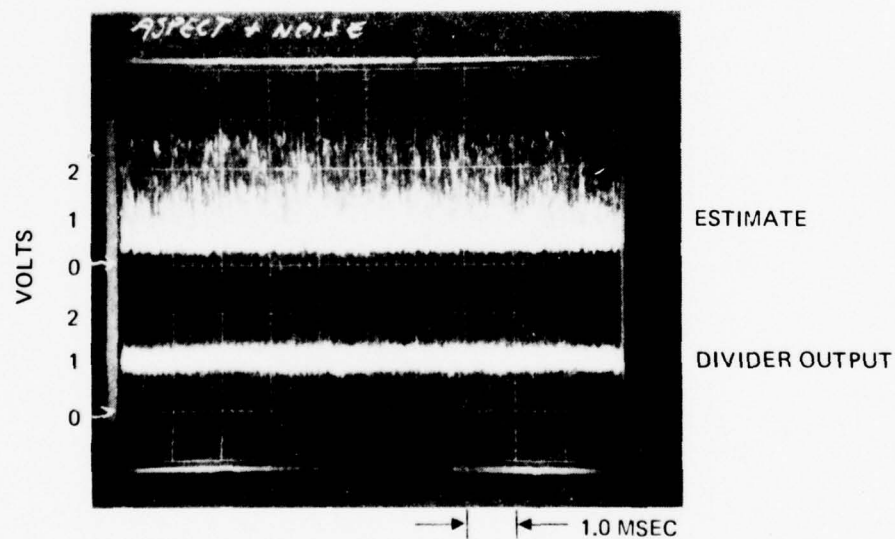
(b) ESTIMATED SPECKLE NOISE AND
DIVIDER OUTPUT VS. TIME

Figure 44. ASPECT restored COAT performance with the modulation formation of Figure 35.

117

but not complete cancellation would occur). Direct quantitative
comparisons of experimental data and computer simulations also showed
good agreement.   Based on these results, we feel very confident that
ASPECT is an effective way to cancel speckle interference.

SECTION 6

AUTOMATIC BANDWIDTH ADAPTIVE CONTROL (ABAC)

A. GENERAL DESCRIPTION

Previous work[1,2,12] has shown that there is a direct correlation
between the amount of COAT performance degradation due to specile inter-
ference and the magnitude of the system's servo bandwidth.* That is to
say, there will be less speckle degradation at smaller bandwidths and
vice versa. Conversely, if one wants to compensate a dynamic phase error,
such as atmospheric turbulence, the opposite holds true. Too small a
bandwidth will prevent the servo from compensating the rapidly changing
phase errors. Clearly, there is some optimum value of bandwidth, above or
below which the performance degrades. However, it is impossible to anti-
cipate what value this should be because it is a function of the amplitude
and frequency distribution of both of the turbulence and the speckle,
making it different for every scenario. The ABAC system is designed to
actively and automatically seek this optimum bandwidth for all scenarios.

In Figure 45, let the signal S_o from the COAT receiver be given by
Eq. 3.16. A dither modulation of the COAT servo bandwidth f_s at frequency
ω_g produces a temporal modulation of the target glint intensity, given by

$$\Delta i_g = \frac{\partial I_g}{\partial f_s} \Delta f_s \sin(\omega_g t) \quad , \tag{6.1}$$

where Δf_s is the amplitude of the bandwidth dither. If there is very
little speckle modulation at the dither frequency, then, after synchro-
nously detecting and low-pass filtering signal S_o, we get the gain or
bandwidth correction signal, $G(t)$ given approximately by

---

* The term bandwidth, as used throughout this section, refers to the value
of bandwidth at full convergence. Section 7.A discusses how the band-
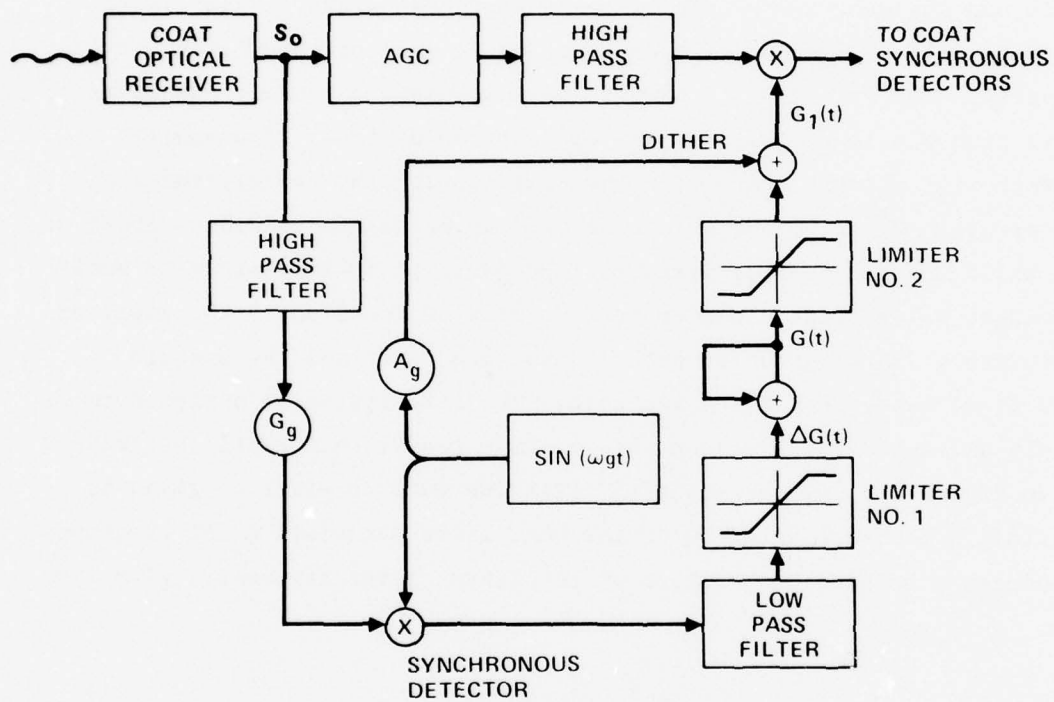width varies with convergence level.

119

Figure 45. Schematic of ABAC servo.

$$\Delta G(t) \simeq \frac{1}{2} KG_g \frac{\partial I_g}{\partial f_s} \Delta f_s , \qquad (6.2)$$

where

$K \equiv$ optical detector constant

$G_g \equiv$ the adjustable gain parameter in the ABAC loop.

Eq. 6.2 illustrates a fundamental problem associated with the ABAC servo. The derivative

$$\frac{\partial I_g}{\partial f_s}$$

cannot be anticipated without a priori knowledge of the nature of the speckle and turbulence degradation that will be encountered in a given COAT/target scenario. Therefore, it is impossible to select an optimum value for the gain parameter G_g. This problem can be overcome by setting the value of G_g very high so that the magnitude of the correction signal would always be too large. If a signal limiter is then placed after the low-pass filter following the synchronous detector, as shown in Figure 45, only the polarity of the correction signal will need to be correct, because the magnitude will almost always be the same. Thus, the ABAC servo will change the gain in the COAT servo at a fixed rate in either a positive or negative direction. The magnitude or clipping level of the signal limiter should be adjusted so that the gain does not change significantly (e.g., ±10%) during one dither period.

In addition, if there is significant speckle modulation at the band-width dither frequency, then there will be a spurious error signal created, just as there is in the normal COAT servo. There appears to be no way to avoid this problem other than to keep the ABAC servo bandwidth low enough to keep the speckle noise power below the true signal power. This would result in a very slow servo; however, there are other reasons for wanting a slow servo, as discussed below.

It is rather straightforward to conclude that a very low dither frequency for the ABAC servo (as compared to COAT dithers) is highly desirable if not an absolute necessity. Just for mechanical reasons, the dither period must be longer than twice the characteristic response time of a COAT servo (on the order of a few milliseconds). Furthermore we must recognize that the mean Strehl ratio on target from a speckle- or turbulence-degraded COAT system is not well defined for short periods of time. It usually requires 10 to 20 times a typical COAT convergence time (on the order of 10 msec or more) for a well-defined average convergence level to be established. Thus, for the change in target intensity as a function of change in bandwidth (i.e., $\frac{\partial I_g}{\partial f_s}$ in Eq. 6.2) to be well defined, the bandwidth dither period must be sufficiently long. Also, because of speckle modulations, it will probably require more time for the COAT receiver intensity to establish a well-defined mean level than it does at the target. The conclusion from all of this is that low dither frequencies are most desirable. A bandwidth dither frequency of 10 Hz for a 1000-Hz bandwidth COAT servo is probably reasonable.

Unfortunately, at the beginning of this program we did not expect that the dither would have to be this slow. Only the mechanical consid-erations were anticipated. Thus, we felt that a 300- or 400-Hz dither frequency and a 1000-Hz COAT servo would be adequate. The original 18-channel servo simulation was modified to simulate this configuration.

The nominal bandwidth of the 18-channel servo code[1,5] is generally between 300 and 500 Hz. Increasing the maximum allowable COAT servo bandwidth to 1000-Hz would increase the response time, thus allowing faster dithering of the bandwidth, which in turn would decrease the total time necessary to run each simulation. To implement this scheme, we had to increase the frequency spacing between the usual COAT dither channels from 1400 Hz to 4000 Hz. The 18th dither frequency then became 80.2 kHz, which is more than double the previous value of 32 kHz. Consequently, to maintain the same numerical accuracy as before would require us to decrease the integration step size by more than a factor of 2. Therefore, we chose to reduce the number of channels from 18 to 12, thereby reducing

122

the maximum dither frequency so that the integration step size could be left approximately the same, $\delta t = 4$ μsec. With these modifications, combined with computer core constraints, we were able to make simulation runs lasting for 192 msec at reasonable costs. This allowed us to use an ABAC dither frequency of 50 Hz and still run simulations for almost 10 dither cycles. Even through a lower dither frequency and many more dither cycles would be much preferable, the data gathered under these constraints is still fairly conclusive.

A dynamic phase error $\phi_n(t)$ was also introduced into each COAT channel to simulate atmospheric turbulence. This was done, using the following expression for the phase error in an arbitrary channel η:

$$\phi_n(t) \equiv A_{tr} \sin (\omega_{tr}t + \gamma_n), \tag{6.3}$$

where A_{tr}, ω_{tr}, and γ_n are input parameters. The variables γ_n are chosen randomly between 0 and 2π. Including this simulated turbulence gives us a more realistic perspective of ABAC operations.

B. COMPUTER SIMULATION RESULTS

We have run closed loop simulations of the ABAC servo system using simulated turbulence and the same three speckle modulation functions described earlier in Section 4.C. We will refer to them by specifying the target rotation rate. The magnitude of the turbulence in each case was $A_{tr} = \pi/3$ rad, and the frequency was 1256.64 rad/sec (200 Hz). Some open loop results are given below to give the reader a feel for what one should expect from an ABAC system. Figures 46, 47, and 48 show the average Strehl ratios for the 12-channel COAT system described in Section 6.A as a function of servo bandwidth. These averages were obtained from computer simulation runs of the COAT system operating at fixed bandwidth and subjected to the indicated speckle and turbulence degradations. These data show approximately where the optimum bandwidth for each scenario should be. However, there is a great deal of fluctuation from
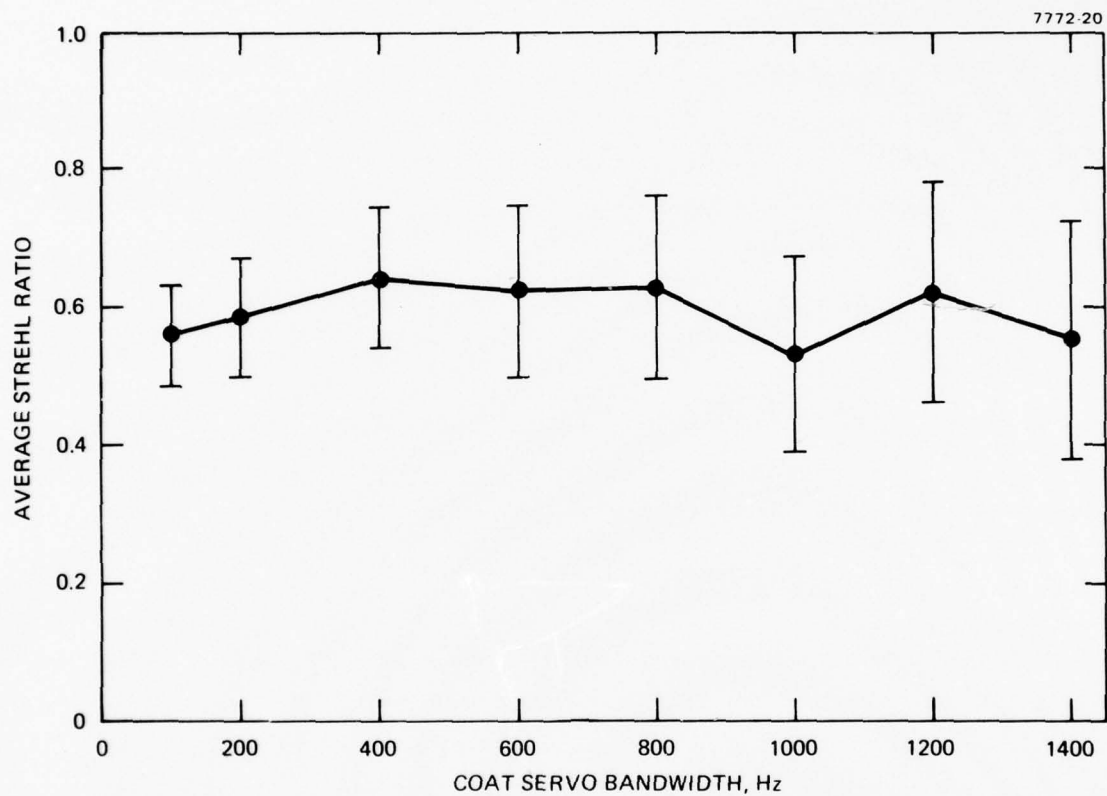
Figure 46. COAT system performance at fixed bandwidth target rotation rate 0.4 rad/sec.
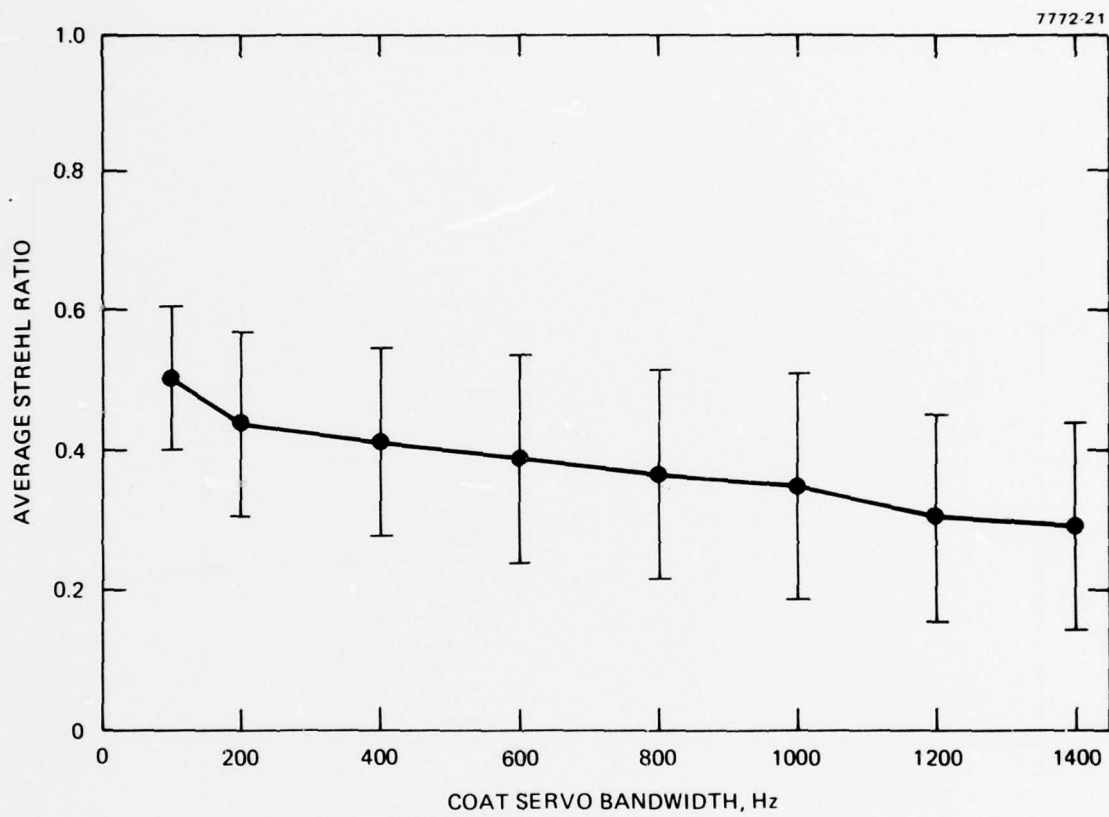
Figure 47. COAT system performance at fixed bandwidth targer rotation rate
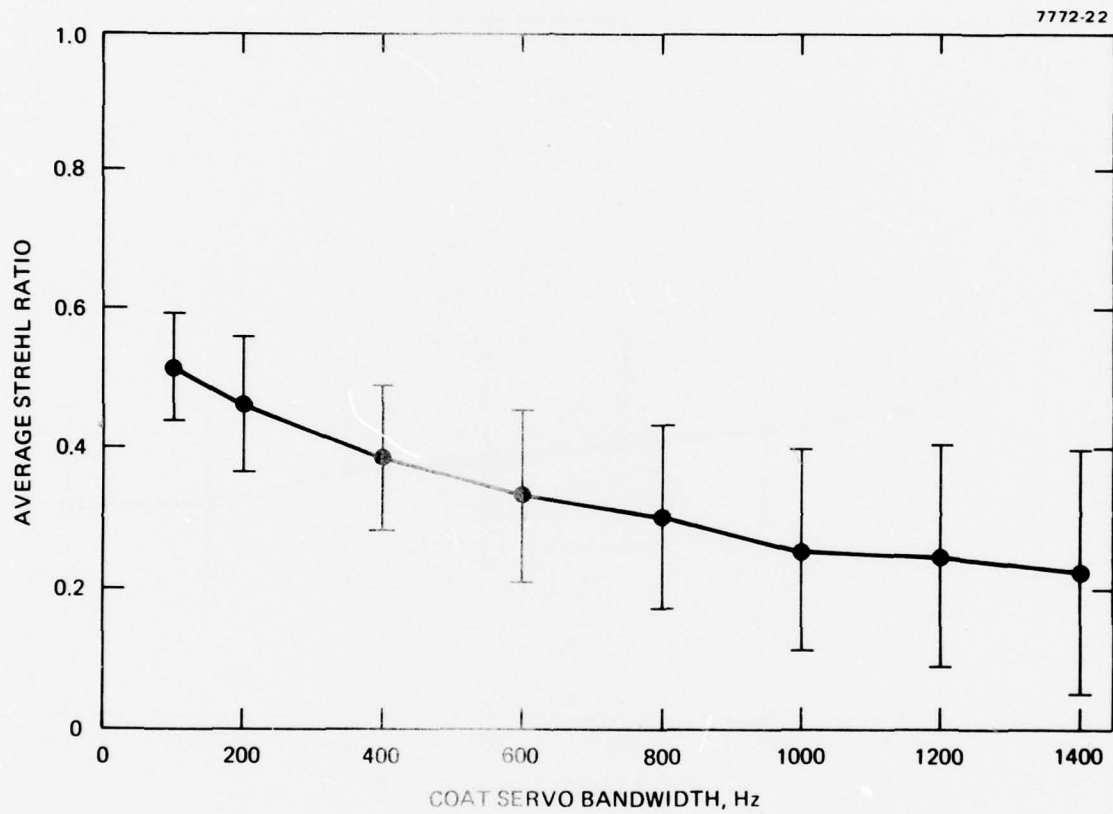2.0 rad/sec.

Figure 48. COAT performance at fixed bandwidth. Targert rotation rate 10.0 rad/sec.

these average Strehl ratios at any given bandwidth for short periods of
time. The error bars in each figure indicate the standard deviation.
These fluctuations can cause the average Strehl ratio, over time periods
on the order of a bandwidth dither period, to vary considerably from this
mean value. Figures 47 and 48 show that the optimum bandwidth for target
rotation rates 2.0 and 10.0 rad/sec, is 100 Hz or less most of the time.
But for short periods of time, some higher bandwidth may be optimum.
This phenomena is more apparent in Figure 46, where it is difficult to
determine what the optimum bandwidth for a target rotation rate of
0.4 rad/sec really is. Since the ABAC servo responds on a time scale
much shorter than the 192 msec over which these data were gathered, these
fluctuations do not really present a great problem. The ABAC servo
simply tries to compensate these fluctuations by changing the bandwidth
in a direction that increases the Strehl ratio. In other words, ABAC
does not really seek a long time optimum bandwidth; rather, it seeks a
long time optimum Strehl ratio, which is really the parameter we wish to
optimize.

This can best be appreciated in Figures 49 and 50. Figure 49(a)
shows COAT performance with a closed-loop ABAC servo in the form of tar-
get Strehl ratio versus time. Figure 49(b) shows the ABAC bandwidth
correction signal. As discussed above, only the polarity of this signal
is important because the ABAC servo generates a constant change in band-
width in either the positive or negative direction in accordance with
this polarity. The large oscillations at the beginning of the plot are
system transients due to the initial conditions. Figure 49(c) is a plot
of the average Strehl ratio over 24-msec intervals superimposed on a plot
of ABAC-generated COAT servo bandwidth. The bandwidth, which was
initialized to 600 Hz, starts to decrease when the ABAC servo is turned
on 40 msec after the start of the simulation. The bandwidth continues
to decrease as long as the Strehl ratio increases (or remains constant).
When the bandwidth goes below 300 Hz, the Strehl ratio decreases slightly
and the ABAC system reverses the change in bandwidth, with a resultant
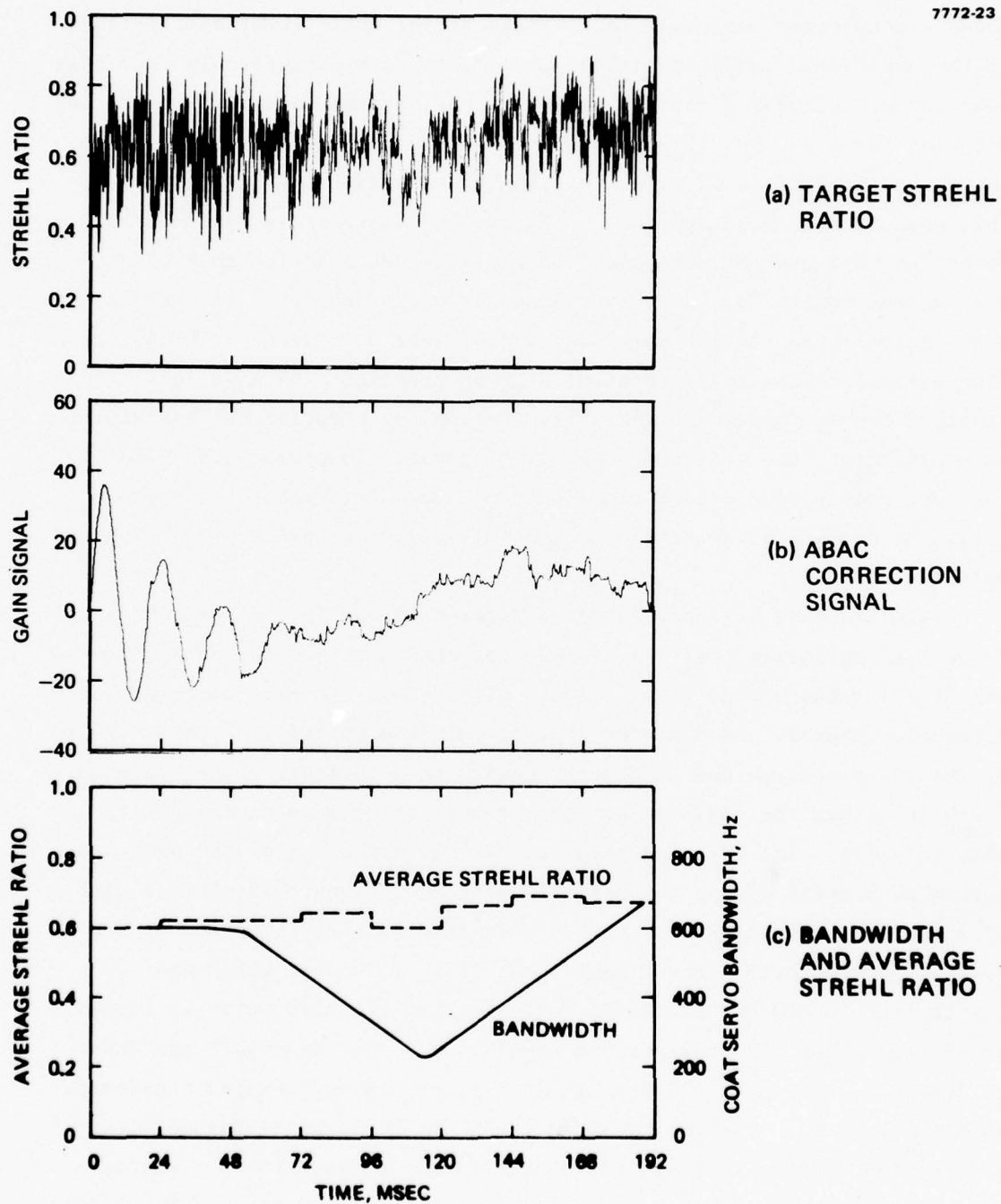further increase in the Strehl ratio. The final bandwidth after 192 msec

Figure 49. COAT system performance with open loop ABAC system. Case: GRC-1. Initial bandwidth: 600 Hz.

128

is almost 700 Hz. From Figure 49(b), however, it appears that the ABAC servo correction signal was just about to change polarity again which would have caused a reversal of the bandwidth increase. It is unlikely that the ABAC servo would have found an optimum bandwidth in this case. It seems more likely that it would continue searching somewhere between 200 and 800 Hz. This search would not be random, however, because the servo would constantly be trying to maintain the highest Strehl ratio possible over any given dither period. The open loop data of Figure 46 is quite consistent with this interpretation because there is only a small amount of variation in average Strehl ratio over this range of bandwidth and there is considerable fluctuation.

To be sure that the ABAC system would approach the same state or the same optimum bandwidth from above or below, we chose to run each scenario twice, once with the bandwidth initialized at 600 Hz, and once with the bandwidth initialized at 100 Hz, and then compare the results. Figure 50 shows the same data as shown in Figure 49, for a 100-Hz initialization. As is the case in Figure 49(c), Figure 50(c) does not appear to show a long time optimum bandwidth. These two figures are poor examples to compare this way because of the lack of definition of the final state; therefore, we proceed to cases where the target rotation rates are 2.0 and 10.0 rad/sec and the comparison is more meaningful.

These two scenarios are very similar in their effect on COAT performance, and a judgment of ABAC performance is quite simple to make. In Figures 51 through 54 (which are formatted the same as Figures 49 and 50), the ABAC servo in each case simply drives the COAT servo bandwidth to 100 Hz and keeps it there.[*] This result is consistent with the open loop data of Figures 47 and 48, where 100 Hz or less is clearly the optimum bandwidth. Starting the simulations from either 600 Hz or 100 Hz clearly produces the same final bandwidth.

_____

[*] Because there is always a plus and minus 100 Hz dither associated with the ABAC system, 100 Hz is the lowest limit which we allow the bandwidth to reach. Therefore, in effect, the final COAT servo bandwidth is not 100 Hz but varies between 0 and 200 Hz.

129

(a) TARGET STREHL
RATIO

(b) ABAC
CORRECTION
SIGNAL

(c) BANDWIDTH
AND AVERAGE
STREHL RATIO

Figure 50.   COAT system performance with open loop ABAC system.   Case:
GRC-1.   Initial bandwidth: 100 Hz.

(a) TARGET STREHL
    RATIO

(b) ABAC
    CORRECTION
    SIGNAL

(c) BANDWIDTH
    AND AVERAGE
    STREHL RATIO

AVERAGE STREHL RATIO

BANDWIDTH

Figure 51.   COAT system performance with open loop ABAC system.   Case:
             GRC-2.   Initial bandwidth: 600 Hz.

131

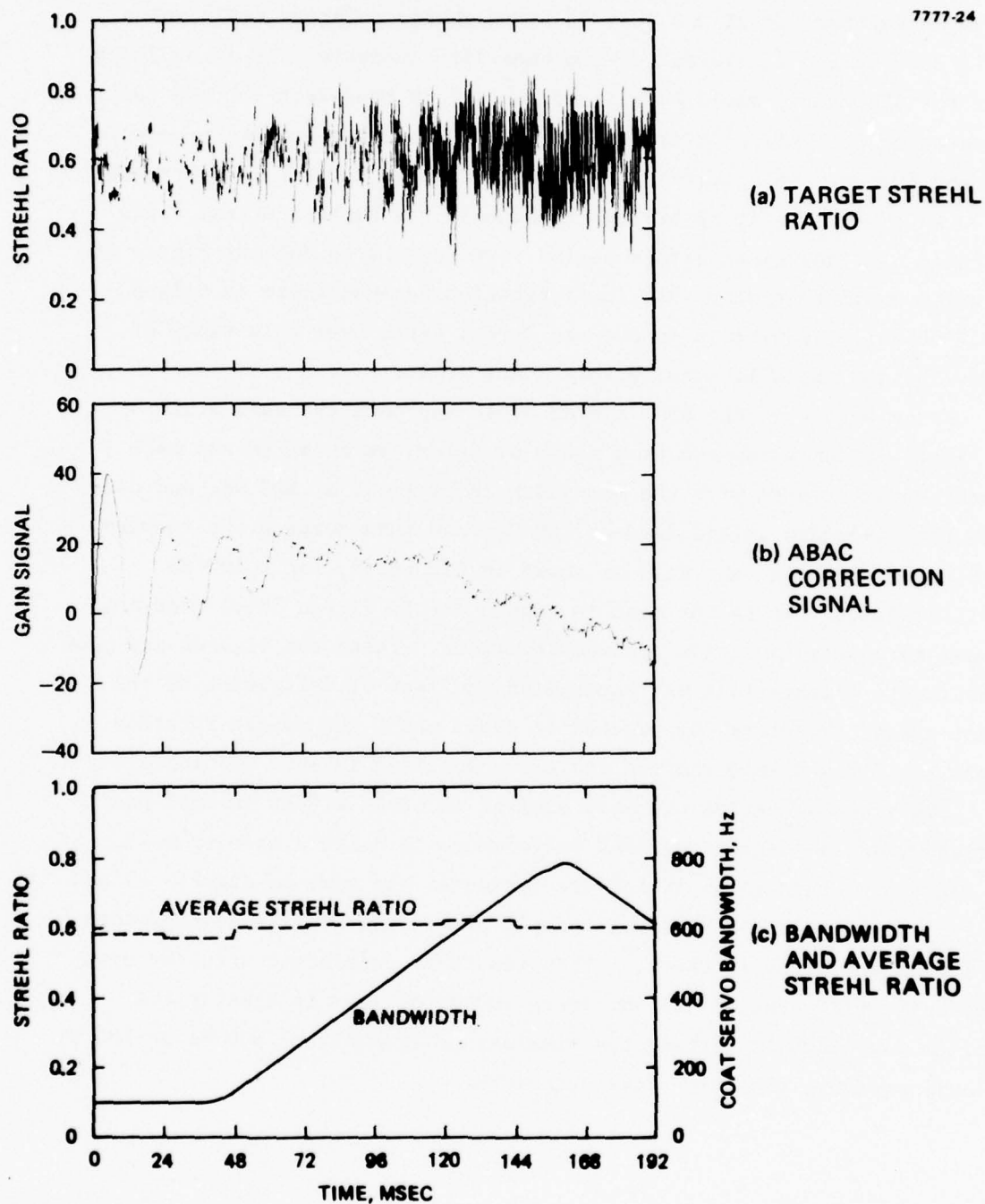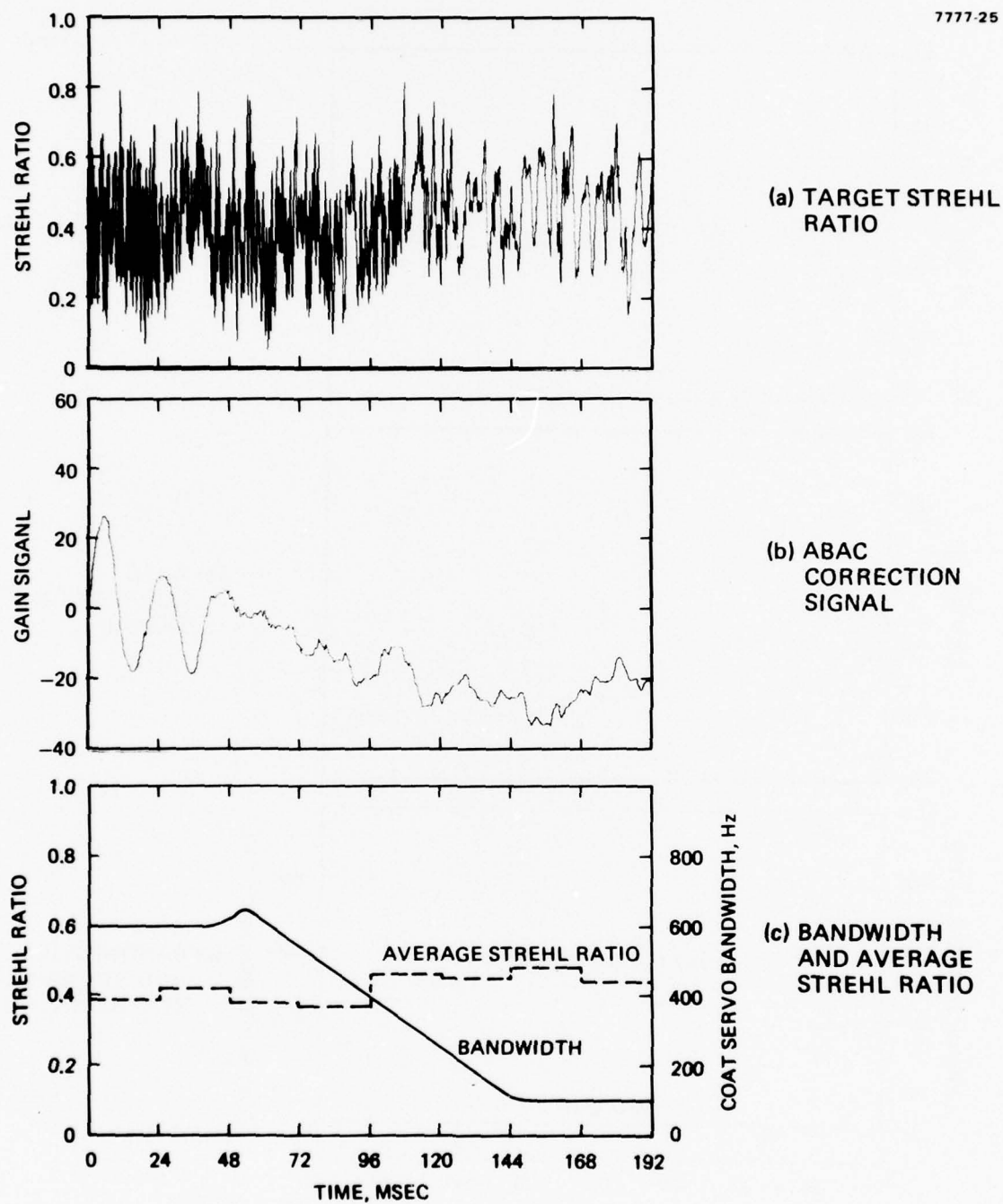Figure 52. COAT system performance with open loop ABAC system. Case: GRC-2. Initial bandwidth: 100 Hz.

132

Figure 53. COAT system performance with open loop ABAC system. Case: GRC-3. Initial bandwidth: 600 Hz.
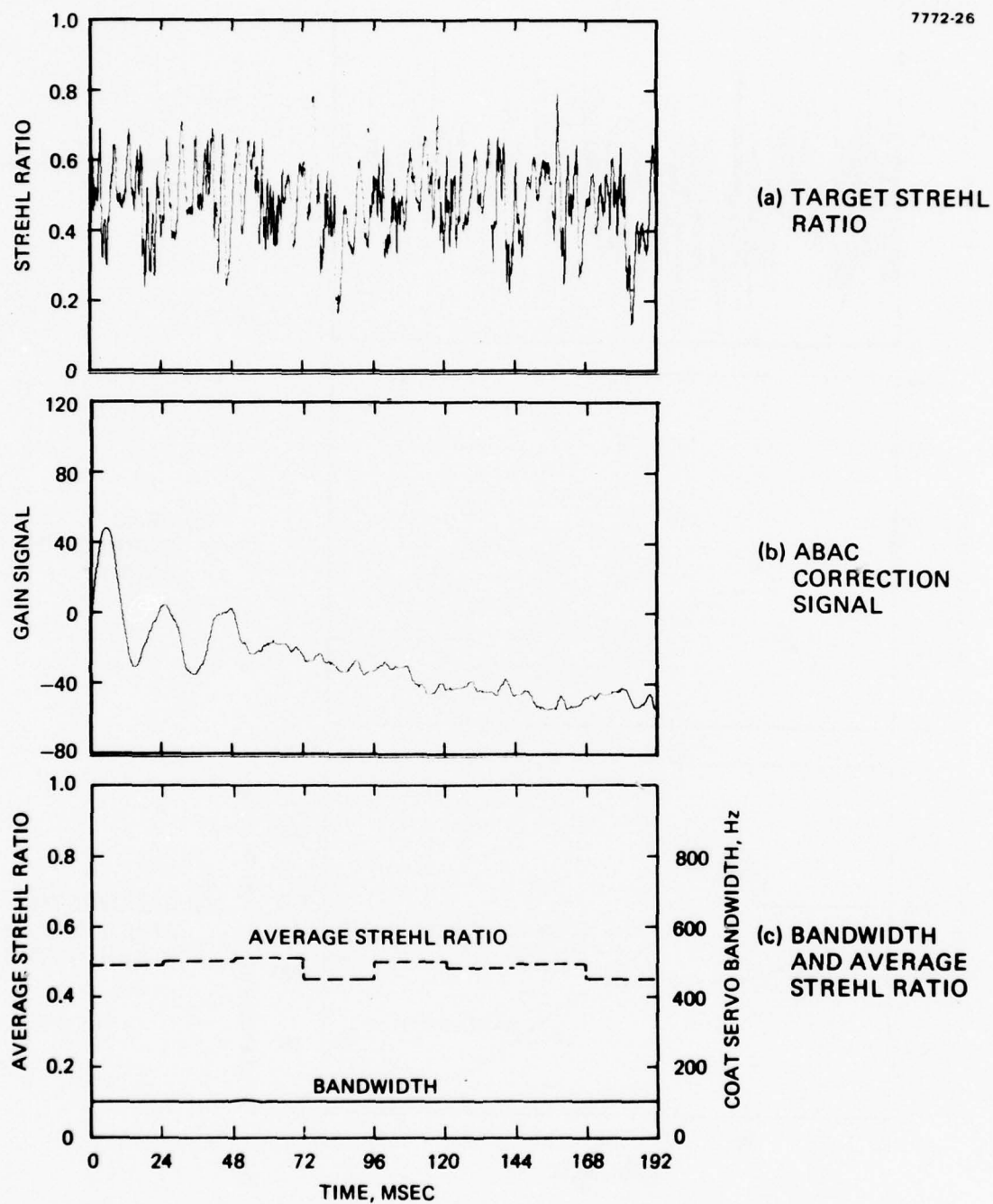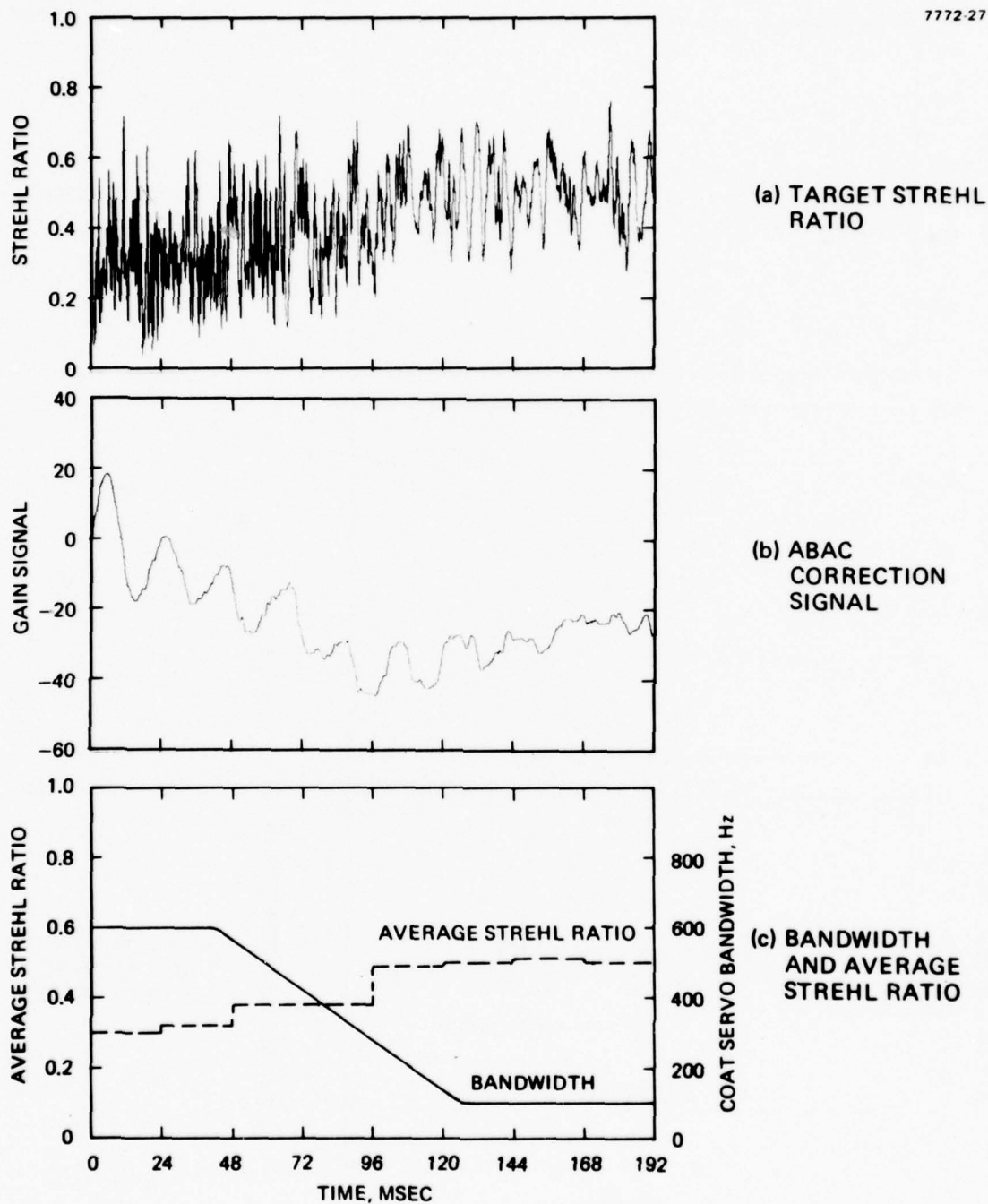
(a) TARGET STREHL RATIO

(b) ABAC CORRECTION SIGNAL
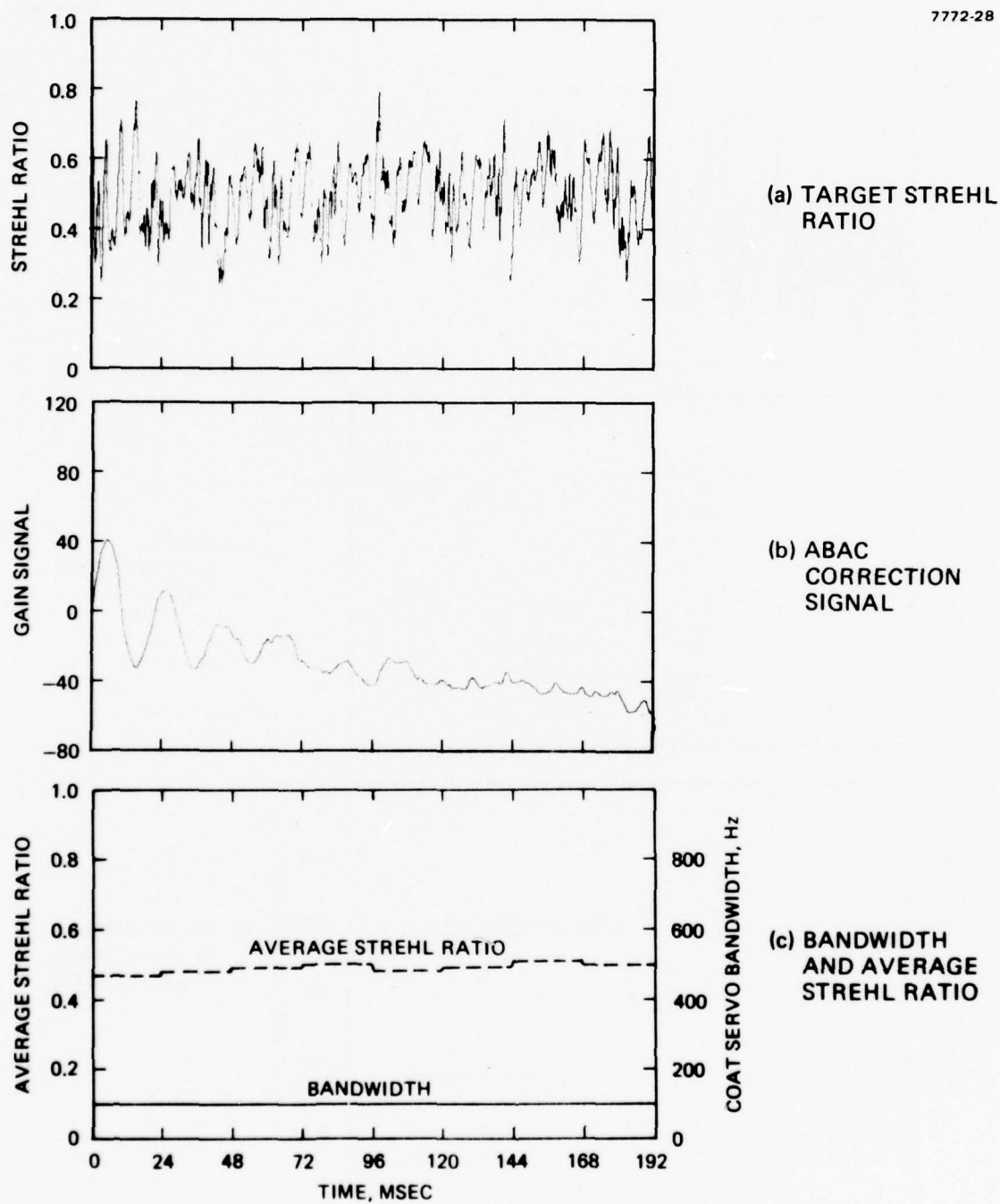
(c) BANDWIDTH AND AVERAGE STREHL RATIO

Figure 54. COAT system performance with open loop ABAC system. Case: GRC-3. Initial bandwidth: 100 Hz.

C.   CONCLUSIONS

This section has demonstrated that an ABAC servo can optimize COAT servo bandwidth and can do this regardless of the source of the performance degradation. As long as these degradations are bandwidth-related, the ABAC servo will seek the optimum bandwidth under the given constraints. This optimization is accomplished by dithering the COAT bandwidth and then synchronously detecting the correction signal at the dither frequency. Since this signal is proportional to the magnitude of the change in the Strehl ratio (or convergence level) in response to a smal change in bandwidth, and since the response of the COAT system to such a change in bandwidth is very slow, particularly under conditions of speckle interference, the bandwidth dither must also be very slow. We have found that the dither frequency should be about two orders of magnitude lower than the COAT servo bandwidth.

By examining Figures 49 through 54, one might conclude that ABAC, or more generally bandwidth variation, is only a marginally useful concept because the improvement in Strehl ratio in any one scenario is not that dramatic. The most impressive performance is shown in Figure 53, where the Strehl ratio increases from about 0.3 to 0.5. However, a realistic COAT target will not be a sphere rotating at a constant rate such as the ones modeled in these simulations. A real target would most likely have complex geometry and move about at various and continually changing velocities and angular velocities. This would produce a constantly changing speckle pattern. This, combined with atmospheric turbulence and any other bandwidth sensitive distortions, would create an ever changing scenario. It is ABAC's ability to adapt the bandwidth to the scenario in an optimum manner that best illustrates its utility.

SECTION 7

ANALYTICAL PREDICTIONS OF SPECKLE-RELATED PERFORMANCE DEGRADATION
OF MULTIDITHER COAT SYSTEMS

This section expands on an analysis originally developed under
contract D30602-76-C-0021 and reported in Refs. 1 and 12. In that
analysis, we were able to calculate the time-averaged convergence level[*]
of a COAT system subjected to multiplicative noise caused by speckle as
a function of the relative noise energy. More precisely, we calculated
the convergence level as a function of a parameter called speckle coeffi-
cient, or C_s, which is just the square root of the average noise power
within the COAT dither frequency bands. If we assume, as we did in the
original analysis, that the gain or bandwidth characteristics of a COAT
system are independent of convergence level, then a knowledge of these
and the spectrum of the speckle modulation function is all that is
necessary to compute a single value of C_s, which then allows us to calcu-
late the convergence level. In real multidither COAT systems, however,
the open loop dc gain varies with convergence level. Therefore in prin-
ciple there exists a separate value of C_s for every value of convergence
level. This dependence of C_s on convergence level can be thought of as
a constraint relationship, whereas the original relationship which allows
us to calculate the average convergence level as a function of C_s is a
statistical relationship based on physical principles. Both of these
relationships must be satisfied simultaneously to represent a real COAT
system in a true physical scenario. Since the latter relationship is
already known from Ref. 1, we now proceed to derive the constraint
relationship. To do this requires calculating the open loop dc gain
associated with the speckle interference in an arbitrary channel n.

In Ref. 1, we have shown that the synchronously detected signal in
each channel consists primarily of the sum of two components: the true

---

[*] In this context, the convergence level is just the Strehl ratio on a
target glint.

error correction signal and the interference signal caused by speckle. Furthermore, we have demonstrated that the convergence level attained by the COAT system was always such that the average power after synchronous detection was equal in each of these signals. Therefore, we assumed that the average open loop dc gain associated with the speckle interference is the same as that for the true error signal. Based on this, we can calculate the expectation value of this parameter in an arbitrary channel n of an N-channel multidither COAT system.[*]

Eq. 11 of Ref. 1 exprsses the normalized sum of all the COAT receiver intensity modulations at the dither frequencies. The modulation at the nth frequency I_n, is just one term in that sum. Therefore, I_n can be written as

$$I_n = -\frac{4J_o(\psi_o)J_1(\psi_o)}{N^2} \left[\sum_{\substack{m=1 \\ m \neq n}}^{N} \sin(\beta_n - \beta_m) \right] \sin\omega_n t, \qquad (7.1)$$

where the variable t is time, ψ_o is the amplitude of the dither modulation in radians of wavelength, J_o and J_1 are the zeroth and first Bessel functions, ω_n is the dither frequency, and β_m is the average phase at the target associated with COAT channel m. Using trigonometric identities, Eq. 7.1 can be rewritten as

$$I_n = -\frac{4J_1(\psi_o)}{N^2} V_{Rn} \sin(\beta_n - \beta_{Rn}) \sin\omega_n t, \qquad (7.2)$$

where V_{Rn} and β_{Rn} are defined as the resultant amplitude and phase of the following vector sums:

---

[*] We will assume a COAT system without an AGC, as was done in the original analysis.

138

$$V_{Rn} \cos(\beta_{Rn}) \equiv \sum_{\substack{m=1 \\ m \neq n}}^{N} J_o(\psi_o) \cos(\beta_m) \qquad (7.3)$$

$$V_{Rn} \sin(\beta_{Rn}) \equiv \sum_{\substack{m=1 \\ m \neq n}}^{N} J_o(\psi_o) \sin(\beta_m). \qquad (7.4)$$

Physically, β_{Rn} is the average relative phase of the resultant field at the target glint associated with all COAT cahnnels except channel n, and V_{Rn} is proportional to its amplitude. This can be seen as follows. In the original statistical analysis (see Ref. 1), we assumed that the target glint was illuminated by N identical sources, each having a field amplitude of N^{-1} and a phase of $\beta_n + \psi_o \sin\omega_n t$, where n refers to the nth element or channel in a zonal multidither COAT system. Since the dither phase $\psi_o + \sin\omega_n t$ changes at a much faster rate than the means phase β_n, we may represent the nth element field at the target by an average phasor quantity $\overline{V}_n$, which is the time average of the true field over a dither period T_n:

$$\overline{V}_n \equiv \frac{1}{NT_n} \int_o^{T_n} dt \, e^{i(\beta_n + \psi_o \sin\omega_n t)} = \frac{J_o(\psi_o)}{N} e^{i\beta_n} . \qquad (7.5)$$

Except for the normalization factor N^{-1}, the summations in Eqs. 7.3 and 7.4 are just the component vector sums of average fields defined this way. Thus, $\beta_n - \beta_{Rn}$ in Eq. 7.2 is just the phase error in channel n that must be corrected by the COAT servo.

The correction signal S_n is proportional to the amplitude of the dither modulation at frequency ω_n. Thus, using Eq. 7.2 we define:

$$S_n \equiv \frac{G_1}{2} \left[-\frac{4J_1(\psi_o)}{N^2} V_{Rn} \sin(\beta_n - \beta_{Rn}) \right] , \qquad (7.6)$$

139

where G_1 is a proportionality constant as well as an adjustable gain parameter (see Figure 13) and the factor 1/2 comes from the synchronous detection process. The open loop dc gain in channel n is defined as

$$g_n \equiv \left| \frac{S_n}{(\beta_n - \beta_{Rn})} \right| = \frac{2G_1 J_1(\psi_0)}{N^2} V_{Rn} \frac{\sin(\beta_n - \beta_{Rn})}{(\beta_n - \beta_{Rn})} \quad . \qquad (7.7)$$

We are now in a position to calculate the expectation value of g_n based on the statistical model developed in Ref. 1. To do this, we will first derive the relationships among β_n, V_{Rn}, and β_{Rn} at a specified convergence level. The total average resultant amplitude V_R and phase β_R associated with the entire field at the target glint, analogous to the resultant field defined in Eqs. 7.3 and 7.4 can be defined[*] as

$$V_R \cos(\beta_R) \equiv \sum_{m=1}^{N} J_0(\psi_0) \cos(\beta_m) \qquad (7.8)$$

$$V_R \sin(\beta_R) \equiv \sum_{m=1}^{N} J_0(\psi_0) \sin(\beta_m) \quad . \qquad (7.9)$$

The variable V_R can easily be related to the mean convergence level I_M defined in Eq. 10 of Ref. 1:

$$V_R^2 = N^2 I_M - N [1 - J_0^2(\psi_0)], \qquad (7.10)$$

V_R and V_{Rn} are just the amplitudes of phasors $\overline{V}_R$ and $\overline{V}_{Rn}$:

$$\overline{V}_{RM} \equiv V_{Rn} e^{i\beta_{Rn}} \qquad (7.11)$$

---

[*] This definition of β_R is inconsistent with Ref. 1. The β_R in Ref. 1 is identical to β_{Rn} in this report.

$$\overline{V}_R \equiv V_R \, e^{i\beta_R} \; . \tag{7.12}$$

Their phasor relationship is shown graphically in Figure 55. It can be expressed mathematically as:

$$V_R = V_{Rn} \cos(\beta_{Rn} - \beta_R) + J_o(\psi_o) \cos(\beta_n - \beta_R) \tag{7.13}$$

$$0 = V_{Rn} \sin(\beta_{Rn} - \beta_R) + J_o(\psi_o) \sin(\beta_n - \beta_R) \tag{7.14}$$

Using Eqs. 7.10, 7.13, and 7.14, it can readily be shown that Eq. 7.7 may be rewritten as:

$$g_n = \frac{2 J_1(\psi_o) \, G_1 \sin(\beta_n - \beta_R)}{N^2 (\beta_n - \beta_{Rn})} \left\{ N^2 I_M - N[1 - J_o^2(\psi_o)] \right\}^{1/2} . \tag{7.15}$$

The phase angle β_R, which is the resultant absolute phase of the total field at the target glint, can have any arbitrary value. It is convenient for computation to define it to be zero. We can then compute $\langle g_n \rangle$, the expectation value of the open loop dc gain, consistent with the statistical model of reference 1, by using the following relationship:

$$\langle g_n \rangle \equiv \frac{1}{\alpha} \int_{\alpha/2}^{\alpha/2} d\beta_n \, g_n$$

$$= \frac{2 J_1(\psi_o) \, G_1 \{ N^2 I_M - N[1 - J_o^2(\psi_o)] \}^{1/2}}{\alpha N^2} \int_{-\alpha/2}^{\alpha/2} d\beta_n \, \frac{\sin\beta_n}{(\beta_n - \beta_{Rn})} \; .$$
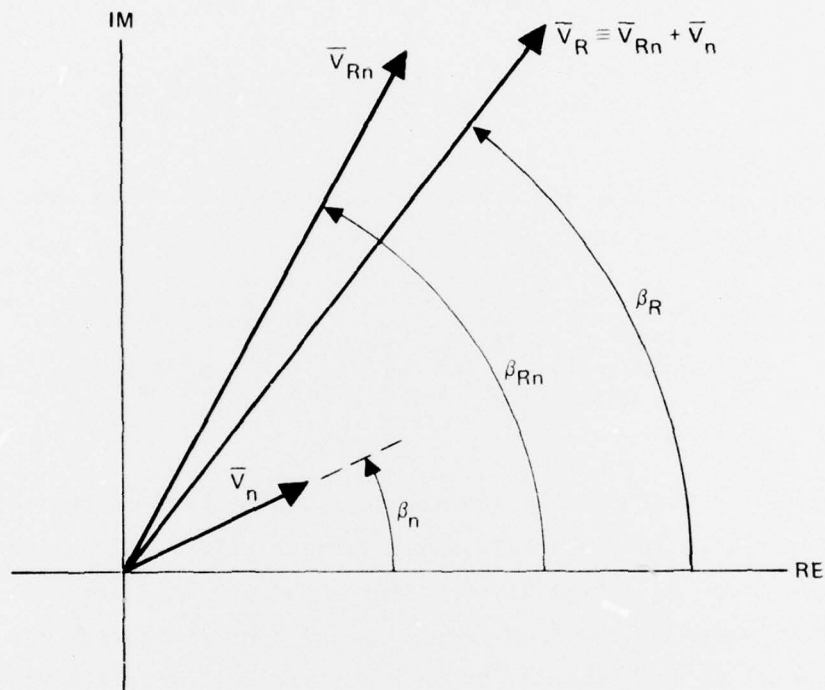
$$\tag{7.16}$$

141

Figure 55. Phasor diagram showing relationship among $\overline{V}_R$, $\overline{V}_{Rn}$, and $\overline{V}_n$.

The factor α^{-1} is the probability density as defined in Ref. 1. The limits of integration in Eq. 7.16 are chosen to be consistent with the choice of $\beta_R \equiv 0$. The phase variable β_{Rn} can be defined in terms of β_n using Eqs. 7.13 and 7.14 and the integral in Eq. 7.16 can be computed numerically to give the expectation value of g_n at any specified convergence level.

The COAT servo bandwidth characteristics are obtained by multiplying the open loop dc gain by $T(\omega)$, the transfer function of the low-pass filter following the synchronous detectors. Thus, the expected open loop gain $g(\omega)$ is:

$$g(\omega) = \langle g_n \rangle T(\omega). \tag{7.17}$$

The average closed-loop complex gain $G(\omega)$ is then given by the usual relationship:

$$G(\omega) = \frac{g(\omega)}{g(\omega) + 1} . \tag{7.18}$$

If desired, the average servo bandwidth for any specified convergence level and C_s at that level can be calculated as described in Ref. 1.

A more accurate way of computing C_s is to first calculate the average power contributed by the speckle modulations in each channel using the complex gain profile $G(\omega)$ and then to sum over all channels to get the total average power. Thus, we present the following modified definition of C_s:

$$C_s \equiv \left\{ \sum_{n=1}^{N} \int_{\infty}^{\infty} d\omega \frac{a(\omega-\omega_n) a^*(\omega-\omega_n) G(\omega) G^*(\omega)}{2T} \right\}^{1/2} \tag{7.19}$$

The variable T is one-half the time period over which the speckle modulations are defined and over which the mean convergence level is to be predicted. The function $a(\omega)$ is the Fourier transform of the speckle

143

modulation function, and ω_n is the nth dither frequency. The frequency shift of the function $a(\omega)$ in Eq. 7.19 accounts for the synchronous detection process. Even though the limits of integration in Eq. 7.19 are $\pm\infty$, the values of $G(\omega)$ beyond several servo bandwidths are typically so much lower than those near zero frequency that an adequate numerical value of C_s may be obtained by integrating over plus and minus several bandwidths.

A computer program which calculates C_s as a function of convergence level in the manner described above has been coded. This program also calculates the predicted convergence level as a function of C_s based on the original analysis of Ref. 1. A typical program output is shown in Figure 56. The curve marked physical relationship corresponds to the analysis of Ref. 1, while the one marked constraint relationship corresponds to the present analysis. The mean Strehl ratio or convergence level where the two relationships have simultaneous solution (i.e., where the two curves inversect) is the analytically predicted value, about 0.45 in this case.

In both of these computations, we have assumed a 12-channel multi-dither COAT system having a dither amplitude of $\psi_o = 0.349$ rad of wavelength in each channel. The dither frequencies range from 8.0 to 52.0 kHz separated by intervals of 4.0 kHz. In calculating C_s, we used the speckle modulation function from Figure 12 in Ref. 1. The transfer function $T(\omega)$ was

$$T(\omega) = (1 + i\frac{\omega}{\omega_o})^{-1} (1 + i\frac{\omega}{\omega_1})^{-4} , \qquad (7.20)$$

where $\omega_o = 20$ πrad/sec, and $\omega_1 = 1000$ πrad/sec (representing the five-pole low-pass filter which follows the synchronous detector in each COAT channel). The loop gain parameter G_1 was set at 14,830. Using Eq. 7.17, this corresponds to an open loop, unity gain servo bandwidth of 400 Hz at full convergence. We refer to this as the nominal servo bandwidth.
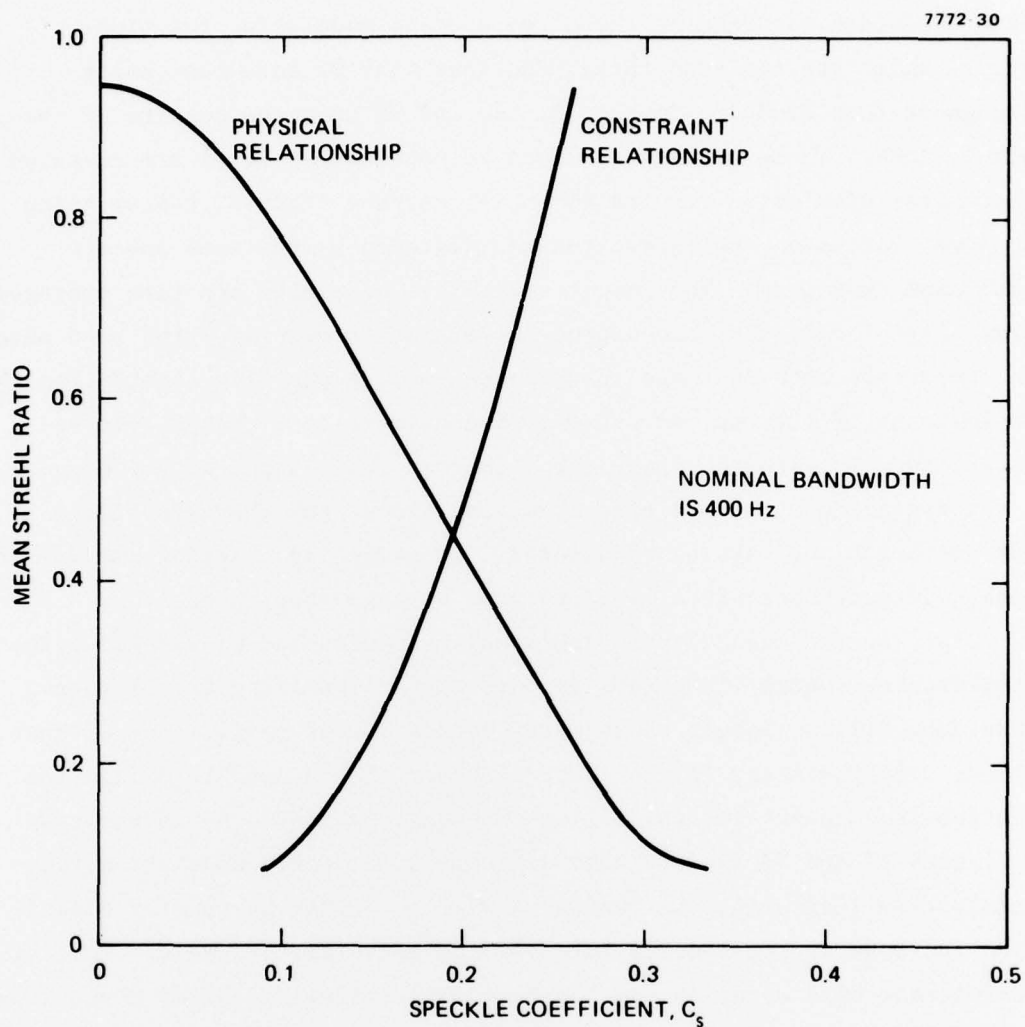
Figure 56. Typical analytical output. (This case predicts degrada-
tion of lines from the speckle modulations of Figure 12,
Ref. 4.)

These calculations were repeated at six different values of nominal servo bandwidth for each of the three speckle modulation functions of Ref. 1, which are the same three functions that we have been using throughout this study. Figures 57, 58, and 59 show the results of these calculations. These predicted values of convergence level are compared to computer simulation results shown in the same figures, representing the same COAT servo configurations and degraded by the same speckle modulation functions. The computer simulation results are time averaged target Strehl ratios or convergence levels taken over a period of 8 msec. The comparison between these results are good, especially considering the complexities of the real situation. The gain in each channel varies instantaneously with the phase error in that channel and with the state of convergence of the remaining channels. Thus, the channels always have different and varying bandwidths. Consequently, varying amounts of speckle interference are allowed to pass through each channel.

Also, once a channel has been completely disabled by speckle noise interference, further increases in noise power resulting from larger bandwidths will no longer cause more degradation of performance of that channel. Furthermore, if the spectral power of the speckle modulation function is concentrated in the low-frequency channels, as is the case in Figures 57 and 58 (and to some degree in all speckle modulation functions), then increasing the bandwidth will not cause an equally distributed increase in the speckle interference among all channels. Most of the increase will occur in the low-frequency channels. After these low-frequency channels are completely disabled, then further increases in bandwidth will cause a proportionately lower decrease in overall COAT performance. This is probably the reason for the consistently greater discrepancy between analysis and computer simulations results at the higher nominal bandwidths. The computer simulations reflect the true situation, while the statistical analysis which treats all channels as having the same average phase error related to the total average power cannot account for this phenomenon.
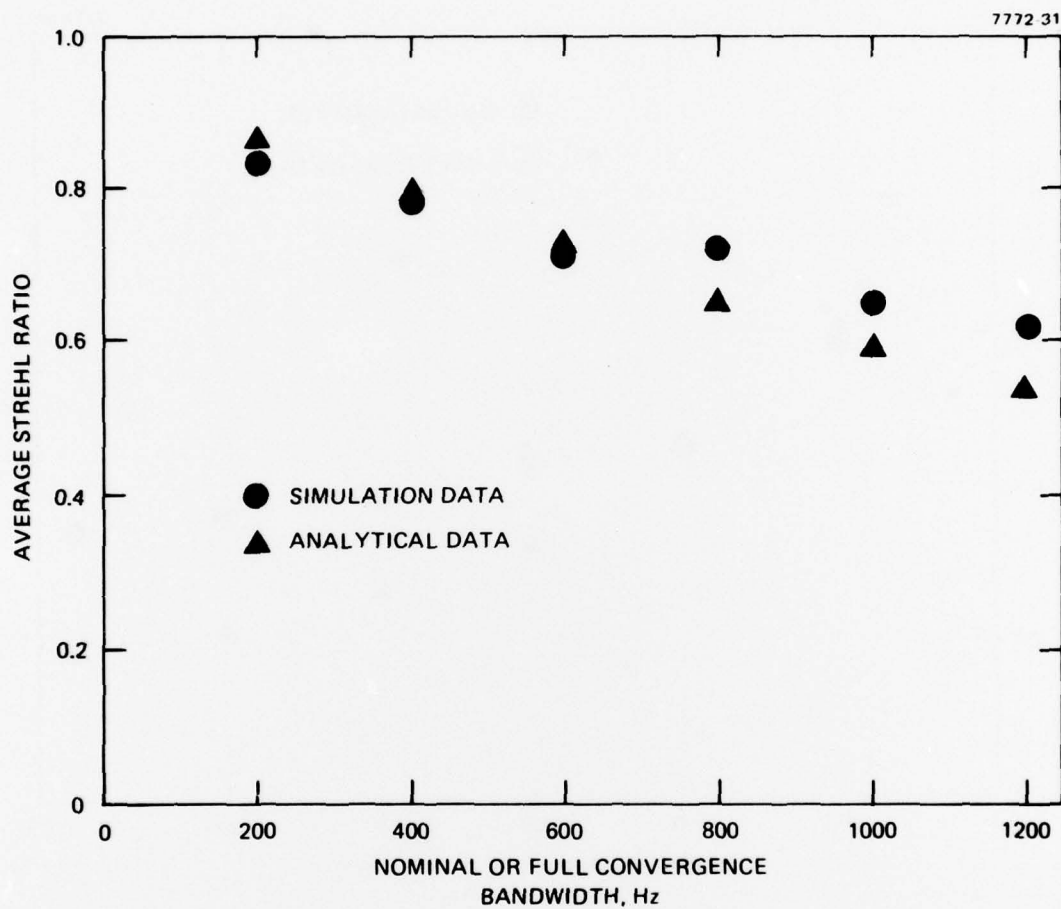
146

Figure 57. Comparison of analysis and computer simulations using speckle modulations from Figure 10, Ref. 1.
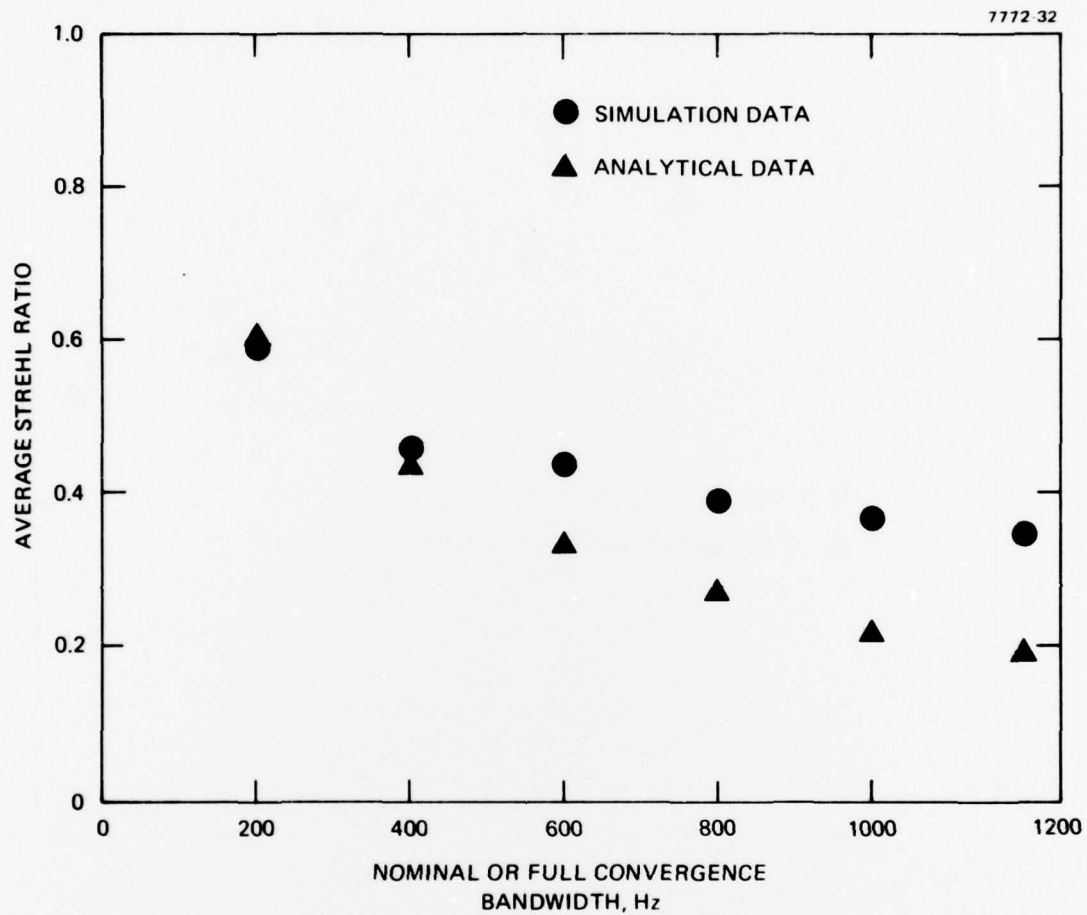
Figure 58.   Comparison of analysis and computer simulations using speckle
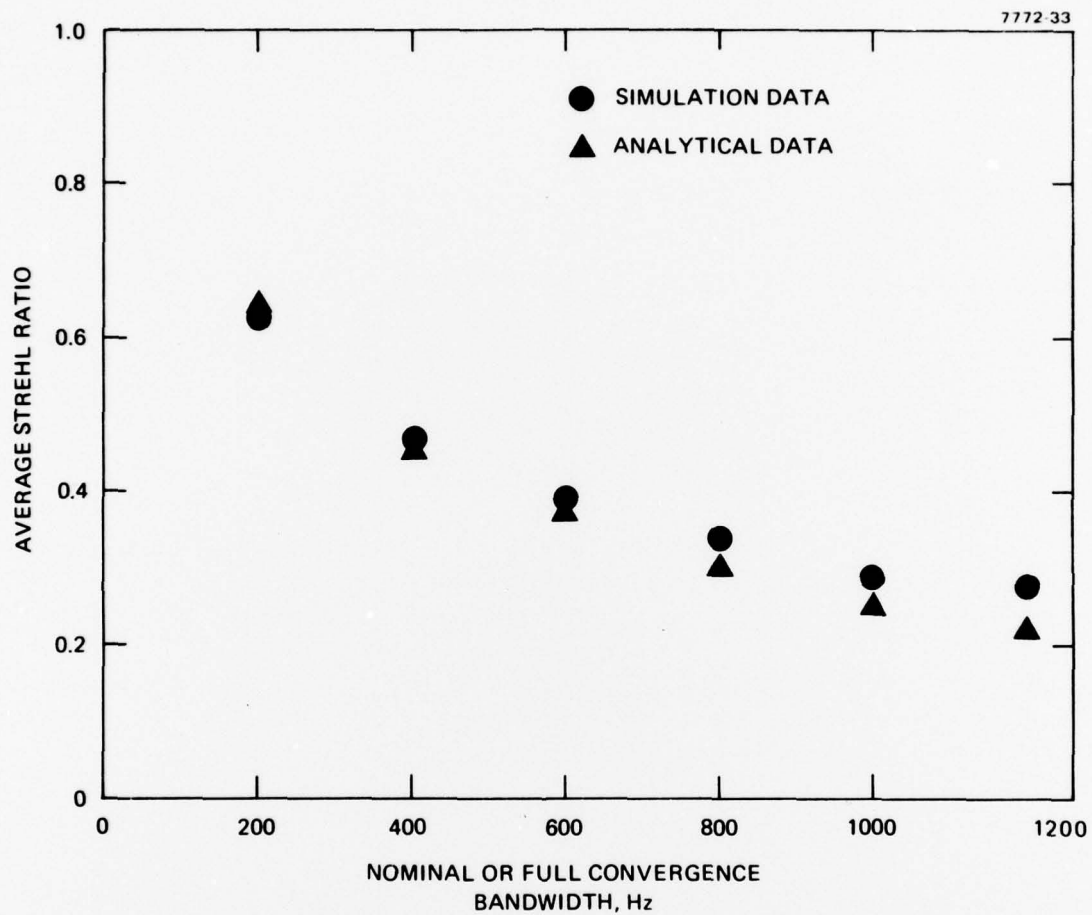modulations from Figure 11, Ref. 1.

Figure 59. Comparison of analysis and computer simulations using speckle modulations from Figure 12, Ref. 1.

REFERENCES

1. Kokorowski, S.A., Pedinoff, M.E., and Pearson, J.E., "Analytical, Experimental, and Computer-simulation Results on Interactive Effects of Speckle with Multidither Adaptive Optics Systems," *J. Opt. Soc. Am.* 67:333, (1977).

2. Pearson, J.E., Kokorowski, S.A., and Pedinoff, M.E., "Effects of Speckle in Adaptive Optics," *J. Opt. Soc. Am.* 66:1261, (1976).

3. Gurski, G.F., Nomiyama, N.T., Radley, R.J., and Wilson, J., "An Initial Evaluation of Performance of Adaptive Optical Systems with Extended Dynamic Targets," *J. Opt. Soc. Am.* 67:345 (1977).

4. Bridges, W.B., Brunner, P.T., Lazzara, S.P., Nussmeier, T.A., O'Meara, T.R., Sanquinet, J.A., and Brown, W.P., Jr., "Coherent Optical Adaptive Techniques," *Appl. Opt.* 13:291 (1974).

5. Pearson, J.E., Bridges, W.B., Hansen, S., Nussmeier, T.A., and Pedinoff, M.E. "Coherent Optical Adaptive Techniques: Design and Performance of an 18-element, Visible, Multidither COAT system," *Appl. Opt.* 15:611 (1976).

6. Pearson, J.E., Hansen, S., "Experimental Studies of a Deformable-Mirror Adaptive Optical System," *J. Opt. Soc. Am.* 67:325 (1977).

7. Goldfischer, L.I., "Autocorrelation Function and Power Spectral Density of Laser Produced Speckle Patterns," *J. Opt. Soc. Am.* 55:247 (1965).

8. Goodman, J.W., "Some Fundamental Properties of Speckle," *J. Opt. Soc. Am.* 66:1145 (1976).

9. Dainty, J.C. (Editor), "Laser Speckle and Related Phenomena," *Topics in Applied Physics* Vol. 9, Springer-Verlag (1975).

10. George, N., "Speckle from Rough, Moving Objects," *J. Opt. Soc. Am.* 66:1182 (1976).

11. Erdmann, J.C., Gellert, R.I., "Speckle Field of Curved, Rotating Surfaces of Gaussian Roughness Illuminated by a Laser Spot," *J. Opt. Soc. Am.* 66:1194 (1976).

12. Pedinoff, M.E., Kokorowski, and J.E. Pearson, "COAT/Target-Signatures Interactions," Technical Report, Contract No. F30602-76-C-0021, 1976, A030055.

13. O'Meara, T.R., "The Multidither Principle in Adaptive Optics," *J. Opt. Soc. Am.* 67:306 (1977).

APPENDIX

SYSTEM SAFETY ANALYSIS

The contract statement of work requires that a system safety analysis be performed in accordance with paragraph 5.8.2.1 of MIL-STD-882. Such an analysis was performed during the contract work to identify and, where necessary, correct possible hazards associated with the operation of the system, known as the "multidither COAT experimental model" (hereafter called "the COAT system"), used in the experimental tasks of this contract. The analysis performed follows a similar analysis[*] performed for the same COAT system when it was located in a different area.

There are two potential hazard sources for users of this system within the laboratory environment, where this contract work was performed: (1) electrical shock and (2) eye damage by laser radiation. Appropriate safety precautions were taken as part of the Hughes Industrial Safety Program to ensure sufficient fire protection, clearance for egress from the laboratory, access to power-line breakers, etc., so that the requirements of the California OSHA codes were satisfied.

Electrical shock from the COAT system was assessed to be in Category I — Negligible as defined in paragraph 3.14 of MIL-STD-882. Proper design of the electrical parts of the system ensures that no personnel can encounter lethal or hazardous electrical voltage and/or current levels.

The hazard level for optical eye damage was assessed to be in Category II — Marginal. The nature of the program required working with two laser sources, a 30-mW He-Ne unit operating at 0.6328 μm and a 1.5-W argon unit with an output wavelength of 0.488 μm. Various system optics reduce the maximum potential power levels to 10 mW at 0.6328 μm and 100 mW at 0.488 μm. The potential hazard is adequately controlled by providing

---

[*] W.B. Bridges et al., RADC-TR-74-108, Jan. 1974, Contract F30602-73-C-0248, 779668/3GI.

153

safety glasses for all personnel while working on or around the system
and by using masks, optical stops, etc. to confine the optical laser
beams to areas where no personnel can directly view them at day point
where the optical power density exceeds 2.5 mW/cm^2.

Sufficient safety procedures have thus been implemented to ensure
that both the 0.6328 μm radiation (a Class III hazard at the laser output)
and the 0.488 μm radiation (a Class IV hazard at the laser output) are
adequately controlled to reduce the hazard to Category II for personnel
working within the laboratory where the COAT system is operated. In
addition, personnel are instructed in proper safety procedures while
within the laboratory. Appropriate warning signs notify visitors to the
laboratory, and laser safety goggles are available for visitors.

MISSION
of
Rome Air Development Center

RADC plans and conducts research, exploratory and advanced development programs in command, control, and communications (C^3) activities, and in the C^3 areas of information sciences and intelligence. The principal technical mission areas are communications, electromagnetic guidance and control, surveillance of ground and aerospace objects, intelligence data collection and handling, information system technology, ionospheric propagation, solid state sciences, microwave physics and electronic reliability, maintainability and compatibility.

AMERICAN REVOLUTION BICENTENNIAL

1776-1976